STRUCTURE-FUNCTION RELATIONSHIP STUDY OF A LOOP STRUCTURE IN ALLOSTERIC BEHAVIOUR AND SUBSTRATE INHIBITION OF *LACTOCOCCUS LACTIS* PROLIDASE

A Thesis Submitted to the College of

Graduate Studies and Research

In Partial Fulfillment of the Requirements

For the Degree of Master of Science

In the Department of Food and Bioproduct Sciences

University of Saskatchewan

Saskatoon

By

JIAN AN CHEN

Keywords: allosteric subsite, site-directed mutagenesis, X-ray diffraction

Permission to Use

In presenting this thesis in partial fulfilment of the requirements for a Postgraduate degree from the University of Saskatchewan, I agree that the Libraries of this University may make it freely available for inspection. I further agree that permission for copying of this thesis in any manner, in whole or in part, for scholarly purposes may be granted by the professor or professors who supervised my thesis work or, in their absence, by the Head of the Department or the Dean of the College in which my thesis work was done. It is understood that any copying or publication or use of this thesis or parts thereof for financial gain shall not be allowed without my written permission. It is also understood that due recognition shall be given to me and to the University of Saskatchewan in any scholarly use which may be made of any material in my thesis.

Requests for permission to copy or to make other use of material in this thesis in whole or part should be addressed to:

Head of the Department of Food and Bioproduct Sciences

University of Saskatchewan

51 Campus Dr.

Saskatoon, Saskatchewan S7N 5A8,

Canada.

ABSTRACT

Lactococcus lactis prolidase (*Lla*prol) hydrolyzes Xaa-Pro dipeptides. Since Xaa-Pro is known as bitter peptides, *Lla*prol is potentially applicable to reduce bitterness of fermented foods. *Lla*prol shows allosteric behaviour and substrate inhibition, which are not reported in other prolidases. Computer models of *Lla*prol based on an X-ray structure of non-allosteric *Pyrococcus furiosus* prolidase showed that a loop structure ($Loop^{32-43}$) is located at the interface of the protomers of this homodimeric metallodipeptidase. This study investigated roles of four charged residues (Asp^{36}, His^{38}, Glu^{39}, and Arg^{40}) of $Loop^{32-43}$ in *Lla*prol using a combination of kinetic examinations of ten mutant enzymes and their molecular models. Deletion of the loop structure by Δ36-40 mutant resulted in a loss of activity, indicating $Loop^{32-43}$ is crucial for the activity of *Lla*prol. D36S and H38S exhibited 96.2 % and 10.3 % activity of WT, whereas little activities (less than 1.0 % of WT activity) were observed for mutants E39S, D36S/E39S, R40S, R40E, R40K and H38S/R40S. These results implied that Glu^{39} and/or Arg^{40} play critical role(s) in maintaining the catalytic activity of *Lla*prol. These observations suggested that the loop structure is flexible and this attribute, relying on charge-charge interactions contributed by Arg^{40}, Glu^{39} and Lys^{108}, is important in maintaining the activity of *Lla*prol. When the loop takes a conformation close to the active site (closed state), Asp^{36} and His^{38} at the tip of the loop can be involved in the catalytic reaction of *Lla*prol. The two active mutant prolidases (D36S and H38S) resulted in modifications of the unique characteristics; the allosteric behaviour was not observed for D36S, and H38S *Lla*prol showed no substrate inhibition. D36E/R293K, maintaining the negative charge of position 36 and positive charge of position 293, still possessed the allosteric behaviour, whereas the loss of the charges at these positions (D36S of this study and R293S of a previous study (Zhang et al., 2009 BBA-Proteins Proteom 1794, 968-975) eliminated the

allosteric behaviour. These results indicated the charge-charge attraction between Asp^{36} and Arg^{293} is important for the allostery of *Lla*prol. In the presence of either zinc or manganese divalent cations as the metal catalytic centre, D36S and H38S enzymes also showed different substrate preferences from WT *Lla*prol, implying the influence of Asp^{36} and His^{38} on the substrate binding. D36S and H38S also showed higher activities at pH 5.0 to 6.0, in which range WT *Lla*prol steeply decreased its activity, indicating Asp^{36} and His^{38} are involved in the active centre and influence the microenvironment of catalytic His^{296}. The above observations are attributed to modifications of their local structure in the active centre since the temperature dependency and thermal denaturing temperature indicated little effects on the overall structure of the *Lla*prol mutants.

From these results, we concluded that the unique behaviours of *Lla*prol are correlated to $Loop^{32\text{-}43}$ and Asp^{36} and His^{38} on it. When $Loop^{32\text{-}43}$ takes a closed conformation, Asp^{36} interacts with Arg^{293} via charge-charge attraction to form an allosteric subsite. The saturation of the allosteric site with substrates further allowed the communications of His^{38} with S_1 site residues to complete the active site. When the substrate concentration becomes higher than it is required to saturated productive S_1' site, His^{38}, Phe^{190} and Arg^{293} would resemble the residue arrangement of S_1' site residues (His^{292}, Tyr^{329}, and Arg^{337}) and bind to the proline residue of substrates. This non-productive binding would prevent the conformational change of $Loop^{32\text{-}43}$, which further results in the substrate inhibition. For further confirmation of this mechanism, crystallographic studies will be conducted. In this thesis, we have indentified the conditions to produce crystals of *Lla*prol proteins.

ACKNOWLEDGMENTS

I would like to express my gratitude to my supervisor Dr. Takuji Tanaka for offering me this graduate study opportunity. I appreciate his vast knowledge and skill in many areas, and his assistance in writing reports. Without his incredible patience and support, I could not fulfill the tasks in my research and thesis.

Many thanks go to my other advisory committee members: Drs. Pawel Grochulski, George Khachatourians, and the late Louis Delbaere for the assistance they provided at all levels of the research project. Also I would like to express a special thanks to the graduate chairs, Drs. Phyllis Shand and Vladimir Vujanovic for helpful comments. Finally, I appreciate Dr. Mary D. Pato from the Department of Biochemistry for taking time out from her busy schedule to serve as my external examiner.

I must also acknowledge Yetty Y. (Julie) Gunawan, Eunyoung Baik and Jori Harrison for their efforts involved in my research. Discussions with my other colleagues: Keke Hu, Douglas Grahame, Tae Sun Kang, and Dr. Madhavi Arla, are always appreciated.

For X-ray diffraction experiments in Canadian Light Source and Saskatchewan Structural Science Centre, the help and support from members of Dr. Louis Delbaere's group and Dr. Pawel Grochulski are greatly appreciated. Dr. Peter Yu is also acknowledged for his generosity to allow me to use the equipment in his lab.

Last but not least I would like to express my gratitude to my friends for encouraging me: Hayley Rutherford, Aura Helena Quinonez Corredor, Henry Cao, Hsiang Yun Chi, Katherine Gui, Li Tan, Prasad Daida, Prabha Medihala, Ricky Lam, Tanya Der and Yit Kheng Goh.

Very special thanks go to Prof. Xueping Meng, without whose encouragement I would not have considered a graduate study in biological research. Prof. Meng is the one professor/teacher who truly made a difference in my life. It was under his tutelage that I developed a focus and

became interested in molecular biology. He provided me with direction, technical support and became more of a mentor and friend, than a professor. It was though his, persistence, understanding and kindness that I completed my undergraduate degree and was encouraged to apply for graduate training. I doubt that I will ever be able to convey my appreciation fully, but I owe him my eternal gratitude.

I would also like to thank my family for the support they provided me through my entire life and in particular, I must acknowledge my girlfriend and best friend, Yan Chen, without whose love and encouragement, I would not have finished this thesis.

In conclusion, I recognize that this research would not have been possible without the financial assistance of Natural Science and Engineering Research Council of Canada (NSERC) and Saskatchewan Health Research Foundation (SHRF), and express my gratitude to those agencies.

TABLE OF CONTENTS

LIST OF TABLES

LIST OF FIGURES

LIST OF ABBREVIATIONS

To specify an amino acid residue in a protein mentioned in this thesis, the amino acid residue is expressed as $Xaa^{\#}$; where Xaa represents the 3 letter code of the amino acid and superscript "#" indicates the position of this amino acid residue in its protein sequence. For example, Arg^{293} displays an arginine residue at the 293^{th} position of its protein sequence.

Other used abbreviations are listed as below.

Δ36-40	The mutant of the deletion of region from position 36 to 40
3D	Three dimension
ABS	Absorbance
APP	Amino peptidase P
Arg^{293}	Arginine residue at position 293 of a protein
ATP	Adenosine-triphosphate
*b*LeuAP	Bovine leucine aminopeptidase
BSA	Bovine serum albumin
BU	Binding unit
CAP	Catabolite activator protein
cAMP	Cyclic adenosine monophosphate
CD	Circular dichroism
cGMP	Cyclic guanosine monophosphate
CLS	Canadian Light Source
D36S	The mutation of aspartic acid to serine at position 36
D36S/E39S	The double mutation of aspartic acid to serine at position 36 and glutamic acid to serine at position 39

D36E/R293K	The double mutation of aspartic acid to glutamic acid at position 36 and arginine to lysine at position 293
DBD	DNA binding domain
DEAE	Diethyl-aminoethyl
DNA	Deoxyribonucleic acid
dNTP	Deoxynucleotide triphosphate
E39S	The mutation of glutamic acid to serine at position 39
E.coli	*Escherichia coli*
*e*MetAP	*Escherichia coli* methionine aminopeptidase
FID	Free interface diffusion
GAF	Domain present in phytochromes and cGMP-specific phosphodiesterases
GRAS	Generally recognized as safe
H38S	The mutation of histidine to serine at position 38
H38S/R40S	The double mutation of histidine to serine at position 36 and arginine to serine at position 40
H	Hill constant
HPLC	High-pressure liquid chromatography
*Hs*MetAP	Human methionine aminopeptidase-2
IBMX	3-Isobutyl-1-methylxanthine
Ip	Ionization potential
IPTG	Isopropyl β-D-1-thiogalactopyranoside
K_i	Substrate inhibition constant
K_m	Michaelis constant
KNF	Koshland-Nemethy-Filmer

L. lactis	*Lactococcus lactis*
*Lla*prol	*Lactococcus lactis* prolidase
$Loop^{32-43}$	A loop secondary structure composed of residues from 32 to 43
*pep*Q	*Lacotococcus lactis* prolidase coding gene
LB	Luria-Bertani broth
Mdeg	Millidegrees
MW	Molecular weight
MWC	Monod-Wyman-Changeux
OD	Optical density
PCR	Polymerase chain reaction
PD	Prolidase deficiency
PDE 2A	Phosphodiesterase 2A
*pep*Q	Prolidase gene
PEG	Polyethylene glycol
*Pf*MetAP	*Pyrococcus furiosus* methionine aminopeptidase-1
*Pf*prol	*Pyrococcus furiosus* prolidase
pK_a	Acid dissociation constant
pI	Isoelectric point
*Ps*CP	*Pseudomonas sp.* carboxypeptidase G_2
Rubisco	Ribulose-1,5-bisphosphate carboxylase/oxygenase
R40E	The mutation of arginine to glutamic acid at position 40
R40K	The mutation of arginine to lysine at position 40

R40S	The mutation of arginine to serine at position 40
RM	Reaction mixture
R state	Relaxed state of allosteric enzyme
[*S*]	Substrate concentration
SDS-PAGE	Sodium dodecyl sulfate polyacrylamide gel electrophoresis
SDM	Site-directed mutagenesis
*Sg*AP	*Streptomyces griseus* aminopeptidase
SU	Stimulating unit
T state	Tense state of allosteric enzyme
TV	Threshold value
SSSC	Saskatchewan Structural Sciences Centre
ν	Velocity
V_{max}	Maximum velocity
WT	Wild type
Xaa	Amino acid

1 INTRODUCTION

Fermented foods attract attention from consumers in terms of their health benefits. One of the major expenses in making fermented foods, such as cheese, is the costs to age the fermented foods to allow development of their distinctive flavours (Fukushima, 1979; Roberts and Vickers, 1994). The ageing processes generally take months to years to complete. This long duration is required to diminish off-flavours which are prominent defects in the early stage of ageing. Efficient reduction of off-flavours would shorten the ageing process of the food fermentation while keeping higher acceptability by consumers. Proline-containing peptides, including Xaa-Pro, largely account for the bitterness of fermented foods, and these peptides are less accessible to general peptidases due to the presence of an imino ring structure. Since Xaa-Pro is an ultimate product of proteolysis by general peptidases, Xaa-Pro dipeptidase (prolidase), which specifically hydrolyzes Xaa-Pro, would be useful in debittering processes and shortening the ageing time for the fermented food industry.

Prolidase is also an essential metabolic enzyme in human bodies. Prolidase deficiency (PD) caused by a malfunction of prolidase results in clinical symptoms, such as severe skin lesions, facial abnormalities, chronic joint dislocations, bacterial infections, and mental retardation (Powell et al., 1974). An enzyme replacement therapy using an activated prolidase is considered to treat PD (Colonna et al., 2008). Furthermore, prolidase is considered as a potential tool to detoxify nerve gas chemicals through their hydrolysis (Ditargiani et al., 2010).

Lactic acid bacteria are well-known as a GRAS (generally recognized as safe) microorganism. Prolidase produced from *Lactococcus lactis* is ideal for food and medical applications. Therefore, a comprehensive understanding of *Lactococcus lactis* prolidase (*Lla*prol)

in terms of its structure and function relationships would provide valuable information to adapt *Lla*prol to such applications.

2 LITERATURE SURVEY

2.1 Biotechnological Applications of Prolidase

2.1.1 Fermented Food Industries

Fermented foods are established and widely accepted as a category of foods. They include many traditional foods, such as cheese (fermented casein), summer sausage, pickled vegetables, miso (salted and fermented soybean paste), soy sauce, fish sauce, natto (fermented soybeans), and katsuobushi (dried fish meat) (Maehashi and Huang, 2009). During processes of the food fermentation, a wide range of peptides are generated through protein hydrolysis and contributes to flavours and off-flavours of the fermented foods. Off-flavours, such as bitterness arisen from bitter peptides, are not preferred in terms of the customer acceptance. To attain customers' acceptance, flavour masking or bitter compound degradation is required. Prolidase would be used as a debittering agent in the preparation of fermented foods through the degradation of bitter peptides into free amino acids, which generally have little flavours.

2.1.1.1 Bitter Peptides in Cheese

Cheese is a traditional dairy food in Western countries. A cheese making process mainly involves three steps: curding, curd processing, and ageing. In the curding step, milk is coagulated into solid curd by adding bacteria culture and coagulating enzymes. The curd is drained, salted, and moulded in curd processing which usually produces a salty yet bland cheese (Walter et al., 1969). In the ageing process (also called ripening), metabolic activities of starter bacteria and their enzymes transform texture and flavours of cheese. The transformation relies on the breakdown of casein proteins and milk fats in unripened cheese into a complex mixture of amino acids, peptides, and fatty acids, which contribute to the distinctive flavours of cheese.

Ageing processes can take from a few months to several years and the length of ageing directly affects the degree of ripening.

The degree of ripening can result in different intensity of bitterness. By using *Lactococcus lactis ssp. lactis* S3 as a starter bacterium, Cheddar cheese is slightly bitter at two, four and six months of ripening, even bitter after two years (Broadbent et al., 1998). When the bitterness is pronounced, it can negatively influencing the acceptance and marketability of cheese. It was reported that the bitter flavour in cheese is due to the degradation of casein proteins to peptides (Bumberger and Belitz, 1993). Past investigations have confirmed that the proteolytic systems in starter bacteria play a crucial role in the flavour formation, including bitterness (Thomas and Pritchard, 1987). The proteinases slowly degrade polypeptides, such as α_{s1}-casein to oligopeptides and free amino acids (Visser et al., 1983). Some of these oligopeptides taste bitter. A study on enzymatic hydrolysis of casein showed that resultant oligopeptides from residue position 49 to 97, comprising a large variety of proline-containing peptides, are the contributors to the bitter flavour (Bumberger and Belitz, 1993). The result of this experiment was further validated by the analysis of isolated peptides from Cheddar cheese (Lee and Warthesen, 1996), which showed that proline-containing peptides are key players in the bitterness of cheeses.

2.1.1.2 Bitter Peptides in Other Fermented Food Makings

Sufu (Chinese soybean cheese) making includes a preparation of the tofu from soybean, solid-state fermentation with fungi (e.g., *Actinomucor elegans*), salting and ripening. Hydrolysis of soybean protein in tofu into peptides and amino acids occurs during the ripening stages, which normally take three to six months (Han et al., 2004). This hydrolysis develops distinctive flavours of sufu. The soybean protein is composed of four main proteins, α, β, γ-conglycinin and 11*S* glycinin (Kim et al., 2003). Kim et al. (2008) showed that 21 bitter peptides are found

in hydrolysate of Soybean 11*S* glycinin. Nine of the 21 peptides are revealed as proline-containing peptides (such as Arg-Pro, Asn-Ala-Glu-Lys-Pro-Asp, Gln-Ala-Leu-Pro-Glu, Gly-Met-Ile-Tyr-Pro-Gly, Ala-Leu-Glu-Pro-Asp-His-Arg, Ile-Tyr-Pro-Gly, and Ile-Tyr-Pro-Gly-Cys-Pro-Ser-Asp).

Fish sauce is a type of food flavouring made through fermentation of fish. Fish sauce that has been only briefly fermented has an apparent fishy taste, whereas extended fermentation gives products nuttier, cheesier and bitter flavours instead. Fish sauce is known for its high contents of oligopeptides formed as a consequence of microbial fermentation. Park et al. (2002) observed that a proline residue exists at the C-terminus of six dipeptides or in the middle of five tripeptides among 17 peptides isolated from fish sauce using HPLC. These proline-containing peptides are bitter tastes based on a sensory evaluation. It was reported that the addition of dipeptidylpeptidases to a fish sauce accelerates the fermentation and yields products with desirable tastes (Raksakulthai and Haard, 2003).

2.1.1.3 Proline-Containing Peptides

Above studies on fermented foods found that the undesirable bitter taste is caused by the formation of bitter peptides during production processes. When the concentration of bitter peptides exceeds taste threshold values (TV), a bitterness defect is detected. As mentioned in section 2.1.1.1 and 2.1.1.2, proline-containing peptides dominate bitterness in fermented products. The molecular mechanism how proline-containing peptides show bitterness attracts research attentions but it is still under debate (Kiw et al., 2008).

Ney (1971) proposed that the bitterness of a peptide is correlated to its *Q*-value ($Q=\Sigma\Delta f/n$), which is an average of the hydrophobicity of the side chain of the constituent amino acid residues (Δf reflects the hydrophobicity of an individual amino acid residue, and n is the number

of amino acid residues). According to the *Q* rule, peptides with molecular weight (MW) less than 6,000 Da and a *Q*-value higher than 1,400 cal/mol are bitter peptides. However, the accuracy of the *Q*-rule is limited because other parameters such as primary and seconday structures of peptides account for the bitter tastes (Asao et al., 1987). For instance proline-containing bitter peptides isolated from Guoda cheese, do not obey this *Q*-rule (Toelstede and Hofmann, 2008).

Otagiri et al. (1985) have reported the Arg-Pro is 1.25-times bitter than caffeine. Threshold values (Table 2.1-1) of Arg-Pro and its similar peptides are determined through structure and sensory analyses by Ishibashi et al. (1988). This article discussed the significant role of proline in the bitterness of peptides, and they proposed a rule to determine the bitterness of peptide using structural factors. Bitterness of peptides is determined by two structural factors: binding unit (BU) and stimulating unit (SU). Bitterness is exhibited when both units exist in a molecule and they simultaneously bind to a bitter taste receptor. Taking Arg-Pro as an example, the imino ring of proline residue acts as BU and the adjacent arginine residue plays the role of SU. They argued that these two units must be adjacent to each other in three-dimensional structure of peptides. As shown in Figure 2.1-1, the steric distance between the two units and the diameter of bitter taste receptor are estimated as 4.1 Å (Ishibashi et al., 1988) and 15 Å (Tamura et al.,1990), respectively.

This group further investigated the role of proline residues in the bitter taste of peptides. They showed that another significant role of the proline residue in bitter peptides is the conformational alteration of the proline-containing peptide molecules. *R*-groups of amino acids can occur in either *cis*- or *trans*-configuration and the bulkiness of *R*-groups of most amino acids normally prefers to take the *trans*-configuration (99.95% probability). However, proline

Table 2.1-1 Threshold values of peptides examined in studies of Ishibashi et al (1998)

Peptides	Threshold value (TV)
Arg-Pro	0.8 mM
Arg-Arg	8.0 mM
Arg-Gly	10.0 mM
Pro-Arg	3.0 mM
Arg-Gly-Pro	13.0 mM
Arg-Pro-Gly	0.8 mM
Gly-Arg-Pro	0.8 mM

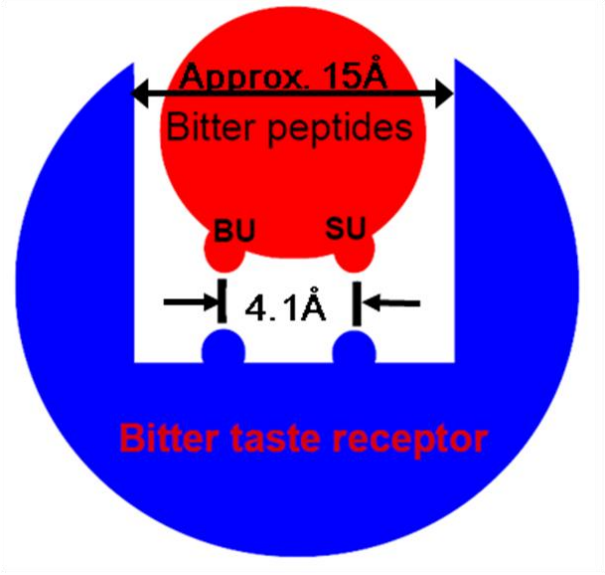

Figure 2.1-1 A model for binding of bitter peptides to bitter taste receptors.
A bitter peptide is shown in red and a bitter-taste receptor is shown in blue. The distance between binding unit (BU) and stimulating unit (SU) in peptides should be around 4.1 Å. The pocket size formed in the bitterness receptor region is approximately 15 Å. (adapted from Ishibashi et al. (1988) and Tamura et al. (1990))

frequently flips between *cis*- and *trans*-configurations than other amino acids, and the probability of *cis*-configuration of proline residues is 5–6 %, which is about 100-times higher than other amino acids (Buxbaum, 2005). This feature of proline allows the conformational isomerization of proline-containing peptides, which may have an influence on the generation of bitterness of these peptides.

2.1.1.4 *Lactococcus lactis* Prolidase in Fermented Food Processing

Milk casein and soybean protein are proline-rich proteins, and proline-containing peptides generated from the hydrolysis of these proteins are reported as key contributors to the bitterness of fermented products (Ishibashi et al., 1988). Attempts have been made to remove or mask the bitterness in fermented foods. It is logical that the use of peptidases to hydrolyze bitter peptides into free amino acids, which normally have less flavour, can reduce the bitterness in fermented foods. However, proline-containing peptides are inaccessible to common exo- and endopeptidases such as general peptidases, di- and tripeptidases (Mcdonald et al., 1969), due to the existence of the imino structure of proline. Thus proline specific peptidases, including proline aminopeptidase P, Xaa-Prolyl dipeptidyl peptidases, proline iminopeptidase, postproline endopeptidase, prolinase, and prolidase are required to hydrolyze proline-containing peptides. Among these enzymes, prolidase and prolinase are two of the most important enzymes because they degrade the ultimate products of general proteolysis, Xaa-Pro and Pro-Xaa, into free amino acids.

Lactococcus lactis is a natural microorganism used as a starter bacterium for making many types of cheeses. Prolidase from *Lactococcus lactis* can be an excellent mediator to remove bitterness arisen from proline peptides in cheese-making. Thus the structure-function

relationship study of *Lactococcus lactis* prolidase (*Lla*prol) shall provide valuable information to further modify *Lla*prol for practical applications.

2.1.2 Prolidase in Human Health

Prolidase deficiency (PD) is a rare recessive disorder caused by mutations in the prolidase gene and characterized by severe skin lesions, facial abnormalities, chronic joint dislocations, bacterial infections, and mental retardation (Endo et al., 1982). The pathogen of PD is still unclear even though it is proposed to relate to the collagen recycling. Collagen protein accounts for 70 % of skin proteins, which contains a large amount of proline residues. Prolidase plays an important role in the breakdown of collagen and intracellular proteins especially in the final stage when peptides and dipeptides contain a high level of proline residue (Palka and Phang, 1997). Due to a malfunction of prolidase, the patients are not able to hydrolyze the proline containing peptides, resulting in the accumulation of proline-containing peptides, which causes the symptom of PD in patients.

To treat PD, enzyme replacement therapy has been considered. Ogata et al. (1981) and Endo et al. (1982) attempted transfusion of PD patients with normal matched erythrocytes. Due to the inactive form of prolidase in erythrocytes, no effect on clinical symptoms of iminodipeptiduria was observed in these two studies. Hechetman et al. (1988) activated the prolidase in erythrocytes with $MnCl_2$ before transfusion, and positive results were obtained, which provided a fresh approach to enzyme replacement therapy in PD. However, further clinical trials are required to evaluate this manganese–activated erythrocyte system to be applied in PD treatment. Colonna et al. (2008) suggested an innovative therapeutic approach for PD with employing prolidase-loaded chitosan nanoparticles and they successfully introduced and restore the active form prolidase into PD fibroblasts for 8 days.

Lactococcus lactis prolidase can be an alternative source to be applied in treating PD, since *Lactic acid* bacteria are recognized as GRAS (generally recognized as safe) microorganisms. The comprehensive understanding of *Lla*prol in terms of structure and function would facilitate its applications in this area.

2.1.3 Prolidase in Nerve Gas Degradation

Nerve gases are a class of extremely-poisonous chemical compounds to human beings and they can disrupt the transduction of nerve signals to organs when these chemicals are absorbed. Prolidase has been considered as an potential target for treating nerve gas contaminations, because prolidases showed activities on P-F and P-O bonds found in organophosphorus compounds, including the nerve gas chemicals (Vyas et al., 2010). To improve the functionality of *Lla*prol in degradations of nerve gases, protein engineering works of *Lla*prol would be necessary. Hence, it is significant for this purpose to elucidate the molecular mechanism of *Lla*prol.

2.2 General Characterizations of Prolidase

2.2.1 Catalytic Mechanism of Prolidase

Prolidase (E.C. 3.4.13.9) is a dipeptidase, which specifically hydrolyzes dipeptides with prolines or hydroxyprolines at their C-terminal, as shown in Figure 2.2-1.

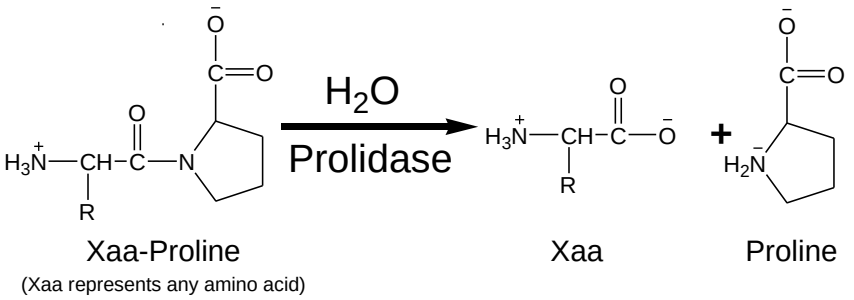

Figure 2.2-1 Chemical reactions catalyzed by prolidase.

Prolidase belongs to a group of enzymes called metallopeptidases, enzymes that require one or two metal cations per active site for their full activities. Through comparison and analyses of metallopeptidases in terms of structure-function relationships, prolidase is classified into a subclass of metallopeptidase that contains a dinuclear active-site metal cluster. Other members of this subclass that have been studied at a structural level, include *Escherichia coli* methionine aminopeptidase (*e*MetAP) (Roderick and Matthews, 1993), *Aeromonas proteolytica* aminopeptidase (Chevrier et al., 1994), bovine leucine aminopeptidase (Strater and Lipscomb, 1995), *Escherichia coli* proline aminopeptidase (Wilce et al., 1998), human methionine aminopeptidase-2 (Liu et al., 1998), *Pyrococcus furiosus* methionine aminopeptidase-1 (Tahirov et al., 1998), *Streptomyces griseus* aminopeptidase (Gilboa et al., 2001), and *Pseudomonas sp*. carboxypeptidase G_2 (Rowsell et al., 1997). These enzymes share high homology at the amino acid level and have a dinuclear metal centre bridged by a water molecule or a hydroxide ion. The metal cluster can coordinate with a bound substrate, activate a nucleophile for catalysis, and presumably stabilize the transition state (Lowther and Matthews, 2002).

The high similarity in three-dimensional structures among prolidase, methionine aminopeptidase (MAP), amino peptidase P (APP) and creatinase (Coll et al., 1990) has these enzymes further cluster into a smaller subclass of metalloenzymes known as “pita-bread enzymes”. Although each of these enzymes have different substrate specificities, they share common metal binding residues which are two aspartate, two glutamate and one histidine residues as shown in Figure 2.2-2, suggesting that they can have a conserved catalysis mechanism (Bazan et al., 1994).

The proposed catalytic mechanistic scheme for the “pita-bread” enzymes is presented in Figure 2.2-3 with *e*MetAP as the model. The carbonyl and amine groups of the peptide bond in

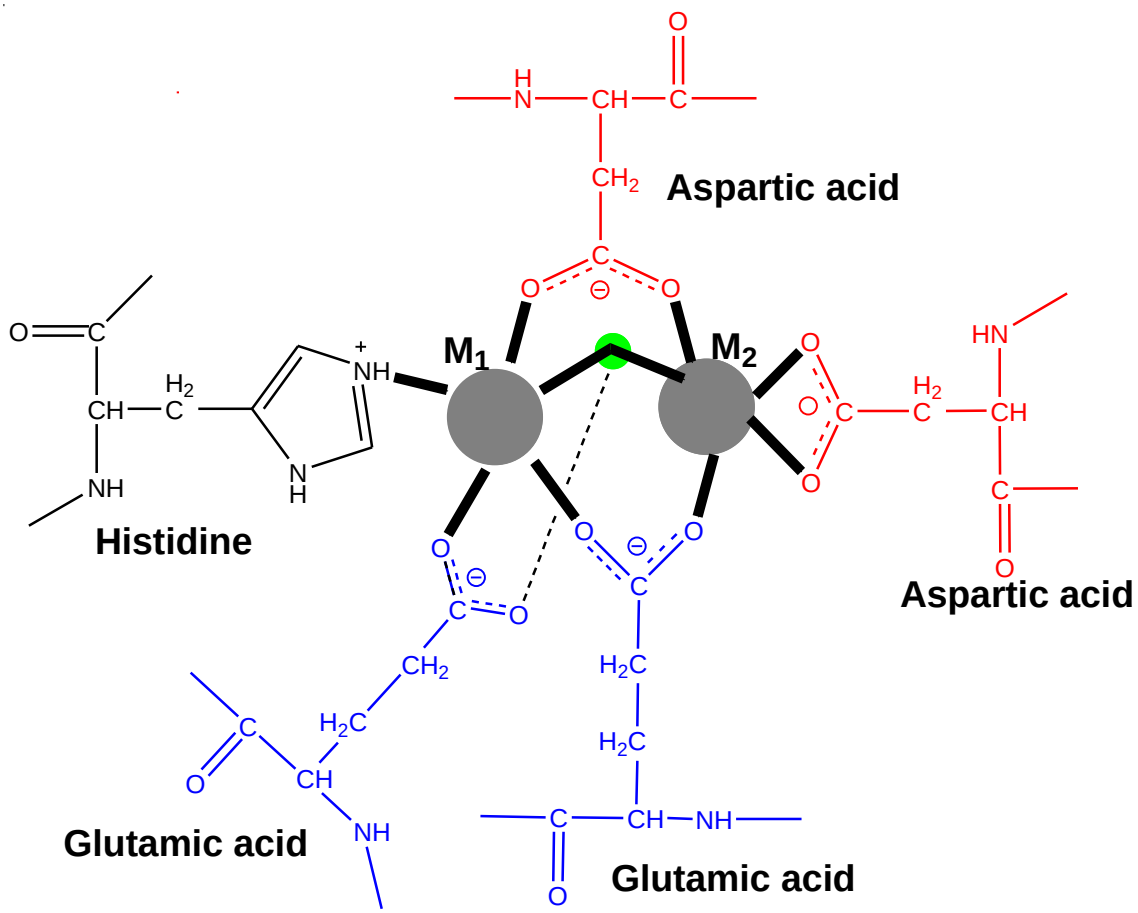

Figure 2.2-2 Schematic diagram of the conserved metal centre possessed by "pita-bread" enzymes.
The two metal ions are shown in gray and labelled as M_1 and M_2. A water molecule bridging two metal ions is coloured green. Five coordinated amino acid residues are shown as labelled. Existing interactions are shown in bold.

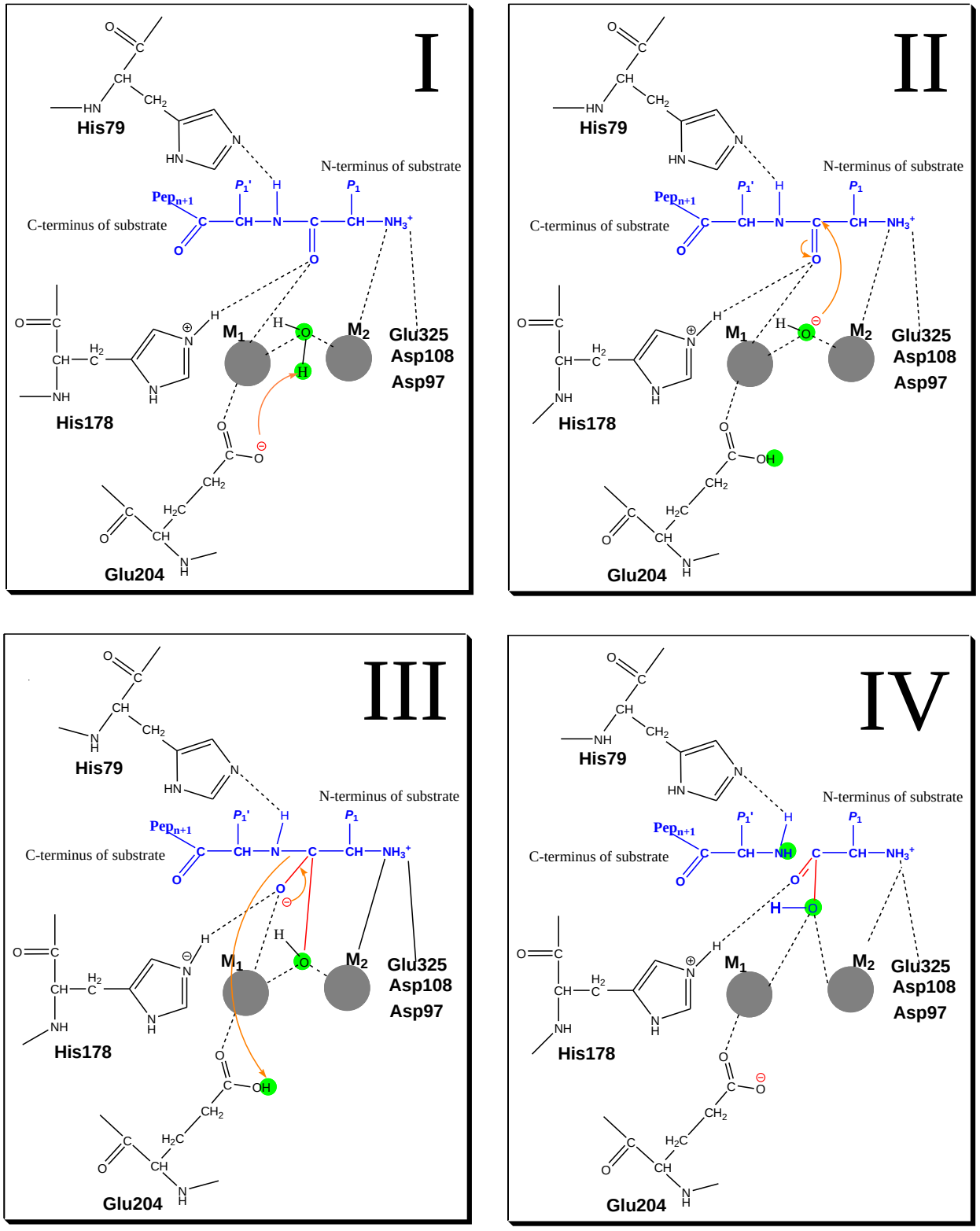

Figure 2.2-3 Schematic view of a proposed catalytic mechanism of a "pita-bread" enzyme, *e*MetAP.

Substrate-peptide is shown in blue. The changes during catalysis are shown in red and orange. Intermediate I: Deprotonated Glu^{204} activates a metal-bound water molecule by accepting a proton; Intermediate II: Resultant metal-bound hydroxyl group attacks the carbonyl carbon of the target peptide bond. Intermediate III: M_1 and His^{178} stabilize the tetrahedral intermediate; When the electron bounces back to form the C=O double bond, the peptide bond breaks and Glu^{204} donates a proton to amine of the leaving group. Intermediate IV: Products are generated and Glu^{204} becomes its original state to perform the next reaction.

substrate are stabilized by M_1 (metal 1), His^{178} and His^{79}. Deprotonated Glu^{204} facilitates the activation of the metal-bound water molecule to become a nucleophilic hydroxide ion (Intermediate I). The activated metal-bound hydroxide ion attacks the carbonyl carbon of peptide bond and an electron of C=O is pushed up to carbonyl oxygen (Intermediate II). When the electron bounces back to re-form C=O, the peptide bond (N-C) is cleaved. Products are generated when Glu^{204} donates a proton to the amine of the cleaved peptide bond (Intermediate III). Two interactions to M_1 and one to His^{178} stabilize the tetrahedral intermediate III during this stage. The resulting product complex (IV) maintains interactions with M_1 and His^{178} (Lowther and Matthews, 2000).

In the case of prolidase, the detailed catalytic reaction is not clear yet due to a lack of structural information in ligand-bound forms. However, because of highly conserved active site residues of "pita-bread" enzymes, prolidase shall share similar catalytic mechanism to other members of "pita-bread"enzymes. When the P_1 (Xaa) and P_1' residues (Pro) are docked in S_1 and S_1' substrate binding sites, respectively, the metal bound water or hydroxyl ion (shown in Figure 2.2-3) can attack the peptide bond of Xaa-Pro. In this process, His^{296} in *Lla*prol (Hu and Tanaka, 2009) or His^{284} in *Pf*prol (Maher et al, 2004) is involved as a proton receptor in the catalytic reaction. Details of the mechanism of prolidase will be further introduced in section 2.4.

2.2.2 Substrate Specificity

Prolidase is found in a wide variety of prokaryotes and eukaryotes. Although physiological functions of prolidase are not clear, this enzyme may play an important role in the recycle of proline. Prolidases are characterized and purified from porcine (Davis and Smith, 1957; Manao et al., 1972; Sjostrom et al., 1973), bovine (Yoshimoto et al., 1983), *Streptococcus cremoris*

(Kaminogawa et al., 1984), human (Myara et al., 1994), *Xanthomonas maltophilia* (Suga et al., 1995), *Aureobacterium esteraromaticum* (Fujii et al., 1996), *Lactobacillus casei* (Fernandez-Espla et al., 1997), *Lactobacillus delbrueckii* (Morel et al., 1999; Rantanen and Palva, 1997), and *Suberites domuncula* (Wiens et al., 1999). Recombinant forms of prolidase expressed in *Escherichia coli* (*E. coli*) are obtained from *Lactobacillus delbrueckii* (Stucky et al., 1995), *Pyrococcus furiosus* (Ghosh et al., 1998), and *Lactococcus lactis* (Yang and Tanaka, 2008). Human prolidase is expressed in Chinese hamster ovary (CHO) cells and *Escherichia coli* (Lupi et al., 2006). Substrate preferences of some prolidases were reported. Prolidases are able to hydrolyze Xaa-Pro dipeptides but they have a preferential activity on Xaa-Pro dipeptides that have hydrophobic amino acid residue at the N-terminal. *Lactobacillus delbrueckii* prolidase is able to hydrolyze Ala-Pro, Ile-Pro, Leu-Pro, Val-Pro, His-Pro, Phe-Pro, Tyr-Pro, and Met-Pro, but it shows no activity to Gly-Pro and Pro-Pro (Morel et al., 1999). Prolidase from *Lactobacillus casei* subsp. *casei* IFPL 731 can hydrolyze Leu-Pro, Ile-Pro, Phe-Pro, Ala-Pro, Val-Pro, Ala-Ala and Ala-Phe (Fernandez-Espla et al., 1997). Both native and recombinant form of *Pyrococcus furiosus* prolidase (*Pf*prol) show activities on Xaa-Pro, such as Met-Pro, Leu-Pro, Val-Pro, Phe-Pro, Ala-Pro, and Lys-Pro, except Gly-Pro (Ghosh et al., 1998). Park et al. (2004) observed *Escherichia coli pep*Q prolidase shows activity on proline dipeptides with polar and nonpolar amino acid residues at the N-terminus, and they also reported *pep*Q prolidase can also hydrolyze nerve gas chemicals (phosphate esters such as soman) in much lower turnover numbers than for the dipeptides. *Lactococcus lactis* prolidase *(Lla*prol*)* prefers Leu-Pro, Val-Pro, and Phe-Pro as its substrates and has considerable activities to Lys-Pro and Arg-Pro but activity toward Gly-Pro, Pro-Pro, Glu-Pro, Asp-Pro and tripeptides are not observed (Yang and Tanaka, 2008).

2.2.3 Metal Ion Selectivity

*Lla*prol can be activated with divalent Zn^{2+} and Mn^{2+} but not by other metal ions (Yang and Tanaka, 2008). *Pf*prol has natural metal activator Co^{2+}, which can be substituted by Mn^{2+} but not by Mg^{2+}, Ca^{2+}, Fe^{2+}, Zn^{2+}, Cu^{2+}, or Ni^{2+} (Maher et al., 2004). Meanwhile, chelating amino acid residues are conserved among pita-bread enzymes, including prolidases. It raises a question why the natural selection of metal ions to activate these two prolidases is different, despite the conserved metal ion binding residues.

Metal ions of metalloenzymes participate in catalysis either by acting as Lewis acid catalyst or by altering their oxidation states (Suh, 1992). The metal ions discussed in this thesis act as Lewis acid catalyst. Several parameters of ion properties (Table 2.2-1) should be taken into consideration on the specificity and selectivity of metal ions in enzyme systems. As demonstrated in Table 2.2-1, divalent Zn^{2+}, Mn^{2+} and Co^{2+} share very similar properties in term of ionic radius, coordination numbers, geometries and ionization potential (Ip). This implies the reason why these metal ions are observed in the catalytic centres of prolidases. However, it is still unclear whether the metal ions used *in vivo* are inherent to the individual enzymes or are determined by surrounding environment of ions within the organism.

2.3 Unique Properties of *Lla*prol

Yang and Tanaka (2008) observed *Lla*prol possesses unique properties, allosteric behaviour and substrate inhibition, as shown in Figure 2.3-1, which are not reported in other prolidases. These properties may limit further applications of *Lla*prol in industrial and medical practices. To manipulate these behaviours toward target applications via protein engineering, it is necessary to understand the underlying mechanisms of these behaviours at an atomic level.

Table 2.2-1 Relevant properties of metal ions discussed in the thesis.

Metal	Common oxidation states	Electronic configuration	Ionic radius	Common coordination numbers	Common coordination geometries	Hardness	Preferred donor	Redox	Ip (eV)
Zn	+2	[Ar]3d^{10}	0.74	4	Tetrahedral	Borderline	N, S, O	No	17.96
				5	Square pyramidal/ Trigonal bipyramidal				
				6	Octahedral				
Mn	+2	[Ar]3d^5	0.83	4	Tetrahedral	Borderline	N, S, O	Yes	15.64
				5	Trigonal bipyramidal				
				6	Octahedral				
	+3	[Ar]3d^4	0.65	5	Square pyramidal/ Trigonal bipyramidal	Hard	O		33.66
				6	Octahedral				
Co	+2	[Ar]3d^7	0.75	4	Tetrahedral	Borderline	N, S, O	Yes	17.06
				5	Square pyramidal/ Trigonal bipyramidal				
				6	Octahedral				
	+3	[Ar]3d^6	0.61	6	Octahedral	Hard	N, O	Yes	33.5

Note: Ionic radii all refer to six-coordinated, high-spin (when low spin is possible) ions as tabulated in (Shannon, 1976). Coordination numbers and geometries are taken from (Holm et al., 1996). Other properties are taken from (Silva and Williams, 2001). I_P is the ionization potential of M to M^{n+}, and is the same as the electron affinity for the reverse reaction from M^{n+} to M, and is taken as a measure of the Lewis acid strength of the M^{n+} ion.

2.3.1 Allosteric Behaviour

Allostery of enzyme is a behaviour whereby enzyme activity is suppressed at low substrate concentrations. Kinetically, the [*S*]-v plot of an allosteric enzyme shows a sigmoidal curve as shown in Figure 2.3-1, rather than a hyperbolic curve. Hill constant (*h*) is used to determine whether an enzyme is allosteric or not. The value of Hill constant defines the cooperativity of ligand binding as follows. If h=1, then this enzyme does not have allosteric behaviour, in which case the affinity of the enzyme for its substrate is not dependant on the binding of other ligand molecules. If h>1, then this enzyme has allosteric behaviour and shows a positively-cooperative reaction, in which case the affinity of enzyme for its substrate increases once a ligand molecule binds to the enzyme. In allosteric regulation, the binding of ligands at one substrate subsite (effector site) induces a conformational change of the active site, thus activate the enzyme.

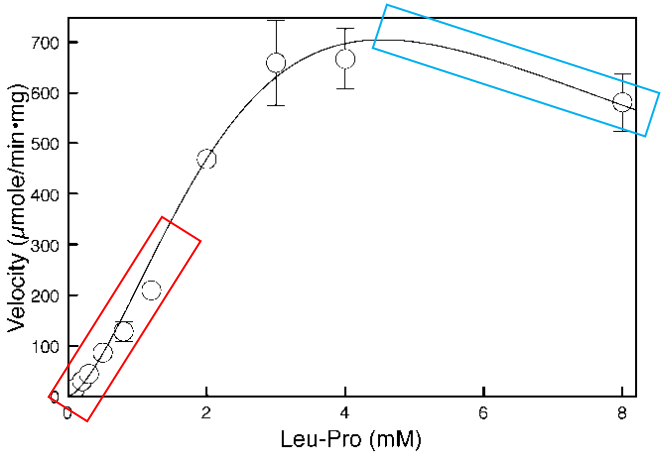

Figure 2.3-1 [*S*]-*v* plot of wild type *Lactococcus lactis* prolidase
The region coloured in red represents the allosteric behaviour that the velocity of the enzyme is suppressed at low substrate concentrations; the region coloured in light blue represents the substrate inhibition where the velocity of the enzyme is decreased at high substrate concentrations (reproduced from Yang and Tanaka, 2008).

Despite the importance of allosteric regulation in metabolism and gene regulation (Monod et al., 1963), the understanding of the structural and energetic basis of allostery has been elusive. For the past 40 years, allostery has been generally explained through either of two classic models: Monod-Wyman-Changeux (MWC) concerted model (also known as population shift model) (Monod et al., 1965) and Koshland-Nemethy-Filmer (KNF) sequential model, i.e., induced fit model (Koshland et al., 1966). In MWC model, the allosteric protein is usually composed of at least two subunits and exists in two conformational states, tense (T) and relaxed (R), and the population ratio of these two states shifts upon ligand bindings. In other words, when allosteric proteins bind to ligands (effectors), a greater population of the proteins shift from the T to R state and allow substrates bind for catalysis. In contrast to the MWC model, the assumptions of the KNF model include that the protein exists in one conformation solely prior to binding of the allosteric effector; upon binding, the ligand induces a conformational change in the subunit to which it is bound. This change may be transmitted to neighbouring vacant subunits at subunit interfaces. For example, if one protein is composed of 100 molecules, in MWC model, before substrate binding, there are 50 molecules in each R and T conformation states, and they are in equilibrium. Upon binding to an effector, the equilibrium is broken and a new balance will be achieved under the new situation that more molecules stay in R state. After catalysis, the enzyme will recover the previous equilibrium. In contrast, in the KNF model, before binding of effectors, all the 100 molecules are in the T state. Upon binding to an effector, all the molecules assume the R conformational states.

Due to the fast rate of conformational changes in proteins, experiments which discriminate between the induced-fit model and the population-shift model are hard to establish. Volkman et al. (2001) provided a direct experiment evidence for the population-shift mechanism (MWC

model) in a phophorylation regulated signalling protein via NMR relaxation experiments. In addition, this study also suggested that the population of active conformers in nitrogen regulatory protein C ($NtrC^r$) is formed by microsecond time-scale motions.

Mechanisms of many allosteric enzymes were widely studied using high-resolution structural analyses (such as X-ray crystallography) of their various liganded forms. Phosphodiesterase 2A (PDE 2A) is a homodimeric allosteric enzyme as shown in Figure 2.3-2-A and it is an example of the allosteric activation adapting induced fit model. PDE 2A cycles between open (R state) and closed conformations (T state), and H-loop is favoured to occlude the substrate binding site to closed conformation (T state). When the effector-cGMP is present in the enzyme solution, it binds to GAF-B domain, particularly α4, β2 and β3, of PDE 2A (Figure 2.3-2-B). The binding of cGMP to the GAF-B domain leads to the reorientation of a helix (LH2), which is the linker between the GAF-B and catalytic domains. In turn, this rearrangement disrupts the dimmer interface and the H loop is free to swing out to expose the substrate-binding site (Figure 2.3-2-C, D). Functionally, this is observed as an enzyme activation of PDE 2A (Pandit et al., 2009).

The above-mentioned theories are constructed on structural changes to activate the allosteric enzymes. More recent evidences showed that allostery can be mediated solely by protein thermal motions, without the involvement of evident structural changes. Popovych et al. (2006) and Tzeng and Kalodimos (2009) provided direct experiments to support this theory. Catabolite activator protein (CAP) is an allosteric protein and is allosterically mediated by cAMP for DNA binding. cAMP switches CAP from ‘off’ state (inactive) to ‘on’ state (active). The binding of cAMP to a mutant CAP-S62F fails to increase the active conformation yet

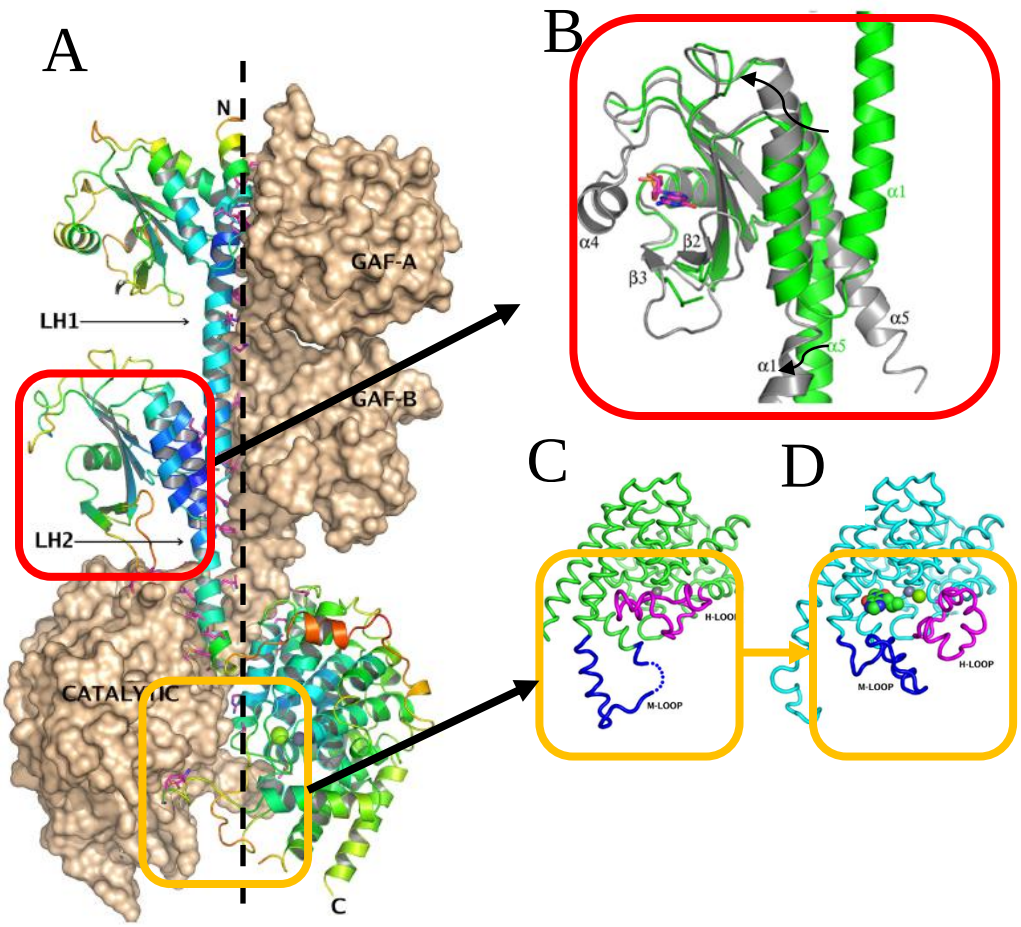

Figure 2.3-2 Schematic view of the structure of Phosphodiesterase 2A.
Panel A: An overall structure of human PDE 2A (residue 215 to 900). Two molecules, A and B are shown in a noncrystallographic 2-fold axis of symmetry, which is shown as a black dashed line. The dimer interface extends over the surface of the entire molecule. Molecule B is shown in surface representation and molecule A is shown in a ribbons representation, with the ribbons coloured by crystallographic B-factor, blue being low and red being high. Three domains (regulatory GAF-A and GAF-B and catalytic domains) are labelled, as well as the linker helices LH1 and LH2 that connect them. The effector binding pocket is shown in red frame and the two catalytic sites occluding each other in the vicinity of the Zn^{2+} and Mg^{2+} ions (shown as gray and green spheres) are located in the orange frame. Panel B: Comparison between the Apo GAF-B domain of human PDE 2A (green) and the cGMP-bound GAF-B domain of mouse PDE 2A (PDB code: 1MCO. grey). The orientations of α_1 and α_5 in Apo form (human) have significant differences from those of effector bound form (mouse). The two helices that define the N and C termini of this domain are rotated by nearly 180^{o} and 30^{o}, respectively, between human and mouse PDE 2A. Panel C: Structure of the unliganded catalytic domain that shows the H-loop folded into the catalytic site and displacing the Mg^{2+} ion. The Zn^{2+} ion is shown as a gray sphere. Panel D: Structure of the catalytic domain co-crystallized with 3-isobutyl-1-methylxanthine (IBMX), showing the H-loop swung out. Zn^{2+} and Mg^{2+} ions are shown as gray and green spheres, respectively. The pictures are adapted with modifications from Pandit et al. (2009)

strongly activates the protein for DNA binding. By comparing the WT CAP and CAP-S62F mutant, they found that the allosteric activation is solely driven by changes in protein motions, which is dominated by conformational entropy. cAMP is able to bind CAP in an active conformation that DNA binding domain (DBD) structurally poises to interact with DNA (Figure 2.3-3-A), whereas cAMP binding to CAP-S62F stabilizes only small populations of active conformations (2 % of the whole populations; Figure 2.3-3-B), failing to elicit the active conformation. However, DNAs can bind to these marginally active DBDs in CAP-S62F-cAMP, and shift inactive conformations into active ones, which are solely driven by the conformational entropy (Tzeng and Kalodimos, 2009).

Allosteric proteins control fundamental biological processes, and malfunction of allosteric proteins can cause metabolic and genetic diseases. However, the biochemical process occurred during allosteric behaviour is still not well understood. Since the allosteric behaviour of industrial enzymes can be interpreted as low efficiency, its modification may be required to quest high efficiency. Understanding the molecular mechanism of allosteric behaviour is significant for guiding the modifications of allosteric enzymes.

2.4 Three-Dimensional Structures of Prolidase

To date, eight three-dimensional structures of prolidases are deposited in the Protein Data Bank (PDB). Three of them are from *Pyrococcus horikoshii* (PDB: 1WY2, 1WN1, 2HOW), two of them are from human (PDB: 2IW2, 2OKN), two from unknown source (PDB: 3N2C, 3MKV), two from *Alteromonas sp.* (PDB: 3L7G, 3L24) and the other one from *Pyrococcus furiosus* (PDB: 1PV9). Through studies on the crystal structures of native *Pyrococcus furiosus* prolidase (*Pf*prol) and its complex with inhibitor (2S, 3R)-3-Amino-2-Hydroxy-5-methyl-hexanoyl-proline (AHMH-pro), Maher et al. (2004) elucidated the detailed structure of the active site and how

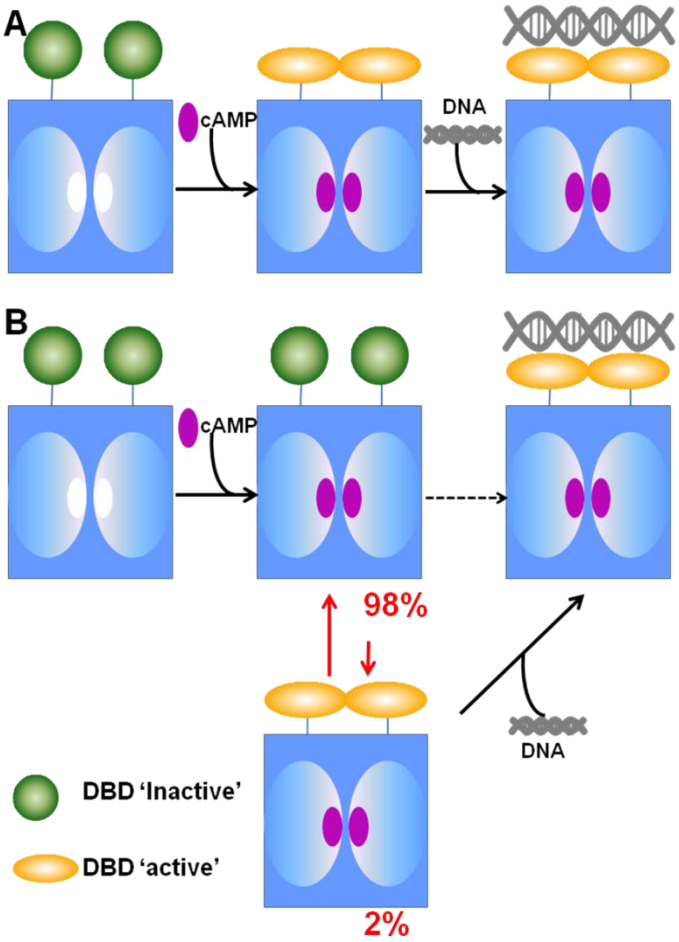

Figure 2.3-3 Model of allosteric regulation driven by entropy.
Panel A: Allosteric activation pathway of WT-CAP; cAMP binding to WT-CAP elicits the active conformation so that DBD becomes structurally poised to interact favourably with DNA. Complex formation is strongly enthalpically favoured and entropically unfavourable. Panel B: allosteric activation pathway of CAP-S62F; cAMP binding to CAP-S62F, active 2 % of the protein. DNA affinity is different between active and inactive conformations of CAP by many orders of magnitude. DNA will bind selectively to the sporadic, active DBD and shift the population from the inactive DBD to the active DBD conformation. DNA binding to CAP-S62F-cAMP2 is entirely driven by entropy, which is dominated by conformational entropy. The red arrows indicate the allosteric transition undergone by DBD. The pictures are reproduced from Tzeng and Kalodimos (2009)

*Pf*prol discriminates against oligopeptides and in favour of Xaa-Pro substrates. *Pf*prol is a homodimer with a subunit molecular mass of 39.4 kDa and its polypeptide fold of a subunit was shown in Figure 2.4-1-A. The subunit has two domains (domain I, residues 1-112; domain II, residues 124-348) and α-helical linker (residues 113-123). The active site is located in an oval depression on the inner surface of a curved β-sheet of domain II. In consistency with the active centre described above for metallopeptidase, in *Pf*prol, the dinuclear zinc atoms are bridged by Asp^{220}, Glu^{327} and a solvent water (W^{176}), as well as coordinate by the side chains of residues Asp^{209}, Glu^{313}, and His^{284}, as shown in Figure 2.4-1-B and in Figure 2.4-1-C (yellow colour). The P_1 binding site in *Pf*prol is formed by hydrophobic residues Phe^{178}, Ile^{181}, Ile^{290} and by Leu^{37} (red colour in Figure 2.4-1-C). The binding site for proline (P_1') is lined by His^{280}, Tyr^{317}, and Arg^{325} (blue colour in Figure 2.4-1-C). They also indicated that two polypeptide segments, which are two loops (residues 291-300 and residues 36-39) as shown in Figure 2.4-1-C, can fold down toward the active site. They argued that the proximity of these loops to the dinuclear metal site in *Pf*prol accounts for the preferences of the enzyme for dipeptide substrates (Maher et al., 2004).

*Lla*prol shares 61.9 % similarity with *Pf*prol at the amino acid level, as demonstrated in the alignment in Figure 2.4-2. Thus, Dr. Tanaka's research group constructed sequence-based computer model of *Lla*prol on the basis of *Pf*prol crystal structure (Yang and Tanaka, 2008). To clarify the unique properties possessed by *Lla*prol, such as substrate specificity, and allosteric behaviour, Zhang et al. (2009) examined the importance of Arg^{293}, His^{303}, and Ser^{307} through the studies on their mutants, and they indicated Arg^{293} besides the active centre (Figure 2.4-3) is an important residue contributing to the allosteric behaviour and substrate inhibition of *Lla*prol. Hu and Tanaka (2009) further tested the roles of Phe^{190}, Leu^{193}, and Val^{302}, which are corresponding

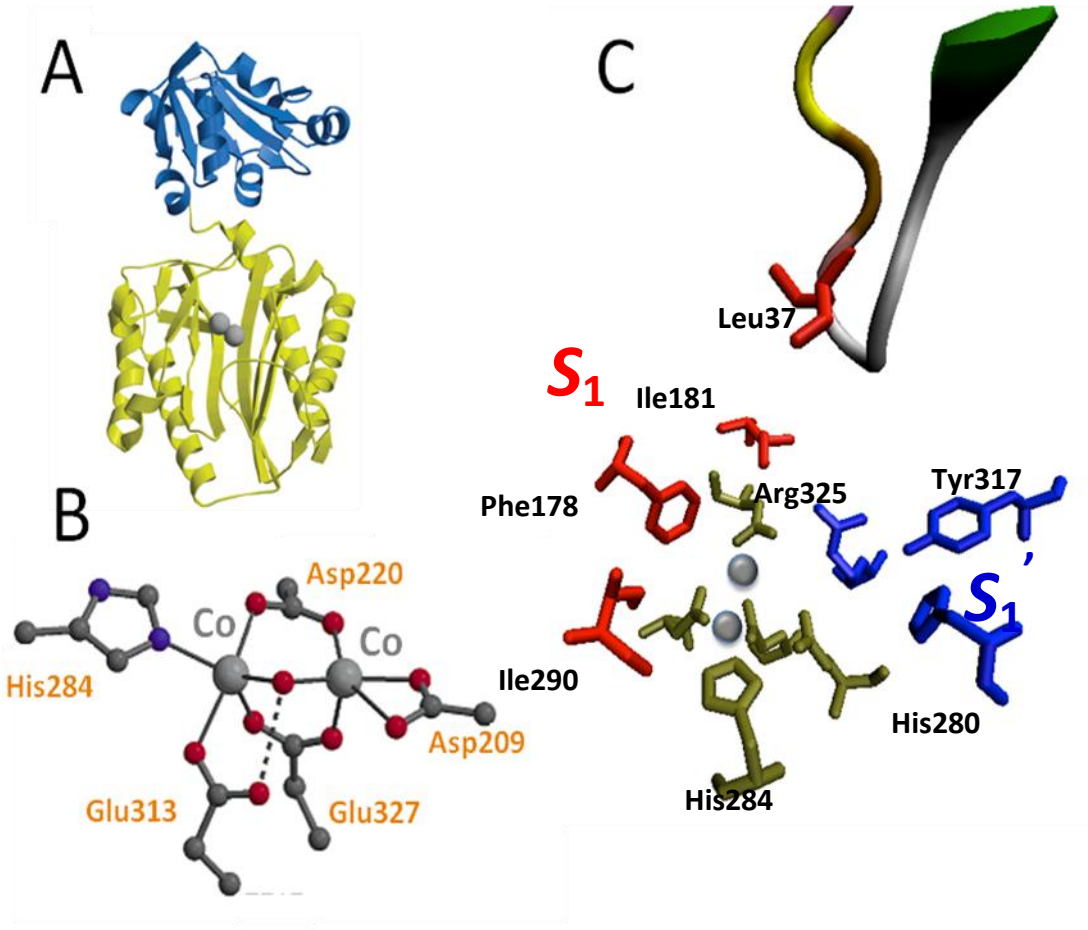

Figure 2.4-1 Models of important residues in *Pf*prol.
Panel A: The structure of a monomer of *Pf*prol. Ribbon drawing highlighting the domain structure; N-terminal domain is in blue and the C-terminal domain is yellow. The Zn atoms are shown as gray spheres. Panel B: the active centre of *Pf*prol; Metal atoms in *Pf*prol are cobalt. The positions of coordinated amino acid residues are labelled. Panel C: Active site residues are coloured gold yellow and the metal ions are coloured gray sphere; besides the active centres, substrate binding sites S_1 and S_1' are coloured in red and blue. Above the active centre, a loop structure (position-33 to 40) is shown in a ribbon model.

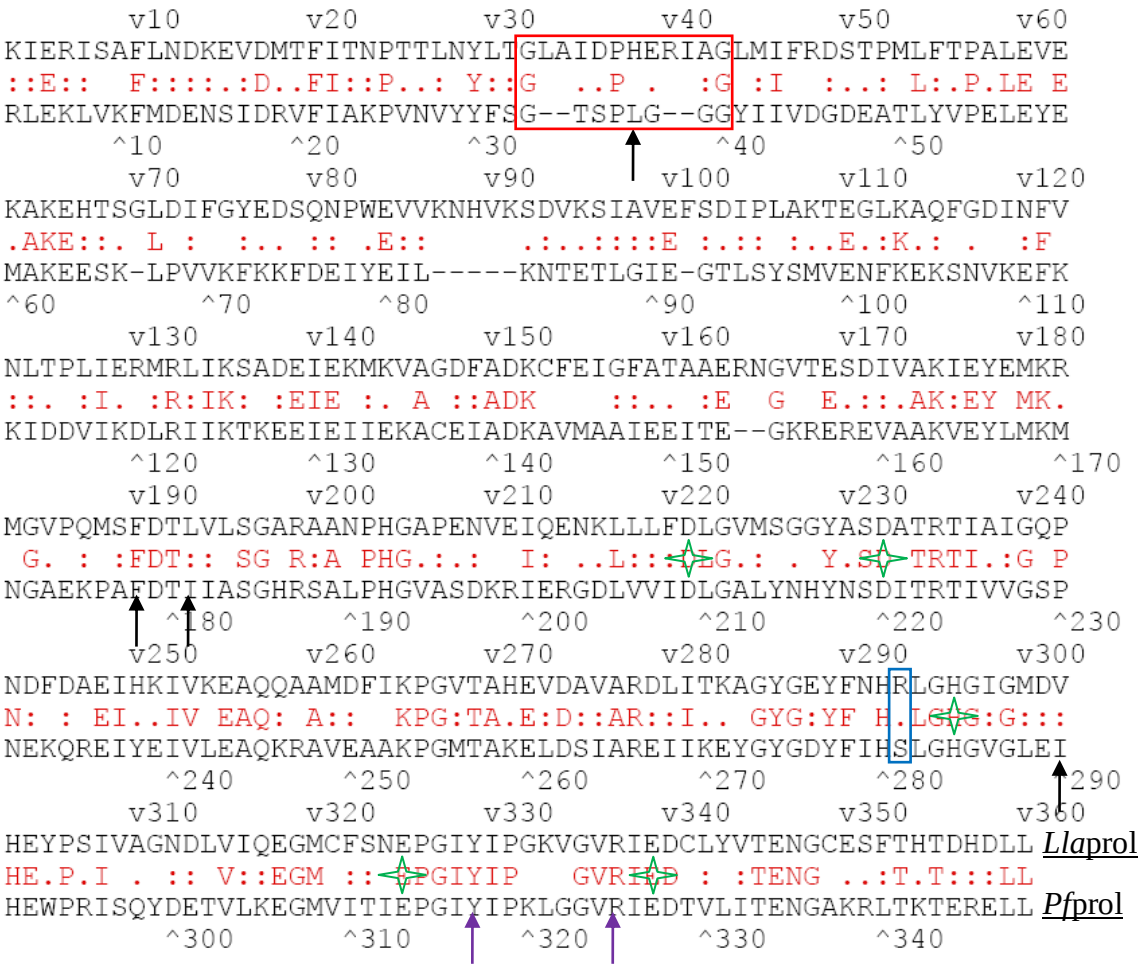

Figure 2.4-2 Alignment of the amino acid sequences of *Lla*prol and *Pf*prol.
The sequences showed in red colour are the consensus sequence between primary sequence of *Lla*prol and *Pf*prol. The red frame indicates the loop segments in both prolidases; the blue frame indicates the position 293 in *Lla*prol and the corresponding residue in *Pf*prol; the green stars represent the metal-chelating residues in both prolidases. Black and purple arrows indicate the S_1 site and S_1' site residues, respectively. The amino acid sequences were obtained from NCBI (GenBank accession code for *Lla*prol: EU216565; PDB accession code for *Pf*prol: 1pv9) and aligned using Clustal W (Thompson et al., 1994).

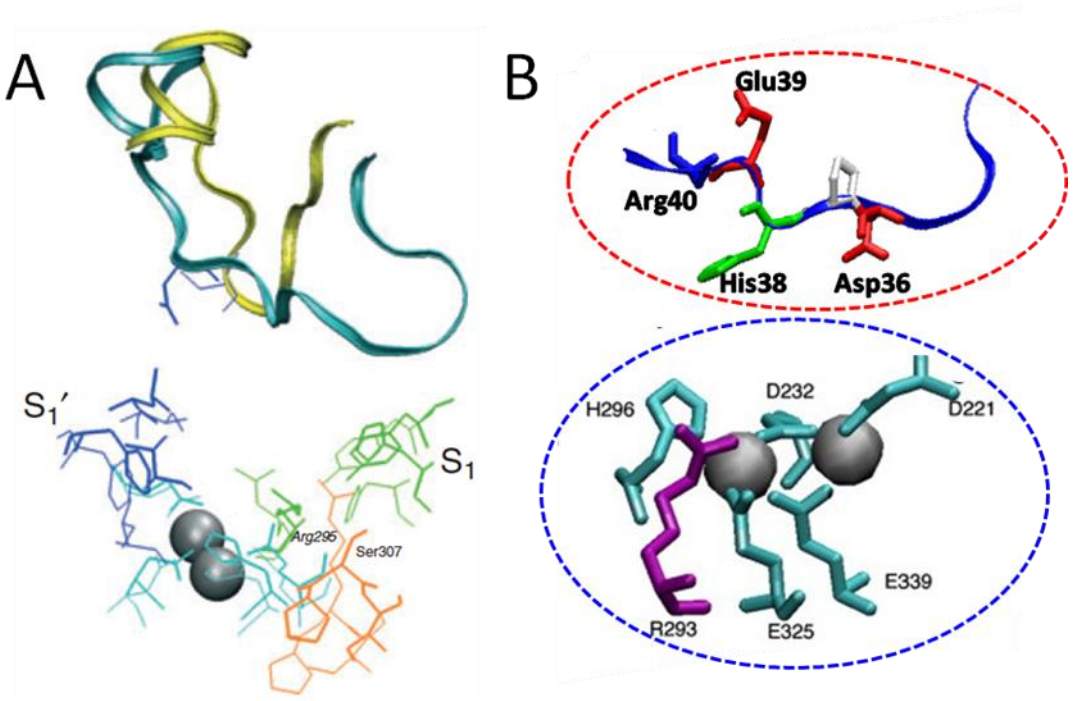

Figure 2.4-3 The loop structures and active sites in *Lla*prol and *Pf*prol.
Panel A: The active site is around two metal atoms (gray spheres). The thick and thin lines represent the *Lla*prol and *Pf*prol, respectively. S_1 and S_1' residues are coloured blue (Phe[190], Leu[193] and Val[302]) and green (His[292], Tyr[329], and Arg[337]), respectively. Chelating residues are shown in cyan. Substrate size-limiting residues (Pro[306], Ser[307] and lle[308]) are shown in orange. Above the active sites, loop structures of *Pf*prol (yellow) and *Lla*prol (cyan) are shown. The Panel B: A computer model of the active site and Loop[32-43] in *Lla*prol. Allosteric determing residue Arg[293] is coloured purple, chelating residues are illustrated in cyan, and the four charged residues on Loop[32-43] are labelled.

to Phe^{178}, Ile^{181}, and Ile^{290}, in the S_1 site of *Pf*prol. Results from this study demonstrated Leu^{193} and Val^{302} contribute the hydrophobic pocket of substrate binding site and they can interact with Arg^{293} to influence the allostery. Besides, they also suggested His^{296} corresponding to His^{284} in *Pf*prol is the proton acceptor in the catalysis, which participate in the catalytic process as mentioned in section 2.2.1. Protonated His^{296} stabilizes the intermediate stage when the metal bound hydroxide attacked the peptide bond of substrates.

These two reports about *Lla*prol also indicated that a Loop$^{32\text{-}43}$ structure near the active site would contribute to the unique characteristics, i.e., allosteric behaviour and substrate inhibition. They also illustrated that a notable difference in the active sites between *Lla*prol and *Pf*prol is the length of the loop structure that is contributed by the other subunit and cover the S_1 site (as shown in Figure 2.4-3-A). The longer loop in *Lla*prol is due to four charged residues (Asp^{36}, His^{38}, Glu^{39} and Arg^{40}), which are located in the middle of Loop$^{32\text{-}43}$ (as shown in Figure 2.4-3-B).

2.5 Loop Structure–Function Relationships

α-helices, β-sheets and reverse turns are three common known secondary structures. α-helices and β-sheets are termed as regular structures whereas reverse turns are considered as non-regular structures. In 1986, another type of non-regular secondary structures of protein was categorized as the protein loop. The protein loop, defined as a segment of contiguous polypeptide chain that traces a "loop-shaped" path in the three-dimensional space, is proposed to be a novel category of non-regular secondary structure (Leszczynski and Rose, 1986). Since then, loop structures have been emerging as functionally important components in proteins. These functional loops are observed in a wide range of enzymes such as aspartic proteinases,

glutathione synthetase, tryptophan synthase, adenylate kinase, lactate dehydrogenase, and ribulose-1,5-bisphosphate carboxylase.

In aspartic proteinase, a loop commonly known as a "flap" is found to extend over the active site and is implicated in the catalytic process (Kempner, 1993; Sielecki et al., 1990). This flap opens to allow substrate access to the active site cleft, closes on substrate bindings and opens again to allow products to leave. Aguilar et al. (1997) found that, in *Saccharomyces cerevisiae* proteinase A crystal structure, a loop$^{72\text{-}81}$ extends over the active site that has been implicated in catalysis. Li et al. (2000) reported this loop region of *Saccharomyces cerevisiae* proteinase A is the most flexible portion. The largest conformational change observed among different structures of this enzyme is up to 8.7 Å. Moreover, polypeptide residues ~Tyr-Gly-X-Gly~ on this loop are highly conserved among aspartic proteinases from different sources. In pepsin, a corresponding Loop$^{71\text{-}80}$ with Tyr^{75}-Gly^{76}-Thr^{77}-Gly^{78}-Ser^{79} at its tip, locates near the active site and changes its position upon substrate binding. Tyr^{75} participates in substrate alignment and anchors the flap in pepsin (Tanaka et al., 1998). Thr^{77} is responsible for forming hydrogen bonds with substrates and for constructing a proper geometry in a transition state during the catalysis (Okoniewska et al., 1999). Gly^{76} and Gly^{78} act as the hinges of the flap to enable Thr^{77} at the tip of the flap to form hydrogen bonds with active site residues (Okoniewska et al., 2000).

A flexible loop (Ile^{226}-Gly^{242}) in *Escherichia coli* B glutathione synthetase stabilizes the acylphosphate intermediate by preventing its decomposition with water (Tanaka et al., 1992; 1993). They hypothesized that the flexible loop extends over the bound substrates in the active site, moving from an “open” position in the unliganded enzyme into a “closed” position when substrates bind to the active site of the enzyme. Subsequently, Kato et al. (1994) constructed and crystallized a loopless mutant to investigate the function of the loop in the *Escherichia coli*

enzyme. They found the crystal structure of the loopless mutant is similar to that of the wild type while the activity of the loopless mutant is $3x10^4$ less than that of the wild-type enzyme. These studies elucidated that the loop has a hyperfunction that is not only a stabilization of the transition states and/or the intermediate of the reaction but also the coupling of ATP hydrolysis with glutathione synthesis through the recognition of the substrates.

Recently, Christen et al. (2008) proposed that residue Ser^{170}, located on a β2–α2 loop in mouse prion protein, has a marked impact on the conformational properties. Hu et al. (2008) speculated that an active site loop of diaminopimelate decarboxylase from *Helicobacter pylori* cycles through down- and up-conformations to stabilize catalytic intermediates and releases reaction products, respectively. These studies demonstrated essential roles of the loop structure play in the process of the enzymatic catalysis.

2.6 Protein X-ray Crystallization

In the late 1950's, Kendrew et al. (1958) solved a crystal structure of sperm whale myoglobin, for which Max Perutz and Sir John Cowdery Kendrew were awarded the Nobel Prize in chemistry in 1962. Since then, up to July 8, 2010, more than 57,402 crystal structures of proteins, nucleic acids and other biological molecules were determined by using X-ray crystallography, while 8,482 structures were solved using NMR, which is normally applied to relatively small proteins with less than 300 amino acid residues (Smialowski et al., 2006). X-ray diffraction methods have provided experimental basis of our present knowledge of protein structures, and they also have been proven as one of the most convincing approaches in investigations of enzyme mechanism.

X-ray is electromagnetic waves that have a wavelength of between 10^{-7} and 10^{-10} m. X-ray waves are scattered when they hit electrons of atoms. It is similar to the way that light waves are

scattered by the engraved lines of a diffraction grate. The regular lattice of a crystal acts like a three-dimensional diffraction grate in scattering a monochromatic beam of X-rays.

A protein crystal has many unit cells with three-dimensionally ordered repeats. Each cell is composed of more than 100,000 electrons. The electron distribution in each cell can be considered as 'electron clouds' localized at the atoms of protein molecules. As shown in Figure 2.6-1-A, when X-ray interacts with electron clouds in a protein crystal, the electric components of the X-ray exert a force on the electrons. This causes the electrons to oscillate with the same frequency as the incident X-ray. The oscillating electrons emit radiations with the same frequency as the incident radiation. The scattered waves interact with each other creating a diffraction pattern (Figure 2.6-1-B). The distribution of diffraction spots reflects the geometry of the unit cell, when relative intensities of the diffracted spots are used in the Fourier transformation to obtain electron density into which a model of the molecule is fitted. However to elucidate the electron density, we need to identify phases of all diffraction spots. One of these known methods of obtaining phases is molecular replacement (MR), letting a model of known molecule to fit into the unit cell of an unknown structure. Afterwards, the electron-density map based on this initial phases is interpreted to produce an atomic model of the molecule via a function as shown in Figure 2.6-1-B. In this way, the three-dimensional structure (the coordination of the atoms in the space) of unknown molecular can be interpreted.

The accuracy of obtained structures depends on both the quality of protein crystals and the resolution of their diffraction. Since a resulting electron density map is an average of all the molecules within the protein crystal, the uniformity of unit cells in the crystal influences the accuracy of the final model. In addition, how far between the atoms in molecules can be

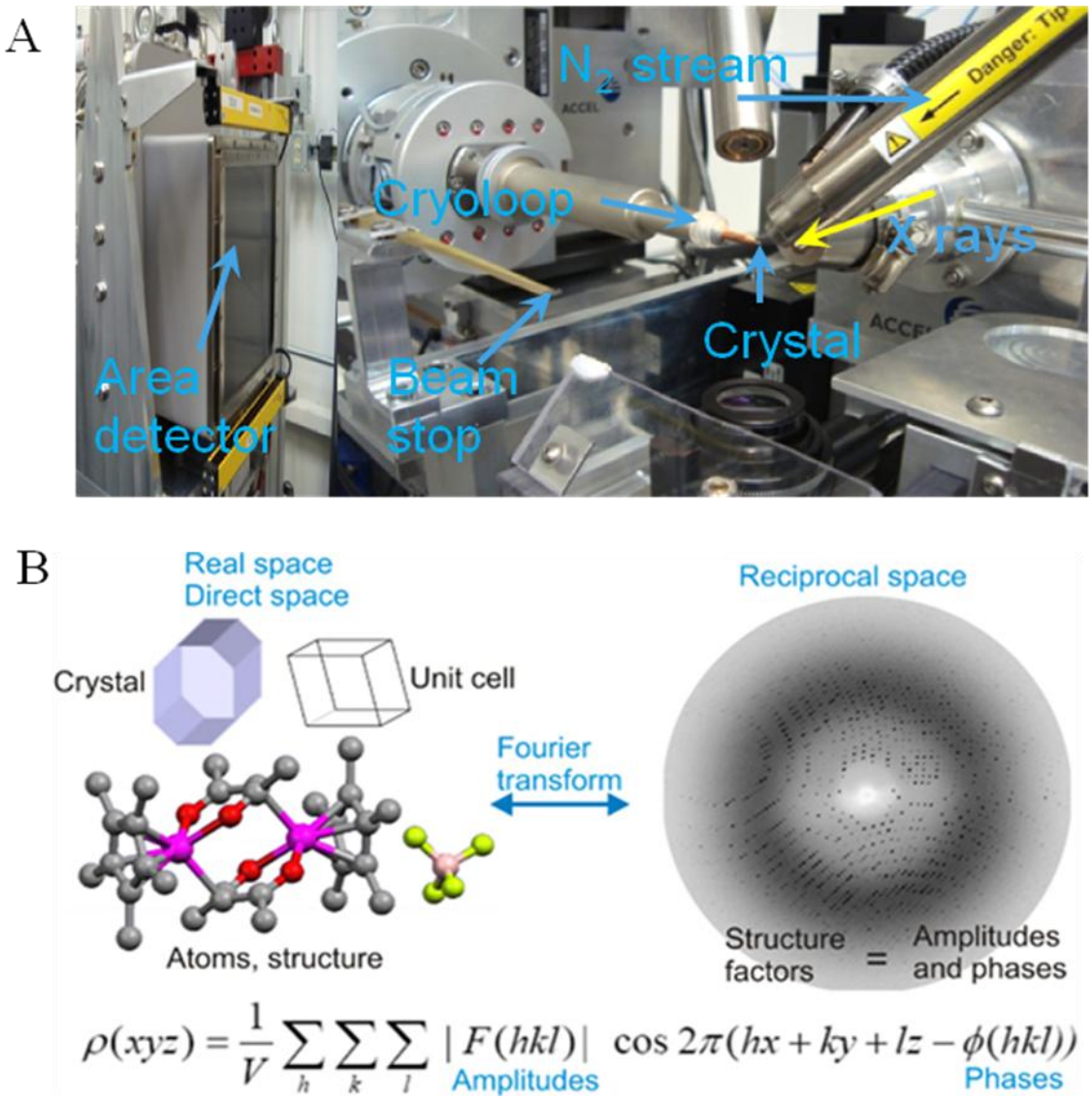

Figure 2.6-1 Schematic view of the process of protein X-ray diffraction
A: The photography presents a diffractometer, an equipment to collect protein X-ray diffraction, at Canadian Light Source. X-ray beamline, beam stop, N_2 stream, area detector and the place where the protein crystal situated are indicated in the photo.
B: The diffraction spots showed on the area detector are used to obtain amplitudes and phases of the molecule via Fourier transformation. The inset function is used to calculate the electron density of a target molecule. In this function, V is the volume of the unit cell; $F(h,k,l)$ and $\phi(h,k,l)$ are the amplitudes and phases of the molecules, respectively. $\rho(x,y,z)$ is the electron density of the molecule. This picture is adapted from www.xtal.iqfr.csic.es/.

distinguished (defined as the resolution) is also important for accurate interpretation of the crystal structure. At a low resolution, 4 to 6 Å, the electron density map reveals just a little more than the overall shape of the molecule in most cases. At 3.5 Å, it is often possible to follow the polypeptide backbone, but there might be some ambiguous regions. At 3.0 Å, it is possible to begin to resolve the amino acid side chains, and with some uncertainty, to fit the sequence to the electron density. At 2.5 Å, the position of atoms may often be fitted with an accuracy of ±0.4 Å. In order to locate atoms within 0.2 Å accuracy, a resolution at 1.9 Å or less is necessary (Fersht, 1985).

To determine the three-dimensional structure of a protein using X-ray crystallography, the first requirement is obviously to grow crystals of good qualities. Crystallization is a complex and multi-parametric process, which produces high quality well-ordered crystals is a predominant bottleneck in the structure determination. The phase diagram in Figure 2.6-2 illustrates the crystallization process, which is associated with the states (liquid, crystalline, or precipitate) with several parameters. Chayen and Saridakis (2008) distinguished the diagram in four areas: an area of very high supersaturation, where the protein will precipitate; an area of moderate supersaturation, where the protein will nucleate spontaneously; an area of lower supersaturation below the nucleation zone, where crystals are stable and may grow (this area is thought to contain the best conditions for growth of larger, well-ordered crystals); and an understaturated area, where the protein will never crystallize. The choice of the method depends on the protein species. Crystallization phase diagrams (Figure 2.6-2) can be used to understand the design of experiments. Each method forces protein solution to reach the nucleation zone and then the metastable zone through different routes (dashed lines).

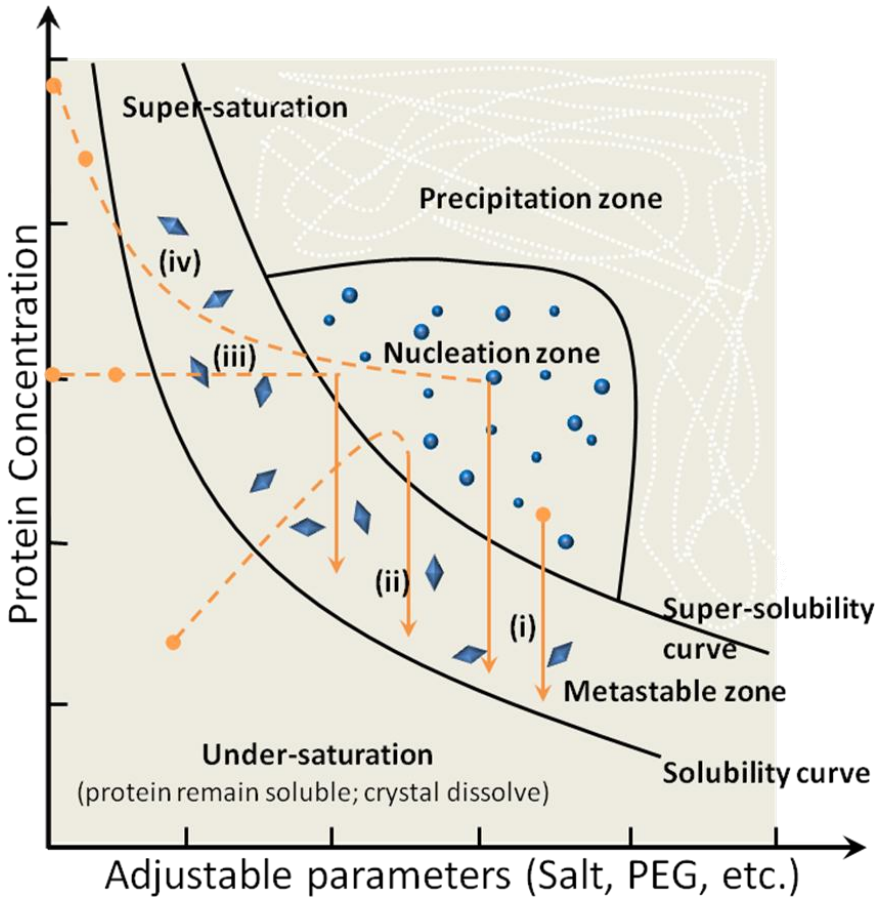

Figure 2.6-2 Schematic illustration of a protein crystallization phase diagram.
Adjustable parameters include precipitant or additive concentration, pH and temperature. The four major crystallization methods are represented: (i) microbatch method, (ii) vapour diffusion, (iii) dialysis and (iv) FID. Yellow dashes and arrows illustrate the crystallization process of each method. (adapted from Chayen and Saridakis (2008))

Several methods, such as vapour diffusion, microbatch, dialysis, free interface diffusion, and in-gel crystallization are available for making protein crystals. Each method has its advantages and disadvantages. The batch method achieves supersaturation immediately upon a mixing, whereas all the other diffusion-based methods gradually bring the protein solution from undersaturation to supersaturation by equilibration with a solution containing the crystallizing agents at target concentrations.

Vapour diffusion is a common method of crystallization. The protein solution is either a hanging or sitting drop that equilibrates in a closed container against the mother liquor which contains higher or lower concentrations of crystallizing agents than those in the drop. The conditions change gradually until the drop and the mother liquor reach equilibrium. Trials are normally conducted in 24-well plates, where each well holds a 0.5-1 mL reservoir solution and is sealed with a siliconized glass or plastic coverslip. The wells are fitted with a support for the sitting drop while hanging drops are hung from the coverslip. A concentrated pure protein at 5-15 mg/mL is usually employed. The advantage of this method is that this method provides a convenient way to adjust conditions precisely in a very small sample. The drawback of this method is the occurrence of skin formation on hanging drops during the diffusion process.

In dialysis methods, a semi-permeable membrane is employed to allow mixing the protein solution gradually, and the protein crystal is obtained from the protein solution, as shown in Figure 2.6-3-B. Typical procedures include the use of a dialysis bag, dialysis buttons or zepperzauer microdiffusion cells. In some cases, the burden of the gradient across the dialysis membrane can result in limiting the number of crystal nucleation sites and reducing the sizes of the protein crystals. Thomas and Pritchard (1987) employed a 'double-dialysis' procedure, which

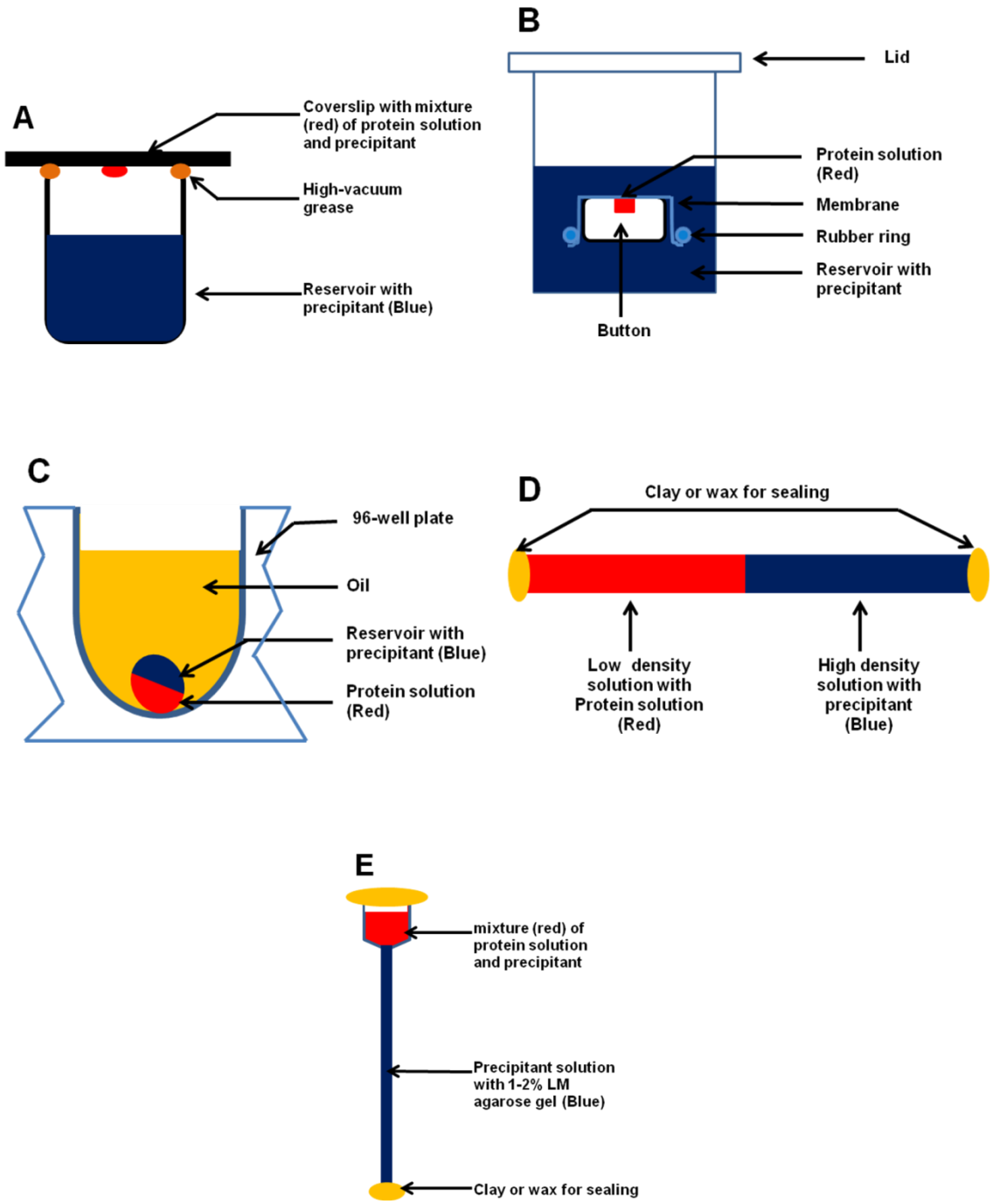

Figure 2.6-3 Schematic Illustrations of Different Crystallization Approaches.
A: Hanging drop vapour diffusion; B: Button dialysis; C: Microbatch; D: FID; E: In-gel crystallization. Protein solutions and screening solution are presented in red and blue, respectively. The materials used for sealing the crystallization condition are coloured yellow.

incorporates a second dialysis membrane to reduce the rate of equilibration in the crystallization experiment.

In microbatch experiments as shown in Figure 2.6-3-C, crystallization trials are dispensed and incubated under low-density paraffin oil. The microbatch method can be used for almost all known precipitants, buffers and additives, including detergents, glycerol and ethanol. It can not be used for crystallization trials containing small organic molecules such as phenol, dioxane or thymol because these molecules dissolve into the oil. Robots can dispense thousands of microbatch trials in small volumes. Depending on the type of oils used, this technique can be harnessed for screening, fine-tuning and optimization experiments. Robotic systems have been employed in obtaining protein crystals (Kelders et al., 1987; Perozzo et al., 1988). A large concern of this automatic procedure was the requirement of relatively large volumes of protein (at least 1-2 μL). Chayen (1990) reported a microbatch automatic system, which routinely dispenses 0.2-1 μL protein, with a final droplet volume of 2 μL.

Free interface diffusion (FID) is a process in which a low-density solution is layered onto a high-density solution. As shown in Figure 2.6-3-D, the two fluids are allowed to mix by direct contact and to reach equilibrium gradually. FID has not been widely used because it requires the use of capillary tubes. To conduct this experiment, 2 to 5 μL of protein sample was transferred into a microcapillary, then 2 to 5 μL of precipitant was slowly loaded into this microcapillary without introducing an air bubble, and the ends are sealed with the wax or clay for crystallization. The advantage of this method is that it requires less purified protein and it also generates protein crystals faster and more cost effectively (Yanicek, 2003).

In-gel crystallization is a crystallization method relying on the microgravity. In comparison of ground-based experiments, the protein crystals grown under microgravity conditions in the US

Space Shuttle Mission STS-95 were more ordered (Boggon et al., 1998). Lorber et al. (1999) observed that the crystals grown in gel on earth, mimicking the microgravity in the space, yielded better crystals obtained in solution. Biertumpfel et al. (2002) reviewed the technique of employing agarose gels in crystallization of biological macromolecules. Sauter et al. (2009) employed agarose gel crystallization and analog of substrates to solve the three-dimensinal structure of aspartyl-tRNA synthetase, which supports the application of gels in the protein crystallization. To perform this experiment, 1-2% agarose gel (low melting temperature) is mixed with screening solution in the ratio of 1:6. The mixed solution is sucked into a capillary and sits until its solidification. Five microliters of protein solution are added on the top of the solidified gel. Lastly, both ends of the capillary are sealed for crystallization (Figure 2.6-3-E).

3 HYPOTHESIS AND OBJECTIVES

The recombinant *Lactococcus lactis* prolidase (*Lla*prol), which is a 67-kDa homodimeric metalloenzyme with the isoelectric point (pI) of 4.6, shows interesting properties: allosteric behaviour and substrate inhibition (Yang and Tanaka, 2008). To elucidate the enzyme mechanisms, structure-function relationship studies on *Lla*prol were performed in previous studies (Hu and Tanaka, 2009; Zhang et al., 2009). Behaviours of allostery and substrate inhibition are not reported in other prolidases and these features are not fully elucidated in terms of their underpinning molecular mechanisms. Direct or indirect manipulations on Arg^{293} cause the loss of allosteric behaviour and substrate inhibition of *Lla*prol, which suggest that Arg^{293} located near the active site is a key residue to contribute these unique features of *Lla*prol (Zhang et al., 2009). From the molecular modelling study, $Loop^{32-43}$ of a subunit located above the active site of the other subunit was proposed to play an important role in the allosteric regulation of *Lla*prol (Yang and Tanaka, 2008). $Loop^{32-43}$ of *Lla*prol is longer than that of non-allosteric *Pyrococcus furiosus* prolidase (*Pf*prol) by four residues. Interestingly, this difference is observed as an addition of four charged residues: Asp^{36}, His^{38}, Glu^{39}, and Arg^{40} on this loop, whereas *Pf*prol does not have charged residues on the corresponding loop. These facts suggest that the $Loop^{32-43}$ can be stretched and its charged residues may offer distinctive properties observed in *Lla*prol.

The hypothesis of this study is that the charged residue(s) on $Loop^{32-43}$ contributes to the allosteric behaviour and substrate inhibition through interactions with Arg^{293} and/or other active site residues. This hypothesis was examined through the analysis of *Lla*prol mutants. Also, it will be necessary to know the actual three-dimensional structure of *Lla*prol in order to interpret

the results from this and future research. Thus a crystallographic study of *Lla*prol was also initiated.

The objectives of this project are as follows:

i) To elucidate the contributions of Loop$^{32\text{-}43}$ by means of a loopless mutant,

ii) To identify the roles of individual residues on the loop structure, and

iii) To crystallize *Lla*prol for X-ray crystallography.

4 MATERIALS AND METHODS

4.1 Materials

pUC18 and pKK223-3 vectors were used for construction and expression of the mutated *Lla*prol genes. *E. coli* TOP10F' (F'[*lac*I^{q} Tn10(*tet*^{R})] *mcr*A Δ(*mrr-hsd*RMS-*mcr*BC) φ80*lac*ZΔM15 Δ*lac*X74 *deo*R *nup*G *rec*A1 *ara*D139 Δ(*ara-leu*)7697 *gal*U *gal*K *rps*L(*Str*^{R}) *end*A1 λ^{-}) was used as the cloning and expression host in this project. These vectors and host were supplied from the lab collection of Dr. Tanaka's laboratory. All the oligonucleotides required in this research were synthesized at Integrated DNA Technology (IDT; Coralville, IA, USA). Restriction enzymes were purchased from Fermentus International (Burlington, ON, Canada). DNA *Pfu* polymerase, dNTPs and T4 DNA ligase were obtained from Invitrogen (Burlington, ON, Canada). Peptone and yeast extract were products of BD (Franklin Lakes, NJ, USA). ATP was obtained from EMD Chemicals (Darmstadt, Germany). IPTG was bought from Omega Bio-Tek (Norcross, GA, USA). Protein Assay Dye Reagent Concentrate was purchased from Bio-Rad (Hercules, CA, USA). Arg-Pro, Pro-Pro, Asp-Pro, Glu-Pro，Leu-Leu-Pro and Leu-Val-Pro were synthesized at GenScript (Piscataway, NJ, USA). Leu-Pro and Lys-Pro were purchased from Bachem (Torrance, CA, USA). Phe-Pro and Val-Pro were products of Sigma (Oakville, ON, Canada). Gly-Pro was obtained from Peptide Institute Inc. (Ibaraki, Osaka, Japan). All other common chemicals are at ACS-grade or better, and obtained from Sigma (Oakville, ON, Canada), EMD Chemicals (Darmstadt, Germany), Fisher Scientific (Ottawa, ON, Canada), and Alfa Aesar (Massachusetts, MA, USA).

4.2 Site-Directed Mutagenesis

E. coli TOP10F' harbouring the *Lla*prol gene on a pUC18 plasmid (pUC-*lac*Q) had been constructed in a previous study of Dr. Tanaka's laboratory (Yang and Tanaka, 2008). Modified Quik-Change site-directed mutagenesis (SDM; Braman et al., 1996) was employed to perform mutagenesis on the pUC-*lac*Q. This method synthesizes mutated DNA with a pair of mutation primers via PCR. pUC-*lac*Q plasmid DNA was purified with an alkalysis method (Birnboim and Doly, 1979) and used as the template DNA. Besides 50~100 ng template DNA, the reaction mixture of the PCR contained a pair of oligonucleotides (20 pmol each), 10 pmol of each dNTPs, and 0.5 units of *Pfu* DNA polymerase. The reaction mixture was incubated in a PCR machine with 16 cycles of 1 min-95 ℃/1 min-55 ℃/4 min-68 ℃ along with the 5 min denaturation at 95 ℃ prior to these cycles and a 10 min elongation period at 72 ℃ after the cycles. The primer pairs to construct each mutant are listed in Table 4.2-1. The PCR products were treated with 10 μL of chloroform, followed by an ethanol precipitation. The resultant DNA molecules were digested with the *Dpn* I restriction enzyme in order to degrade the template DNAs, and further transformed into *E. coli* TOP10F'. Transformants were spread on LB agar plates and incubated at 37 ℃ overnight. Colonies were picked up and their plasmid DNAs were digested with the restriction enzyme that recognizes the sequence incorporated with the oligonucleotides primers (as shown in Table 4.2-1) to identify positive clones for each mutants. The positive clones were further confirmed using DNA sequencing with M13 universal primers (shown in Table 4.2-1) at National Research Council-Plant Biotechnology Institute (Saskatoon, SK, Canada). A double mutant (D36E/R293K) was constructed by introducing R293K mutation on the confirmed D36E mutant gene. Following to the screening, positive clones were subcloned into an expression system. The mutated prolidase genes in the positive clones were PCR-amplified using two

Table 4.2-1 List of primers used in this study.

Primers	Sequences (5' to 3')	Restriction enzymes
Δ36–40	F: ACAGGGCTAGCAATTATTGCCGGCCTGATG R: CATCAGGCCGGCAATAATTGCTAGCCCTGT	*Pdi* I
D36S	F: CTAGCAATTTCTCCTCATGAACGAATTG R: CAATTCGTTCATGAGGAGAAATTGCTAG	*Pag* I
H38S	F: GCTAGCAATCGATCCCAGTGAACGAATTG R: CAATTCGTTCACTGGGATCGATTGCTAGC	*Cla* I
E39S	F: GATCCCCATTCGCGAATTGCTGG R: CCAGCAATTCGCGAATGGGGATC	*Nru* I
R40S	F: CCCCATGAATCGATTGCTGGG R: CCCAGCAATCGATTCATGGGG	*Cla* I
R40E	F: GCAATTGATCCTCATGAAGAAATTGCTGGG R: CCCAGCAATTTCTTCATGAGGATCAATTGC	*Pag* I
R40K	F: GCAATTGATCCTCATGAAAAAAATTGCTGGG R: CCCAGCAATTTTTTCATGAGGATCAATTGC	*Pag* I
D36S/E39S	F: CTAGCAATTTCTCCCCATTCGCGAATTGCTGG R: CCAGCAATTCGCGAATGGGGTGAAATTGCTAG	*Nru* I
H38S/R40S	F: GCAATTGATCCCAGTGAATCGATTGCTGGG R: CCCAGCAATCGATTCACTGGGATCAATTGC	*Cla* I
D36E	F: CTAGCAATTGAACCTCATGAACGAATTG R: CAATTCGTTCATGAGGTTCAATTGCTAG	*Pag* I
R293K	F: GAATATTTCAATCACAAGCTTGGACATGG R: CCATGTCCAAGCTTGTGATTGAAATATTC	*Hind* III
*Lac*Q	F: GGAGAATTCATGAGCAAAATTGAACGTATT R: ATTCTGCAGTTAGAAAATTAATAAGTCATG	*EcoR* I *Pst* I
M13	F: GTTGTAAAACGACGGCCAGT R: CACAGGAAACAGCTATGACC	None

Sequencing pKK223-3	F: GCTGTTGACAATTAATCATCGGC R: TACTGCCGCCAGGCAAATTC	None

Note: Underlined sequences indicate newly-created restriction enzyme sites for identification of mutant genes.

primers (*Lac*Q-F and *Lac*Q-R; Table 4.2-1). Twenty picomoles of each primer were used in the PCR reaction with 10 ng of mutated pUC-*lac*Q DNA, 10 pmol of each dNTP, and 0.5 units of *Pfu* DNA polymerase for a total of 50 μL mixtures. The reaction mixture went through 30 cycles of 1 min-95 ℃/ 1 min-55 ℃/ 1 min-72 ℃ along with the 5 min denaturation at 95 ℃ prior to these cycles and a 10 min elongation period at 72 ℃ after the cycles. The PCR products underwent *Eco*R I and *Pst* I restriction enzyme digestions to generate adhesive ends, along with *Dpn* I restriction enzyme digestions to remove methylated parental DNAs. The DNA fragments of the resultant mutated *Lla*prol gene were ligated into *EcoR* I/*Pst* I digested pKK223-3 plasmids. The ligation mixtures were transformed into *E. coli* TOP10F'. Plasmid DNAs were extracted from the resultant colonies and further digested with the *Nde* I and *Pst* I restriction enzymes. The positive clones were identified to show 3.2 and 2.1 kb fragments on the 1 %-agarose gel electrophoresis. The positive mutated pKK223-3-*lac*Q DNA molecules were confirmed via DNA sequencing using pKK223-3 vector primers (Table 4.2-1) and the confirmed *E. coli* clones were stored in glycerol solution (30 % (w/v)) at -80 ℃ for future uses.

4.3 Expression and Purification of *Lla*prol Mutants

Standard procedures according to a previous study by Dr. Tanaka's group (Yang and Tanaka, 2008) were implemented to express and purify the *Lla*prol mutants. The pKK223-3 clones were inoculated into acidic Luria-Bertani Broth (LB, pH5.5, 900 mL shared equally in nine 500-mL flasks) containing 150 μg/mL ampicillin and the inoculated broth was vigorously shaken (200 rpm) at 16 ℃. To induce the recombinant protein production, IPTG was added at a final concentration of 1 mM to the broth when the optical cell density at 600 nm reached 0.5. The culture was then resumed for additional 72 hours. Cells from the 900-mL culture were harvested through centrifugation (Sorval SS-34, 6,000 ×g, 4 ℃, 10 min) and were suspended into

10 % (w/v) of a 20 mM sodium citrate (pH 6.0)/1 mM zinc chloride/50 mM sodium chloride solution. The suspended cells underwent ultrasonication to release the soluble molecules, followed by centrifugation (Sorval SS-34, 12,000 ×g, 4 ℃, and 20 min). The supernatant was brought to 40 % saturation of ammonium sulfate and kept on ice for 1 hour to precipitate most of nucleic acids and some proteins, which were then removed with centrifuging (Sorval SS-34, 12,000 ×g, 4 ℃, and 20 min). The resultant supernatant was brought to 60 % saturation of ammonium sulfate and was kept on ice for at least 5 hours. After centrifuging (Sorval SS-34, 12000 ×g, 4 ℃, and 20 min), *Lla*prol mutants were recovered as centrifugal pellets. The recovered mutant pellets were dissolved in a 3-mL Buffer A solution (20 mM sodium citrate (pH 6.0)/1 mM zinc chloride). The dissolved protein solution was transferred into a dialysis bag, and then the bag was dialyzed against an 800-mL Buffer A solution for 1 hour at 4 ℃. The dialysis was further conducted in a 2-L Buffer A solution for overnight at 4 ℃. The protein solution was centrifuged (Sorval SS-34, 12,000 ×g, 4 ℃, and 20 min) to remove insoluble matter. The supernatant collected following centrifugation (Sorval SS-34, 12,000 ×g, 4 ℃, and 20 min) was applied on a DEAE Sephacel column (2.5 Φ × 20 cm, GE Health Sciences, Little Chalfont, Buckinghamshire, UK) equilibrated with Buffer A. *Lla*prol mutants were eluted from the column with a 0 to 0.5 M sodium chloride linear gradient in Buffer A. The fractions containing prolidases were identified on 10% SDS-PAGE, and were concentrated to approximately 5 mL with an Amicon YM-10 ultrafiltration (Millipore, Billeric, MA, USA). The condensed sample was loaded on a DEAE 8HR column (Waters, Milford, MA, USA) equilibrated with Buffer A solution. A NaCl linear gradient from 0 M to 0.5 M was used to elute proteins from the column. The fractions containing prolidase were combined after the identification with 10 % SDS-PAGE, and further concentrated with an Amicon YM-10 ultrafiltration. The dimer formations were

examined by estimating the molecular mass through gel filtrations using Bio-Gel P-60, Sephadex G-100, G-150 and Bio-Gel P-200 as described by Yang and Tanaka (2008). The purified prolidases were kept as 50 % glycerol solutions and stored at -20 ℃ for future analysis.

4.4 Enzyme Concentration Determination

To determine protein concentrations during the purification process, a Bradford method (Bio-Rad Protein Assay Dye Reagent Concentrate, Hercules, CA, USA) was employed in this study. In this method, 800 μL of each sample were mixed with 200 μL of the dye reagent concentration, and was incubated at room temperature for at least 5 minutes. The optical absorbance of the samples was then detected at 595 nm using a spectrophotometer Beckman Coulter DU800 (Fullerton, CA, USA). To generate a standard curve of this method, bovine serum albumin (BSA) was used as a standard and the standard BSA samples were prepared in triplicate at several known concentrations (1.2 to 10.0 μg/mL). The standard relationship between BSA concentrations and ABS_{595} was obtained as the following equation.

$$[Protein]\ (mg/mL) = 21.68 ABS_{595} - 0.338 \quad \text{(Equation 4.4-1)}$$

To determine the protein concentration of mutated *Lla*prols, the protein samples were diluted to yield the absorption which falls into the range used to determine the standard curve.

4.5 Enzyme Activity Assay

The prolidase activity was measured using a ninhydrin method (Doi et al., 1981) that determines liberated proline via colourimetric spectrograph. In this method, free proline, which was released from the prolidase reaction, reacted with ninhydrin to generate a chromophore detected as ABS_{515}, while other amino acids are not able to initiate chromophore developing under these conditions. The ninhydrin solution was prepared as 3 g ninhydrin dissolved in a

100-ml organic solvent containing acetic acid and phosphoric acid in a volume ratio of 6 to 4, and heated to 70 ℃ to dissolve ninhydrin completely. A standard curve between different concentrations of free proline and ABS_{515} showed a linear relation, and we determined a coefficient of the proline-ninhydrin chromophore as 0.72555 μM^{-1}.

The standard activity assay was conducted as follows: a 90 μL reaction mixture (RM; 20 mM sodium citrate (pH 6.5)/1 mM zinc chloride/ 2.222 mM Leu-Pro substrate) was preheated at 50 ℃ for 2 min. Then, 10-μL enzyme preparation was added to RM to initiate the reaction, which dilute the substrate concentration to 2.0 mM. At every 1 min (for 4 min), a 20-μL aliquot was sampled and mixed with a 100-μL ninhydrin solution. The mixture was heated at 100 ℃ for 10 min and then chilled on ice. The absorbance values of the samples were detected as ABS_{515} using a Beckman Coulter DU800 spectrophotometer. To generate accurate data, specific dilutions of prolidases were determined to accommodate the absorption changes up to 1.0 during the measurements. The obtained absorbance was converted into the amount of free proline in the samples by multiplying with the coefficient (0.72555 μM^{-1})..

4.6 Determination of Kinetic Parameters

Kinetic parameters were examined with reactions at various Leu-Pro concentrations (0.1, 0.2, 0.3, 0.4, 0.5. 0.7, 1.0, 2.0, 4.0, and 8.0 mM). The reaction mixtures contained 20 mM sodium citrate (pH 6.5), 1mM zinc chloride, and Leu-Pro at an assigned concentration. The reactions were performed following the standard procedure of enzyme activity assay. Michaelis constant (K_m) and maximum velocity (V_{max}) for each prolidase mutant were preliminary determined using the method described by Sakoda and Hiromi (1976), and putative Hill constants were calculated as the slopes of the linear regression of an $Ln(v/(V_{max}-v)) - Ln(S)$ plot. These preliminary values were further applied to fit the S-v data to Equation 4.6-1 using a proFit

program (www.quansoft.com) to determine Michaelis constant (K_m), maximum velocity (V_{max}), Hill constant (h), and inhibition constant (K_i).

$$v = \frac{V_{max} \cdot s^h}{K_m + s^h + \frac{K_m \cdot s^{2h}}{K_i}} \qquad \text{(Equation 4.6-1)}$$

4.7 Substrate Specificity

To investigate the substrate specificity of mutant prolidases, 11 peptides (Leu-Pro, Phe-Pro, Val-Pro, Arg-Pro, Lys-Pro, Gly-Pro, Asp-Pro, Glu-Pro, Pro-Pro, Leu-Leu-Pro and Leu-Val-Pro) were examined as the substrate in prolidase reactions. The reactions were conducted under the standard enzyme activity assay conditions (defined in section 4.5) in the presence of zinc ions using 2 mM assigned peptide substrate.

4.8 Metal Ion Dependency

The activities were assayed in the presence of manganese chloride and different substrates to examine the metal ion dependency. This procedure is the same as the one described in the study of substrate dependency (section 4.7) except substituting 1 mM zinc chloride with 1 mM manganese chloride.

4.9 pH Dependency

In pH dependency study, the enzymatic reactions were performed at various pHs (pH 4.0, 5.0, 5.5, 6.0, 6.5, 7.0, 7.5, 8.0, 9.0, and 10.0). Most pHs required for the study (pH 5.0 to 9.0) were prepared by mixing 20 mM sodium citrate (pH 4.96) and 20 mM sodium borate (pH 9.23) at different ratios. pHs 4 and 10 were achieved using 20 mM citrate-HCl and 20 mM sodium borate-NaOH buffer solutions, respectively. The measurements were followed as the standard

enzyme activity assay procedure described in section 4.5. The activities at each pH were expressed as the activity relative to that at pH 6.5.

4.10 Thermal Dependency

Thermal dependency is used to examine local structural changes of the active site at different temperatures. The reaction mixtures were incubated at a series of temperatures (20.0, 30.0, 35.0, 40.0, 45.0, 50.0, 55.0, 60.0, and 70.0 ℃). The constant temperature was controlled using a water bath and monitored using a digital thermometer. The observed activities were expressed as relative values of the activity at 50 ℃.

4.11 Denaturation Temperature

Thermal denaturation temperature can be an index of the overall structure changes. Far UV-Circular dichroism (CD) spectrophotometer (PiStar-180, Applied Phytophysics Ltd Leatherhead, Surrey, UK) in Saskatchewan Structural Sciences Centre (SSSC) was employed to measure the thermal denaturation temperature by observing melting points of secondary structures of prolidase mutants. To conduct this experiment, 1 mL of 1.0 mg/mL purified enzyme sample was filtered with a 0.25 μm syringe filter and dilute with a buffer solution (20 mM sodium citrate (pH 6.0)) at least 100 times to minimize the influence of pre-existing NaCl. The final solutions were concentrated to 0.8 mg/mL with a MicroSep column (MWCO 10 kDa; Pall Life Science, East Hills, NY, USA) at 8,000 rpm for 30 min using a Sorval SS-34 rotor. Four hundred microliters of each sample were used to perform CD. The CD spectrum was measured over the temperature changes from 25 to 50 ℃ with increments of 5 ℃, 50 to 80 ℃ with increments of 2 ℃, and 80 to 90 ℃ with increments of 5 ℃. Data detected at the wavelength of 222 nm at different temperatures were used to plot the relationship between

temperatures and the angle of polarization (millidegrees (mdeg)). From this plot, the denaturation temperature was defined as the temperature where the rate of change in CD signals reached its maximum which was calculated using Curve Expert 1.4 Program (http://curveexpert.webhop.net/).

4.12 Prolidase X-ray Crystallography

4.12.1 Sample Preparations

To solve the three-dimensional structure of *Lla*prol, wild type *Lla*prol (WT) and loopless *Lla*prol (Δ36-40) were chosen for crystallization experiments. For these experiments, *Lla*prol preparations were purified to 99 % homogeneity as determined on a 10 % SDS-PAGE gel. Since salts such as sodium chloride are easier to crystallize than protein, the interference of these salts should be minimized during the protein crystallization. To remove the excess sodium chloride used during the protein purification process, Buffer A (20 mM sodium citrate (pH6.5)/1 mM zinc chloride) was added to achieve at least 100 times dilution. Then, the protein solution was reconcentrated into in a final concentration of at least 3.5 mg/mL in buffer A with MicroSep columns (Pall Corporation, NY, USA).

4.12.2 Preliminary Crystallization Using Commercial Sparse Matrix Screening

The initial screen solutions, Crystal Screen Kit 1 & 2 (Bukrinsky and Poulsen, 2001) were purchased from Hampton Research (Hampton Research, Aliso, Viejo, CA, USA). The hanging drop vapour diffusion method (Figure 2.6-3-A) was employed in this study to crystallize WT and Δ36-40. Trials were conducted in 24-well cell culture plates, where an 800-µL reservoir solution from the Kit 1 or 2 was placed in the wells and siliconized glass coverslips were used to seal the wells. These plates were kept on a shelf at room temperature for 1-3 weeks. Observations on

these crystallization trials were regularly conducted using a microscope (Leica E-6E, Wetzlar, Germany) and recorded using a Sony camera. This step was to primarily examine conditions (series pH, buffer, additive and precipitant) that WT or Δ36-40 may crystallize.

4.12.3 Optimization of Crystallization

Based on the results from above preliminary crystallization trials, several precipitants, salts, and buffer systems suitable for crystallizing WT and Δ36-40 were identified. These conditions were further optimized to obtain crystals appropriate for X-ray diffraction. Ten series (A to J) of cocktails were prepared according to the matrix design shown in Appendix A. These series were conducted with varying single factor and fixing other factors. Observations and recordings were performed to monitor the growth of crystals.

4.12.4 X-ray Data Collection

The sizes of crystals were measured using an ocular built-in ruler. Crystals were then fished out using a mounting loop and performed room temperature X-ray diffraction measurements with a DX8 Proteum Diffractometer (Bruker, ON, Canada) at SSSC.

A high brilliance beamline 08ID-1 of the Canadian Light Source (CLS) synchrotron was also employed to acquire a crystal structure of *Lla*prol with a high resolution. X-ray diffraction in the CLS should be performed under cryoconditions in order to minimize the damage caused by the synchrotron beam; therefore, crystals should be protected by cryoprotectants. Cryoprotectants such as glycerol and PEG8000 were tested by means of a flash-freezing approach if they could protect crystals in liquid nitrogen. In this approach, crystal screening solutions with different concentrations of glycerol or PEG8000 were tested as follows. A small amount of these solutions were sampled one by one using a mounting loop and were

immediately put into liquid nitrogen for seconds. Clear drop on the loop can be observed if the solution was suitable for cryoprotection. Subsequently, crystals grown in this particular solution under the same conditions previously optimized in this study were brought into X-ray diffraction in the CLS.

5 RESULTS

5.1 Preparations of *Lla*prol Mutants

All of the *Lla*prol mutants (Δ36-40, D36S, H38S, E39S, R40S, D36S/E39S, H38S/R40S, R40K, R40E, and D36E/R293K) were obtained at a homogeneity level. In this section, D36S is representing to show the process and results of SDM, gene cloning and protein purification (Figure 5.1-1). Using pUC-*lac*Q plasmid DNAs (size: 3.6 kb) as the template and D36S-F/R (Table 4.2-1) as the primers, mutated plasmid DNA harbouring ORF encoding D36S was obtained after SDM PCR as shown in Figure 5.1-1-A. Resultant PCR products were transformed into *E. coli* TOP10F'. Positive clones of recombinant *E. coli* whose plasmid DNAs generated a 3.6 kb single band after *Pag* I digestion as shown in Figure 5.1-1-B were identified to carry the mutated *Lla*prol gene and used for further subcloning. Figure 5.1-1-C shows DNA fragments (1.0 kb) of the mutated gene acquired by PCR using primers *Lac*Q-F and *Lac*Q-R (Table 4.2-1). After ligation with digested pKK223-3 vectors, the positive samples were screened with *EcoR* I and *Nde* I digestions. Positive clones showed 2.2 and 3.1 kb bands as shown in Figure 5.1-1-D.

The identities of pKK223-3 clones were confirmed via DNA sequencing and these expression plasmids were transformed into *E. coli* TOP10F' cells to express recombinant *Lla*prols. The purity and homogeneity of prepared mutant *Lla*prols were confirmed on a 10 % SDS-PAGE as shown in Figure 5.1-1-E. Gel filtration tests exhibited the purified *Lla*prol proteins were between 60 and 100 kDa, indicating they form dimmeric structures as observed in WT.

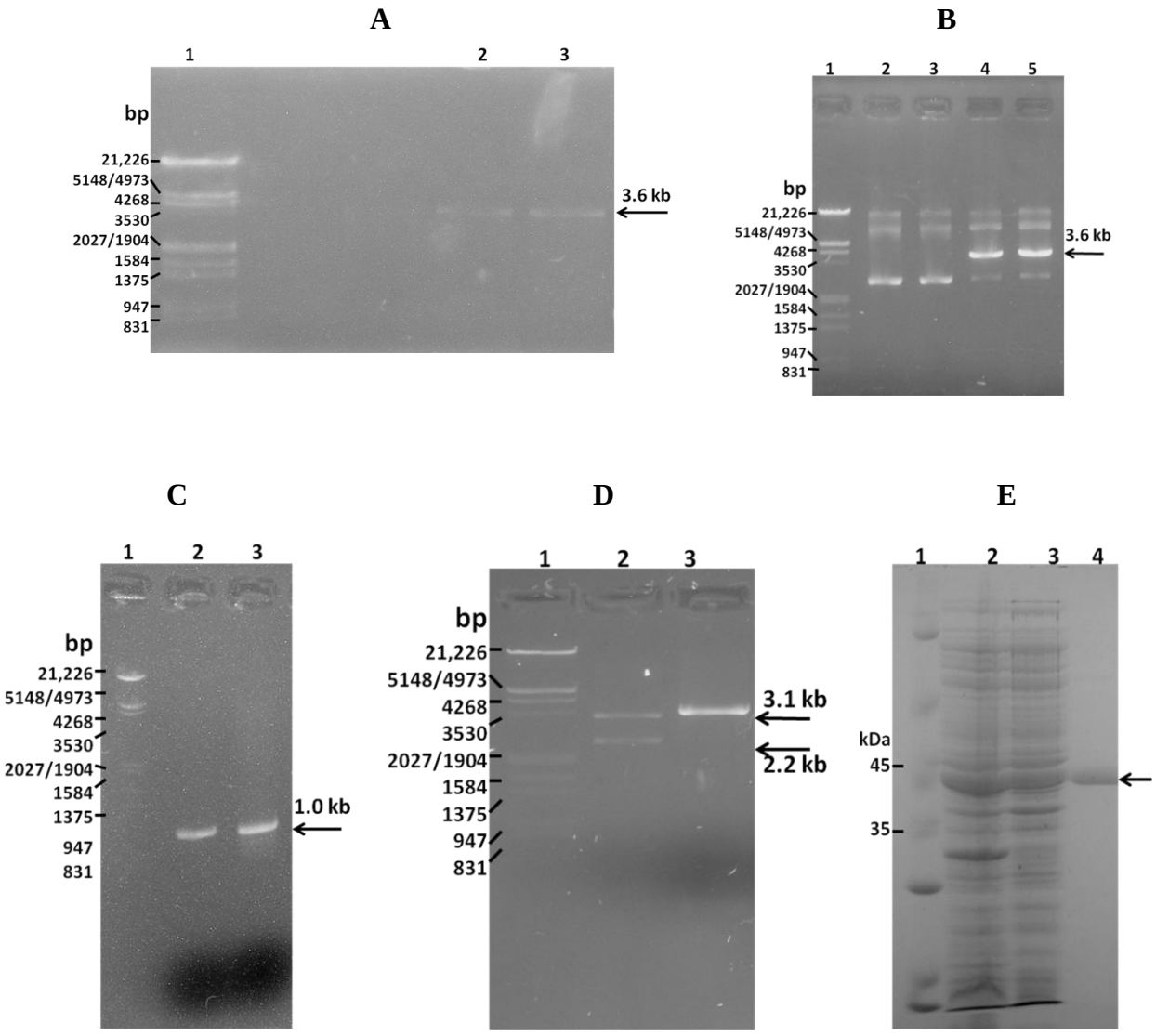

Figure 5.1-1 Results of the preparation of D36S mutant.
Panel A: SDM PCR result of D36S using pUC18-*lac*Q as templates; #1: DNA molecular weight marker; #2, 3: Products of SDM PCR, showing 3.6 kb bands. Panel B: *Pag* I digestion to screen positive clones containing D36S mutation; #1: DNA molecular weight marker; #2, 3: negative controls; #4, 5: positive results, showing linearized plasmids. Panel C: PCR result for the subcloning; #1: DNA molecular weight marker; #2, 3: PCR products showing 1.0 kb bands. Panel D: The *EcoR* I and *Nde* I digestion to screen pKK223-D36S; #1: DNA molecular weight marker; #2: a positive clone showing two bands at 2.2 and 3.1 kb; #3: A negative result; Panel E: A SDS-PAGE gel showing the purified D36S; #1: Protein molecular weight marker; #2: Crude extract fraction of pKK223-D36S/*E.coli* TOP10F'; #3: Dialyzed fraction after 60 % $(NH_4)_2SO_4$ precipitation; #4: DEAE-8HR purified D36S *Lla*prol.

5.2 Characterization of *Lla*prol Mutants

5.2.1 Activity Assay of *Lla*prol Mutants

Before being submitted to detailed enzyme characterizing studies, including [*S*]-ν plot, substrate specificity, metal ion dependency, pH dependency, temperature dependency and denaturing temperature analyses, all *Lla*prol mutants in this study were examined on their activities toward substrate Leu-Pro, which was the most preferred substrate for WT *Lla*prol. Among these mutants, Δ36-40, E39S, D36S/E39S, R40S, R40E, R40K and H38S/R40S were found inactive, and D36S, H38S, and D36E/R293K were active at various levels. Thus, the seven inactive mutants were eliminated from further enzyme characterization studies. However, these mutants indicated the Loop$^{32\text{-}43}$, especially Glu^{39} and Arg^{40} on this loop, played important roles in maintaining the activity of *Lla*prol.

5.2.2 Determination of Kinetic Parameters

According to the methods aforementioned in section 4.5, velocities of each mutant were examined individually at a series of substrate (Leu-Pro) concentrations. The relationship between the reaction rates and substrate concentrations of each mutant is presented in Figure 5.2-1 as the [*S*]-ν plots. The D36S mutant showed a hyperbolic curve up to 4 mM, implying a loss of the allostery in D36S that low concentrations of substrates did not suppress the reaction rates (Figure 5.2-1-B). In a contrast, the H38S mutant showed a sigmoidal curve where its reaction rate slowly increased at a range of low substrate concentrations (Figure 5.2-1-C). This was an indication of the existence of the allosteric behaviour, which is a distinctive property of WT (shown in Figure 5.2-1-A). The h, K_m, K_i, and V_{max} values for each mutant were summarized in Table 5.2-1. The Hill constant of H38S was 1.52 which was close to that of WT (1.58) while

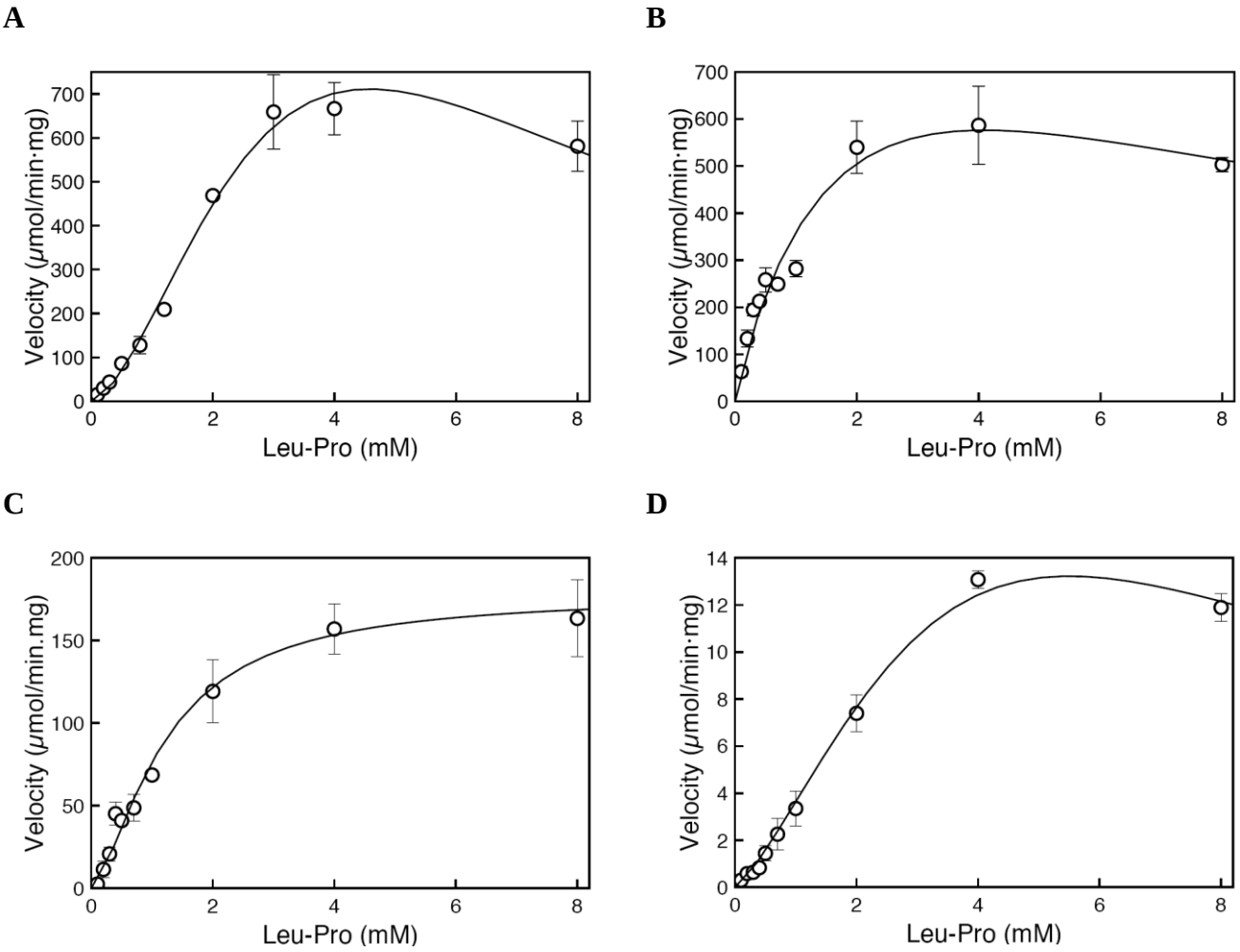

Figure 5.2-1 [*S*]-v plots of *Lla*prol mutants measured using Leu-Pro as the substrate.
A) WT, B) D36S, C) H38S, D) D36E/R293K. The velocity is expressed as the specific activity (μmol/min·mg). The line in each plot shows the calculated relation of [*S*] and *v* according to Equation 4.6-1.

Table 5.2-1 Kinetic parameters of mutant and WT *Lla*prols.

	V_{max} (μmol/min mg)	K_m (or $K_{0.5}$) (mM)	V_{max} /K_m	h	K_i (mM)
WT[a]	1740	8.0	217.3	1.58	15.3
D36S	1673.3	3.4	496.3	0.90	12.6
H38S	178.3	1.3	134.1	1.52	1162.5
D36E/R293K	54.2	13.7	4.0	1.28	78.4
R293S[a]	848.1	23.3	36.4	0.98	∞

a: Zhang et al. 2009

D36S had the Hill constant less than 1.0. These results further confirmed that D36S lost its allosteric behaviour and H38S maintained this behaviour.

Non-allosteric mutant D36S exhibited a V_{max} value similar to that of WT, and its K_m value was 43 % of WT. It can be noted that D36S was saturated at a low substrate concentration and maintained a considerable catalytic efficiency. Its overall catalytic activity (V_{max} /K_m) increased by 2.28-times from WT. Meanwhile, the activity of D36S was inhibited at a high concentration of the Leu-Pro substrate, having a similar K_i value to WT.

The allosteric mutant (H38S) had an appreciable V_{max} (10 % of the WT's value) while showed a higher substrate affinity (K_m: 1.3 mM) than WT (8.0 mM). Also, no substrate inhibition was observed in H38S, as judged from its large K_i value (1162.5 mM).

D36E/R293K was constructed to test an interaction between Asp^{36} and Arg^{293}. When the R293K mutation was introduced with the D36E mutation, the resultant double mutant kept the allosteric behaviour although it suffered a dramatically decrease in activity. The lower V_{max}

(3.1 %) and higher K_m values (1.7-times) than those of WT indicated that the double mutant had a low catalytic efficiency and substrate affinity.

5.2.3 Substrate Specificities

In the presence of zinc or manganese as the catalytic metal ion, all *Lla*prol mutants exhibited similar substrate specificities to WT that they preferred hydrophobic amino acids at the N-terminus of Xaa-Pro dipeptides. Positively charged Arg-Pro and Lys-Pro were also hydrolyzed, whereas the hydrolysis of negatively charged Asp-Pro and Glu-Pro was not observed. All mutants did not hydrolyze other peptides including Pro-Pro, Gly-Pro, Leu-Leu-Pro and Leu-Val-Pro examined in this research. The observed activities of *Lla*prol mutants toward different substrates were summarized in Table 5.2-2.

Although WT and mutant *Lla*prols in this study hydrolyzed the five dipeptides listed in Table 5.2-2, they had different preference profiles toward these dipeptides. Comparing with WT, the D36S mutant appeared to have higher specificities toward Lys-Pro. In the presence of zinc, WT can hydrolyze Lys-Pro at a marginal rate (6.6 %) relative to the most preferred Leu-Pro dipeptides. D36S can digest Lys-Pro at about a half rate of Leu-Pro. Even in the presence of manganese, WT hydrolyzed Lys-Pro at 11.6 % of Leu-Pro, whereas D36S took Lys-Pro at the rate of 68.3 %. It should also be noted that H38S retained its activity at significant levels toward Lys-Pro (70.6 %) and Arg-Pro (119.3 %) in the presence of zinc, comparing with those of WT (6.6 % to Lys-Pro; 12 % to Arg-Pro). In the case of manganese, Lys-Pro hydrolysis by H38S reached 119.5 %, which exceeded that of WT (11.6 %). Whereas D36S and H38S showed the changes in substrate specificities, the D36E/R293K mutant exhibited substrate specificities similar to WT in both metal ions, that is, it recognized Leu-Pro as its best substrates, (Table 5.2-2).

Table 5.2-2 Activities of *Lla*prols for a variety of substrates

	Relative activity (Leu-Pro = 100%)			
	WT [a]	D36S	H38S	D36E/R293K
A) In 1mM zinc chloride				
Leu-Pro	100 ±1.4 (468.7 ±6.6)	100.0 ±2.7 (534.1 ±14.5)	100.0 ±2.6 (162.3 ±4.2)	100.0 ±2.2 (6.7 ±0.14)
Lys-Pro	6.6 ±0.5	51.3 ±4.5	70.6 ±2.2	3.8 ±0.8
Phe-Pro	23.8 ±0.4	44.2 ±1.7	15.8 ±3.9	5.3 ±3.0
Val-Pro	14.4 ±0.4	28.8 ±2.6	4.9 ±1.4	16.3 ±8.5
Arg-Pro	12.0 ±0.9	14.6 ±2.3	119.3 ±5.2	11.2 ±3.5
B) In 1 mM manganese chloride				
Leu-Pro	100.0 (234.5 ±6.3)	100.0 ±11.6 (323.1 ±37.5)	100.0 ±9.5 (140.5 ±13.4)	100.0 (14.7 ±1.4)
Lys-Pro	11.6 ±2.1	68.3 ±5.1	119.5 ±7.0	10.9 ±1.0
Phe-Pro	70.8 ±12.5	23.6 ±3.3	24.8 ±10.8	10.0 ±0.6
Val-Pro	68.1 ±17.5	57.1 ±2.9	12.6 ±3.6	19.5 ±5.4
Arg-Pro	197.7 ±5.6	25.9 ±4.4	86.6 ±9.7	16.7 ±0.6

Note: The number in parentheses indicates the specific activity (μmol/mg min) toward Leu-Pro.
a, Zhang et al. (2009)

5.2.4 pH Dependency

His^{296} acts as a proton acceptor in *Lla*prol reactions (Hu and Tanaka, 2009). Thus the more deprotonated population of His^{296} exists, the higher activity of this enzyme should be shown. D36S showed a much higher activity (129.8 %) at pH 5.5 than WT (5.6 %) and other mutant

*Lla*prols (38.3% for D36E/R293K; 61.1 % for H38S), which was due to the disappearance of the negative charge of position 36.

The data of pH dependency for each *Lla*prol mutants (D36S, H38S, D36E/R293K) are shown in Figure 5.2-2 (B, C, D), with WT *Lla*prol as a reference (Figure 5.2-2-A). Each observed activity toward Leu-Pro at each pH was converted into the relative activity to that at pH 6.5. WT had a working pH range from 6.0 to 8.0. Three mutants examined showed high activities between pH 6.0 and 7.0 as observed in WT, and they lost their activities at pH below 4 and above 8.5. The differences among these mutated and WT *Lla*prol were observed between pH 5.0 and 6.0. At pH 5.0 and 5.5, WT showed little activities (0 and 5.6 %) for Leu-Pro (Figure 5.2.2-A). H38S (Figure 5.2.2-C) and D36E/R293K (Figure 5.2.2-D) showed considerable activities for Leu-Pro at pH 5.5 (61.1 % for H38S; 38.3 % for D36E/R293K). Interestingly D36S (Figure 5.2.2-B) showed a sizable activity at pH 5.0 (40 %) and reached the highest activity at pH 5.5 (129.8 %). These differences indicated the microenvironment in the active site cleft was changed by the disappearance of the charges of Asp^{36} or His^{38}.

5.2.5 Temperature Dependency

Thermal dependency can reflect the local structural rigidity of the active site. Figure 5.2-3-A to D showed the temperature dependency of WT and mutated *Lla*prols. All *Lla*prol mutants showed activities at similar working temperatures from 30 to 60 ℃ as observed in WT. They were barely active at 20 ℃ and lost their activities at 70 ℃. The differences among the WT and mutated *Lla*prols in terms of the temperature dependency were observed at 60 ℃. Mutant D36S retained a high activity (120 %) at 60 ℃ (Figure 5.2-3-B), comparing with that of WT (80 %; Figure 5.2.3-A). In contrast, mutants H38S and D36E/R293K (Figure 5.2-3-C, D) showed the

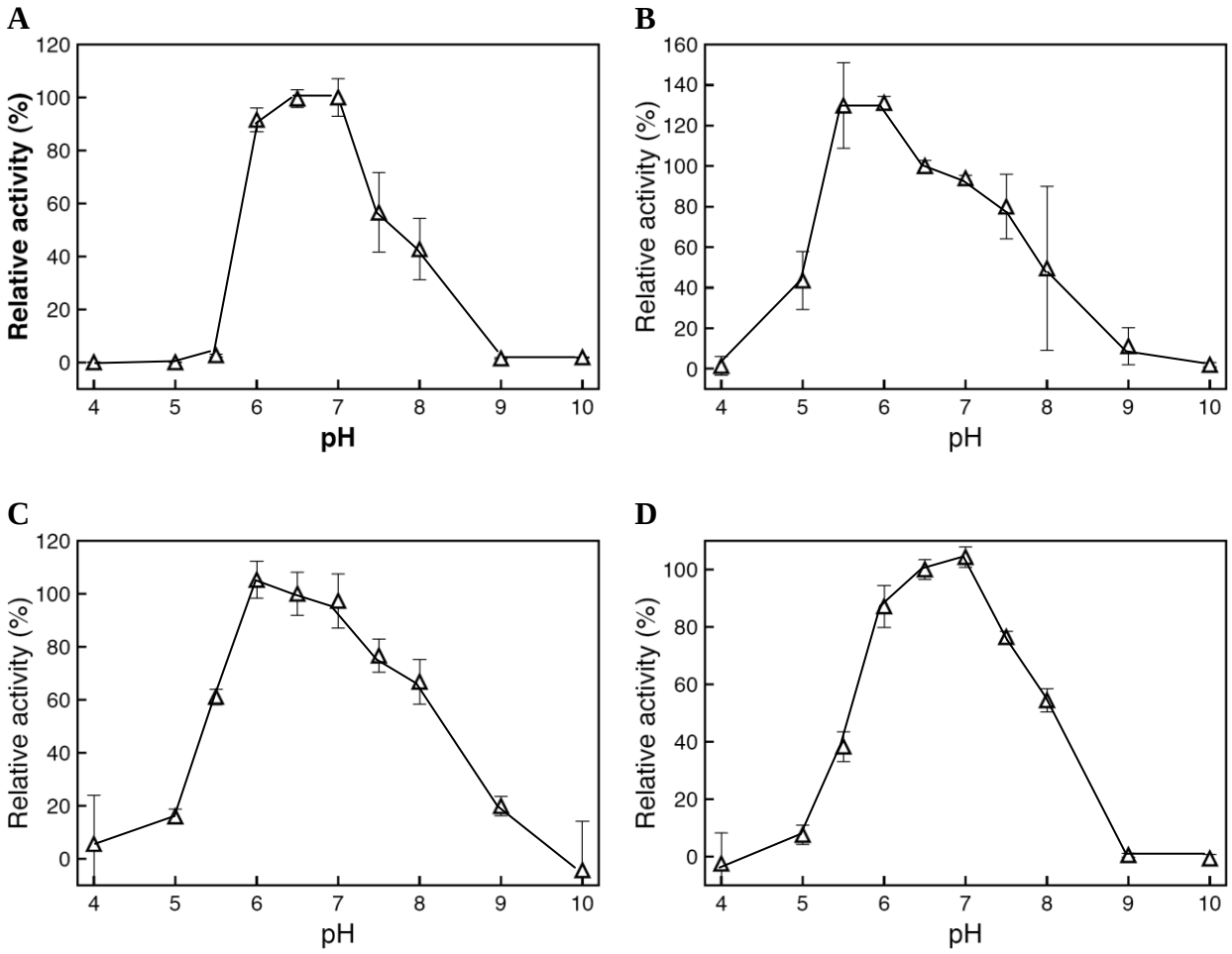

Figure 5.2-2 pH dependency of WT and mutated *Lla*prol
The reactions in this study were performed at assigned pHs (Temperature: 50 ℃; Substrates: 2 mM Leu-Pro; Metal ions: 1 mM $ZnCl_2$). The observed activity at each pH was plotted as relative activity to the activity at pH 6.5 for Leu-Pro. A) WT, B) D36S, C) H38S, D) D36E/R293K.

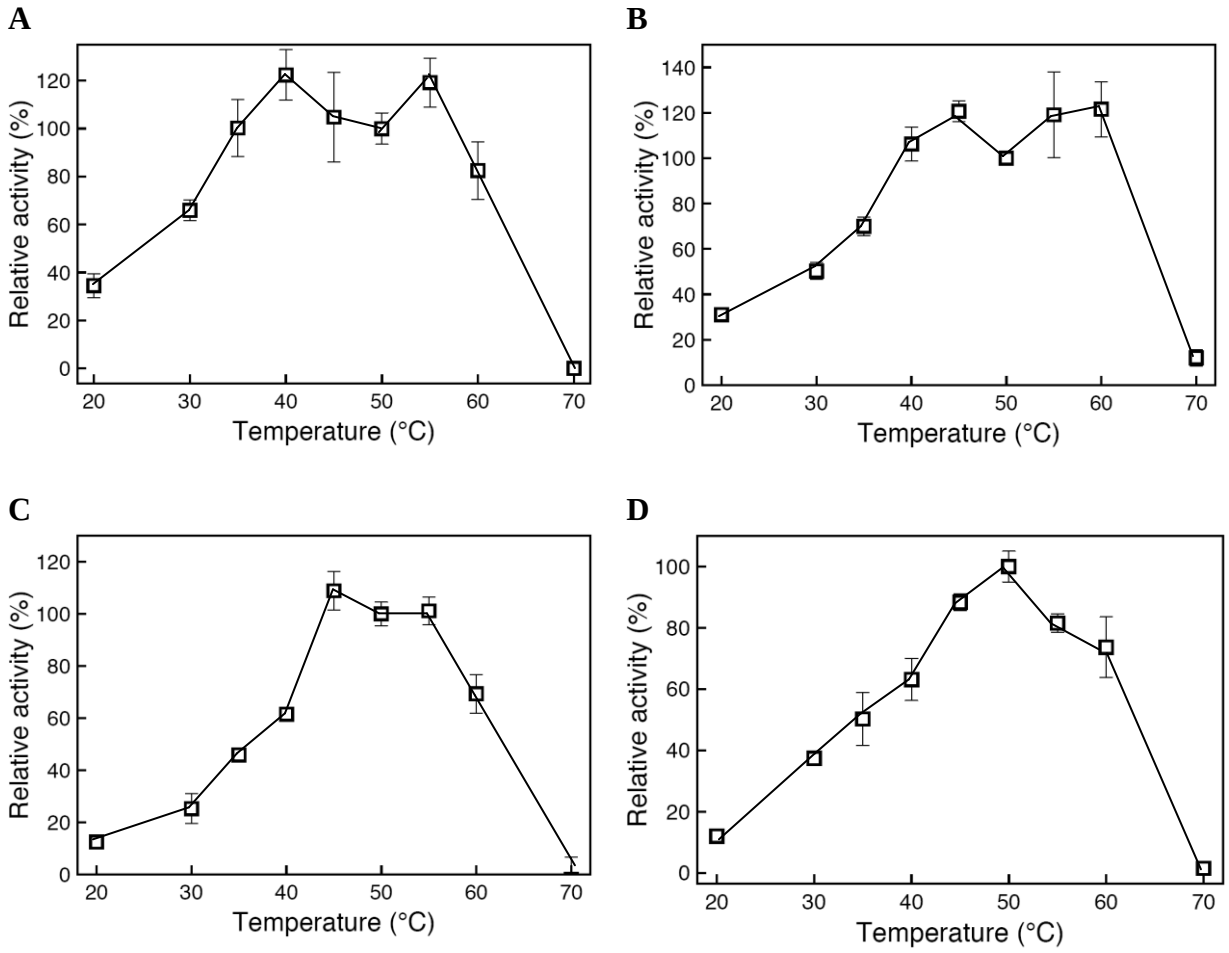

Figure 5.2-3 Thermal dependency of WT and mutated *Lla*prols
The reactions in this study were performed at assigned temperatures (pH: 6.5; Substrates: 2 mM Leu-Pro; Metal ions: 1 mM $ZnCl_2$). The observed activity at each temperature was plotted as relative activity to the activity at 50 ℃ for Leu-Pro. A) WT B) D36S, C) H38S, D) D36E/R293K.

same profile as WT. This suggested that Asp[36] may influence the local structural stability of *Lla*prol.

5.2.6 Denaturation Temperature

By employing circular dichroism (CD) as a tool, denaturing temperatures were determined for D36S, H38S and D36E/R293K. Plots between the temperature and dichroism ellipticity were shown in Figure 5.2-4. These plots showed that the denaturation of secondary structures of *Lla*prol started at 50 ℃, and completed at around 72 ℃. The denaturing temperatures of D36S, H38S, and D36E/R293K determined using Curve Expert 1.4 Program were 68, 67.1, and 67.9 ℃,

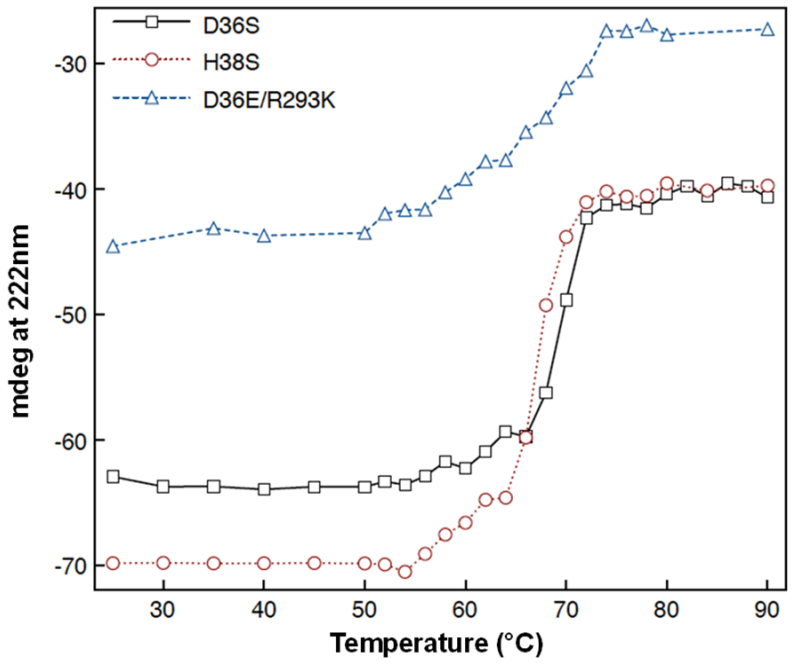

Figure 5.2-4 Thermal denaturation profile of mutated *Lla*prols.
The plots for D36S are shown in squares; for H38S are show in circles; for D36E/R293K are shown in triangles.

respectively. These results indicated the stability of the overall structures of these mutants were similar to that of WT *Lla*prol whose denaturing temperature is 67 ℃ (Yang and Tanaka, 2008). Thus, the mutations introduced by these *Lla*prol mutants did not affect overall structural stability, and their effects are limited to the local structures.

5.3 Preliminary X-ray Crystallography of *Lla*prol

5.3.1 WT *Lla*prol Crystallization from Commercially Kits

When WT *Lla*prol was used for crystallization using Crystal Screen Kit 1 & 2, crystalloid particles of WT were observed in screening solution #18 of Kit 2. Although crystalloid particles were also found in some other solutions in Kit 2, solution #18 allowed the formation of crystals. This solution contained 20 % (w/v) PEG8000, 0.1 M sodium cacodylate (pH 6.5), and 0.2 M magnesium acetate. This condition was further optimized in following studies.

5.3.2 Crystals Obtained Using Self-Made Screening Solutions

Based on the observations in the section 5.3.1, screening conditions were optimized by varying the following factors: precipitant-PEG8000 concentration, pH of sodium cacodylate buffer, and different salts. For this purpose, several series of screening solutions were prepared as shown in Appendix A. Initially, series A to E were used for the WT crystallization. Crystals of three types including a bipyramidal shape, a needle shape and stack of plates were observed in these series. Due to the difficulty to manipulate the needle and plates shape crystals, this study focused on the bipyramidal crystals to apply them for X-ray diffraction studies. Unfortunately, bipyramidal crystals of WT *Lla*prol grown under examined solutions were prone to crack. At the stage of testing F series, loopless *Lla*prol-Δ36-40 was used to crystallize in parallel with WT

*Lla*prol. WT was crystallized in F series but the crystals are cracked as they grow (Figure 5.3-1-A). Interestingly, Δ36-40 was crystallized into a bipyramidal shape in the presence of magnesium acetate and a needle shape in the presence of manganese chloride, as shown in Figure 5.3-1-B, C. Ultimately, the optimal conditions to crystallize the mutant Δ36-40 were determined as 10-12% (w/v) PEG8000/ 0.1 M magnesium acetate/ 0.1 M sodium cacodylate (pH 6.5). Bipyramidal crystals were formed with a reproducible manner under these conditions.

5.3.3 The Effects of PEG8000 on the Crystal Growth of loopless *Lla*prol Δ36-40

To further observe the crystal growth process of Δ36-40, different concentrations of PEG8000 (from 6 to 30% (w/v)) were employed in H series. Results from this experiment were shown in Figure 5.3-2. No crystal was formed at 6 and 8% (w/v) PEG8000 (Figure 5.3-2-A,B) because Δ36-40 was undersaturated (Figure 2.6-2). When the concentration of PEG8000 reached 10 and 12% (w/v), Δ36-40 was in a metastable zone, which was indicated by the well ordered crystals shown in Figure 5.3-2-C, D. When the concentrations of PEG8000 further increased up to 30% (w/v), the smaller and cracked crystals formed, which indicated Δ36-40 arrived at the nucleation zone.

5.3.4 Preliminary X-ray Diffraction

For crystals of loopless *Lla*prol Δ36-40 obtained in solution F17, the X-ray diffraction experiment was performed at SSSC. The diffraction pattern was shown in Figure 5.3-1-D. The crystals diffracted up to 4.6 Å but the space group could not be determined.

To attain a better diffraction, a synchrotron X-ray diffraction analysis was employed for this study. Glycerol and PEG8000 were tested with a flashing-freezing method to examine which is suitable to protect crystals under liquid nitrogen flashing. It was observed mother liquors with an

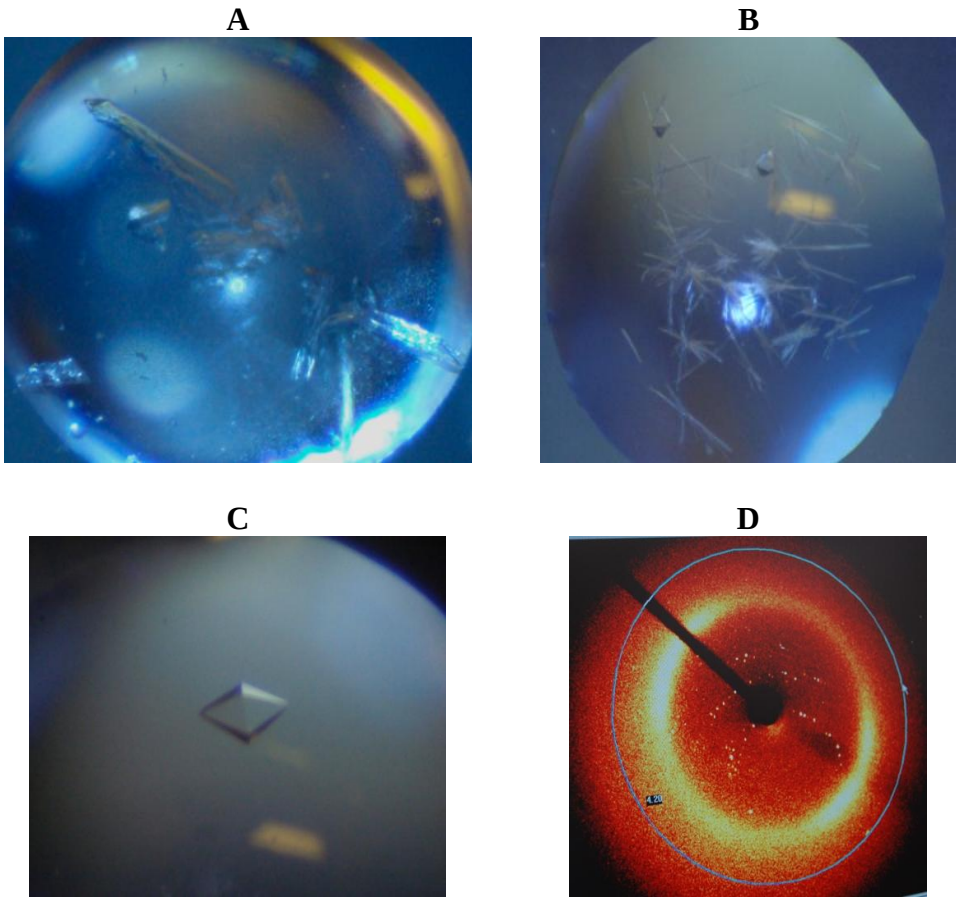

Figure 5.3-1 Crystals obtained in this study and preliminary X-ray diffraction pattern.
A: Cracked WT *Lla*prol crystal grown in 12% (w/v) PEG8000, 0.1M sodium cacodylate (pH 6.5), 0.1M magnesium acetate; B: Needle shaped crystal of loopless *Lla*prol grown in 10% (w/v) PEG8000, 0.1M sodium cacodylate (pH 6.5), 0.1M manganese chloride; C: bipyramidal shaped crystal of loopless *Lla*prol grown in 12% (w/v) PEG8000, 0.1M sodium cacodylate (pH 6.5), 0.1M magnesium acetate; D: X-ray diffraction pattern using a crystal shown in figure 5.3-1-C.

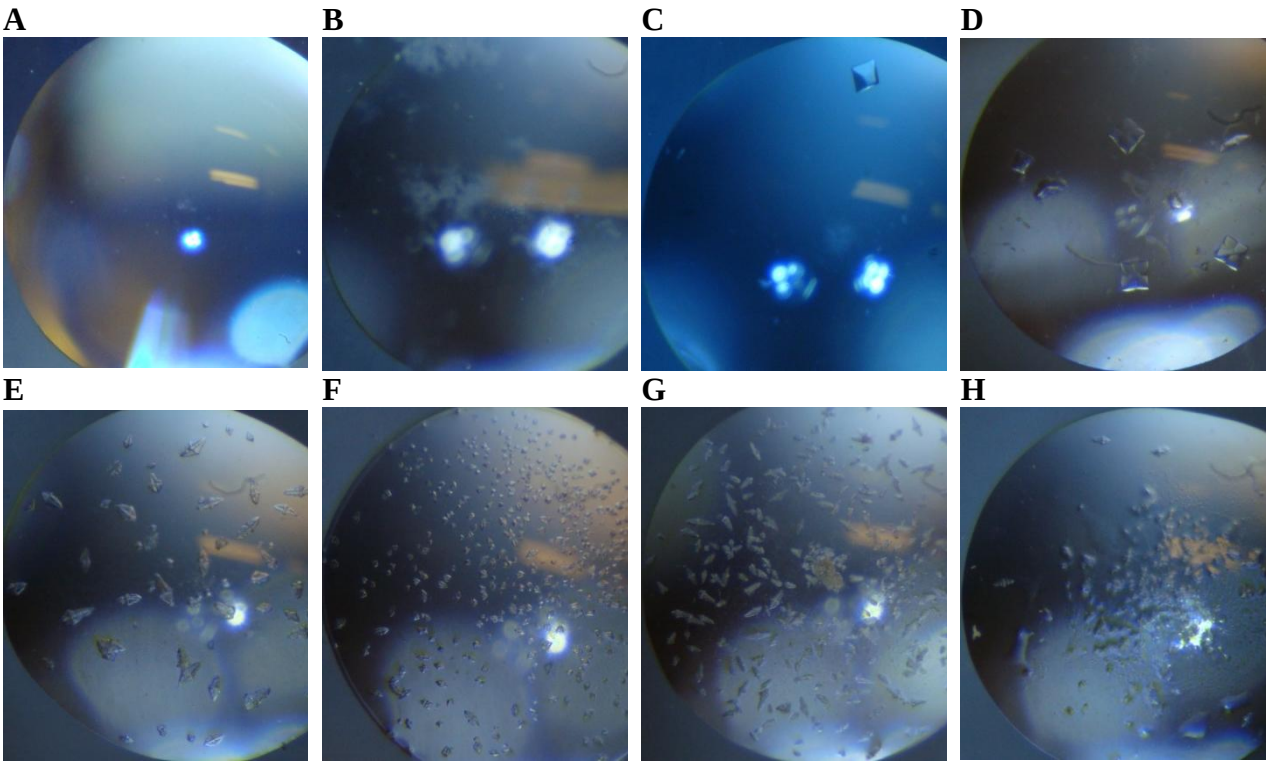

Figure 5.3-2 Effects of PEG8000 concentrations on the formation of crystals
The crystals of Δ36-40 were set at room temperature using a hanging drop method. The mother liquor solutions in this set contained 0.1M sodium cacodylate (pH 6.5), 0.1 M magnesium acetate, and different concentration of PEG8000. The concentrations of PEG8000 from A to H are 6, 8, 10, 12, 20, 22, 25, and 30% (w/v).

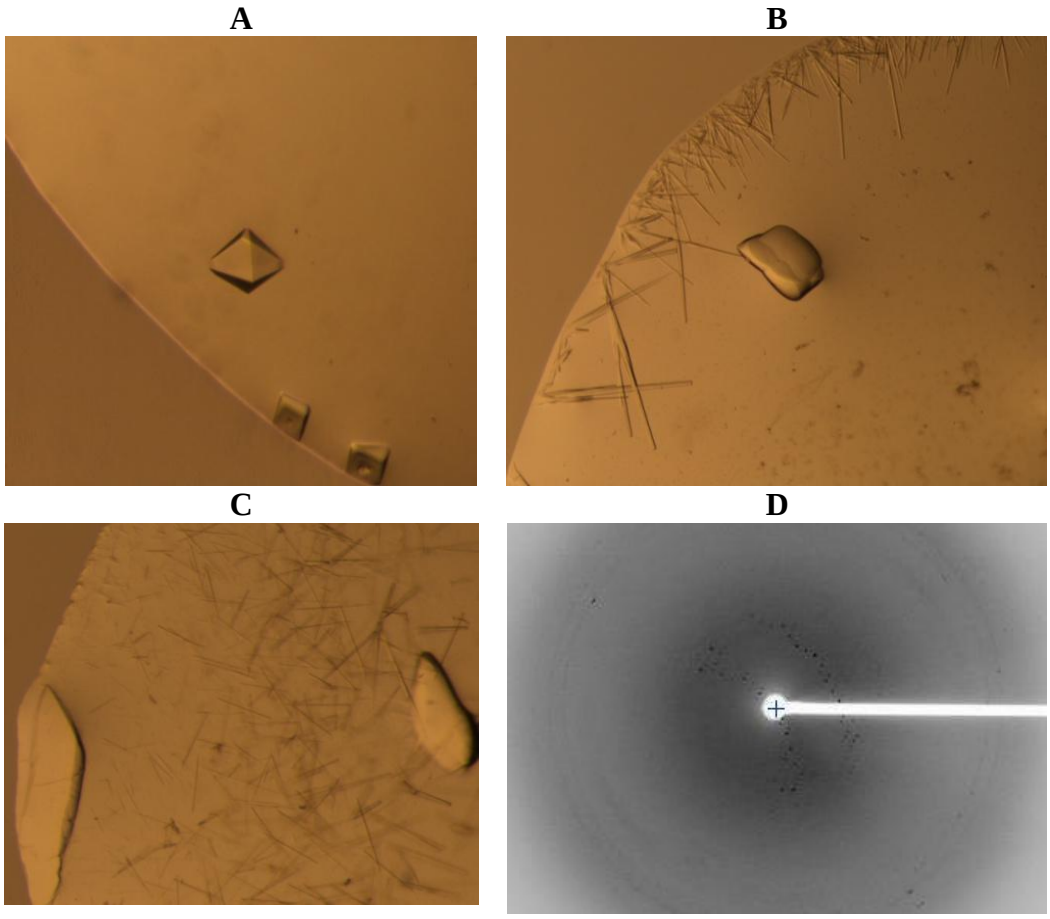

Figure 5.3-3 Cryocondition screening and X-ray diffraction in CLS.
A, B, C: Crystals obtained in the presence of 2 , 4 and 6 % (v/v) glycerol as the cyroprotectant;
D: X-ray Diffraction pattern using a crystal shown in Figure 5.3-3-A in CLS.

addition of glycerol rather than PEG8000 could retain clear drops during the flashing-freezing experiment. Thus, glycerol was used to protect the crystals for synchrotron X-ray diffraction. Δ36-40 was able to crystallize in an ordered form in the presence of low concentrations of glycerol with the optimized crystal growth solution aforementioned (Figure 5.3-3-A). With the increase in the glycerol concentrations, the formation of ordered crystals became difficult as shown in Figure 5.3-3- B and C. Crystals grown in the presence of 2% (v/v) glycerol were submitted to synchrotron X-ray diffraction and the result was shown in Figure 5.3-3-D. The diffraction was still in insufficient qualities that only few diffracted spots were observed, which implied a deficient quality of the crystal.

6 DISCUSSIONS

6.1 Contributions of Loop$^{32-43}$ to the Activity

6.1.1 Loop$^{32-43}$ Protects the Active Site of *Lla*prol

A loop structure is defined as a segment of a continuous polypeptide chain that forms a loop-shaped structure without a regular secondary structure. Loop structures are common structural components of proteins and on an average, five loops on each protein can be observed (Leszczynski and Rose, 1986). One particular type of loops, named as "loop lids" or "flaps" can form a lid structure over an active site of proteins and can play essential roles in protein functions. During catalysis, these loops can be apart from the active site to allow the introduction or release of substrates (open state); they can close over the active site to segregate the catalytic reaction from the environment (close state). This type of loop structure has been observed in many enzymes as mentioned in section 2.5.

A polypeptide segment (Gly^{32}-Gly^{43}) located between the α2 helix and β2 sheet of *Lla*prol forms a loop structure and its functional importance was examined in this study. The computer model of *Lla*prol (Yang and Tanaka, 2008) based on a crystal structure of *Pf*prol shows that the Loop$^{32-43}$ is projected over the active site located in the C-terminal domain of the other subunit, and each end of the Loop$^{32-43}$ is a glycine residue. Glycine residues have great freedom in terms of their conformations due to little steric hindrance of their hydrogen side chains. This nature of glycine can provide the flexibility for adjacent residues. For example, glycine has been shown to act as points of flexibility for hinge-type motions in the active-site loop of glutathione synthetase (Tanaka et al., 1993) and tryptophan synthase (Zhao and Somerville, 1993). Moreover, regions containing Gly-X-X or X-X-Gly are suggested as flexible regions in proteins if either of two X

residues was Val, Leu, Ile, Ala, Ser, Thr and Asp (Yan and Sun, 1997). The loop in *Pf*prol (Gly^{33}-Thr-Ser-Pro-Leu-Gly-Gly-Gly^{40}), which is corresponding to $Loop^{32-43}$, shows its flexibility due to the existence of the glycine residues at the both ends of the loop (Maher et al. 2004). The amino acid sequence of $Loop^{32-43}$ in *Lla*prol is Gly^{32}-Leu-Ala-Ile-Asp-Pro-His-Glu-Arg-Ile-Ala-Gly^{43}, which has Gly-Leu-Ala and Ile-Ala-Gly at the base of the loop. This property allows the flexibility of $Loop^{32-43}$ in *Lla*prol.

In addition, $Loop^{32-43}$ on *Lla*prol is four residues longer than its corresponding loop in *Pf*prol. Coincidentally, there are four additional charged residues (Asp^{36}, His^{38}, Glu^{39} and Arg^{40}, Figure 2.4-3-B) in the middle of *Lla*prol $Loop^{32-43}$, and no charged residue is found on the loop in *Pf*prol. Although $Loop^{32-43}$in the *Lla*prol model was displayed in a tight space (Figure 2.4-3-A) which is calculated based on a short loop structure on *Pf*prol, the different length of the loops between *Pf*prol and *Lla*prol suggested that *Lla*prol $Loop^{32-43}$ can be extended more and potentially had more conformational options than the loop in *Pf*prol.

Implications of the flexible feature of $Loop^{32-43}$ were also obtained from crystallization studies of WT and Δ36-40 *Lla*prol. During the crystallization of WT, cracked crystals were easily formed (Figure 5.3-1-A) either at 4 ℃ or room temperature while loopless mutant Δ36-40 tended to form stable crystals (Figure 5.3-1-B, C). Cracking of crystals observed in this study may be caused by the flexibility of the loop structure present in the protein crystal of WT. The computer model of *Lla*prol shows that $Loop^{32-43}$ is located at the interface between two subunits of *Lla*prol and projects down the active site cleft (Yang and Tanaka 2008). The flexibility of this loop can affect the interaction between two subunits of *Lla*prol, even it may induce a large conformational shift. When a central part of $Loop^{32-43}$ was deleted in Δ36-40, the flexibility of the loop was limited by its length, which resulted in reducing this conformational shift. Thus we

suspect that the cracking tendency of WT *Lla*prol provide another piece of evidence that the loop is flexible dynamically and prevents the formation of well-ordered crystals.

*Lla*prol was inactivated when a central part (Asp^{36}-Arg^{40}) of $Loop^{32-43}$ was knocked out (Δ36-40) or mutations were introduced at either Glu^{39} or Arg^{40} (E39S, R40S, R40K, R40E, D36S/E39S and H38S/R40S). Both D36S and H38S mutants showed different substrate preferences and pH dependency of activity with WT, implying their influence on the substrate binding and the behaviour of the catalyst. These results clearly indicate the importance of $Loop^{32-43}$ in the catalytic efficiency of *Lla*prol. Furthermore, the gel filtration testing on Δ36-40 showed this mutant was a dimer as observed for WT, which suggests the deletion of the loop does not induce an overall change of quaternary structure but a local alteration. For active mutants, D36S and H38S, CD experiments showed their thermal denaturing temperatures were not significantly changed, suggesting their overall secondary structures are similar to WT. Therefore, the introductions of mutations in $Loop^{32-43}$ can cause local structural changes relevant to the enzyme activity, substrate binding and the microenviornment of catalytic residues. This indicates that $Loop^{32-43}$ is a crucial local structure for the enzyme activity of *Lla*prol, and it is likely through influencing the substrate binding and catalysis.

The results and observations discussed above include 1) the location of $Loop^{32-43}$ is situated between two protomers, 2) $Loop^{32-43}$ influences interactions of the protomers, and 3) $Loop^{32-43}$ is critical for substrate binding and catalytic efficiency. These indicate $Loop^{32-43}$ can be defined as a region that exhibits extensive rearrangements during the catalysis. Although some loop structures are involved in catalytic processes without any direct interactions with active sites, as observed in the loop 6 in triose phosphate isomerase (TIM;Kempf et al., 2007), *Lla*prol $Loop^{32-43}$ is believed to affect catalysis through interactions with the active site and substrates. During the

catalysis, Loop$^{32-43}$ is most likely acting as an "active site flap" structure similar to that of aspartic proteinases. It opens to allow substrate access to the active site cleft, closes on substrate binding and opens again to release products. It is also able to stabilize the transition states. To argue the behaviour of Loop$^{32-43}$ clearly, some terms have to be defined before further discussion. In the absence of substrates or ligands, *Lla*prol Loop$^{32-43}$ is believed to have both open and closed conformations. As shown in Figure 6.1-1, at the open state, Loop$^{32-43}$ situated apart from the active site cleft, which is in a flexible state (corresponding allosteric R state); whereas at the closed state, Loop$^{32-43}$ extends over the active site (T state). In the presence of substrates, Loop$^{32-43}$ at the closed state can arrange proper interactions with a substrate and active site residues to initiate the catalytic cycle. The motivation of triggering the maturation of the closed states will be discussed in section 6.1.2.

6.1.2 The Closed Conformation of Loop$^{32-43}$

The results of this research proposed that the Loop$^{32-43}$ plays functional roles through its motion between two major conformational states: open and close. However, it is speculated that Loop$^{32-43}$ has both states in a dynamic equilibrium in an apo enzyme form. More populations take active closed conformation triggered by the ligand-binding in ligand-bound forms. The dynamic nature of Loop$^{32-43}$ over the active site begs the questions of how the residues on the loop contribute to conformational changes of the loop.

Glu^{39} mutants (E39S and D36S/E39S) lost their activities, which imply essential roles of Glu^{39} in the enzyme activity. Glu^{39} is adjacent to one positive charged residue Lys^{108} on the rigid body of N-terminal domain (Figure 6.1-2) which might be essential for maintaining the 'open' conformation of the loop (Figure 6.1-1). E39S or D36S/E39S eliminated this charge-charge interaction between Glu^{39} and Lys^{108}so that Loop$^{32-43}$ couldn't switch back to its 'open'

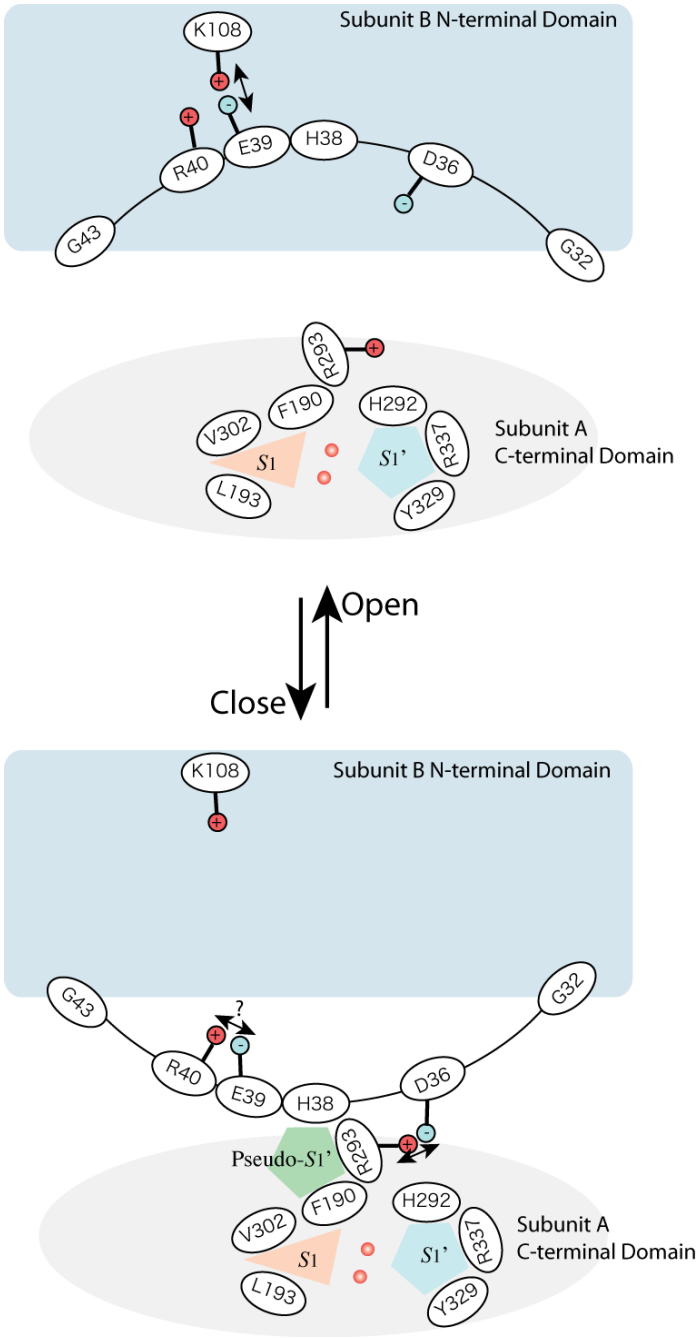

Figure 6.1-1 Schematic view of motions of Loop$^{32\text{-}43}$ in *Lla*prol.
The C-terminal domain of subunit A and N-terminal of subunit B are coloured pink and light blue, respectively. The triangle and pentagon are used to illustrate the S_1 and S_1' sites, respectively, which are located beside the zinc atoms (red spheres). In the open state of Loop$^{32\text{-}43}$, charge-charge interaction between Glu^{39} and Lys^{108} may be responsible for maintaining this position. In the closed state of Loop$^{32\text{-}43}$, Glu^{39} and Arg^{40} may be responsible for this position, where the S_1' site is bound with the P_1' residue (proline) and the charge-charge interaction between Asp^{36} and Arg^{293} would form the allosteric subsite. The closed state brings His^{38} in the position to form the pseudo-S_1' site that is responsible for the substrate inhibition.

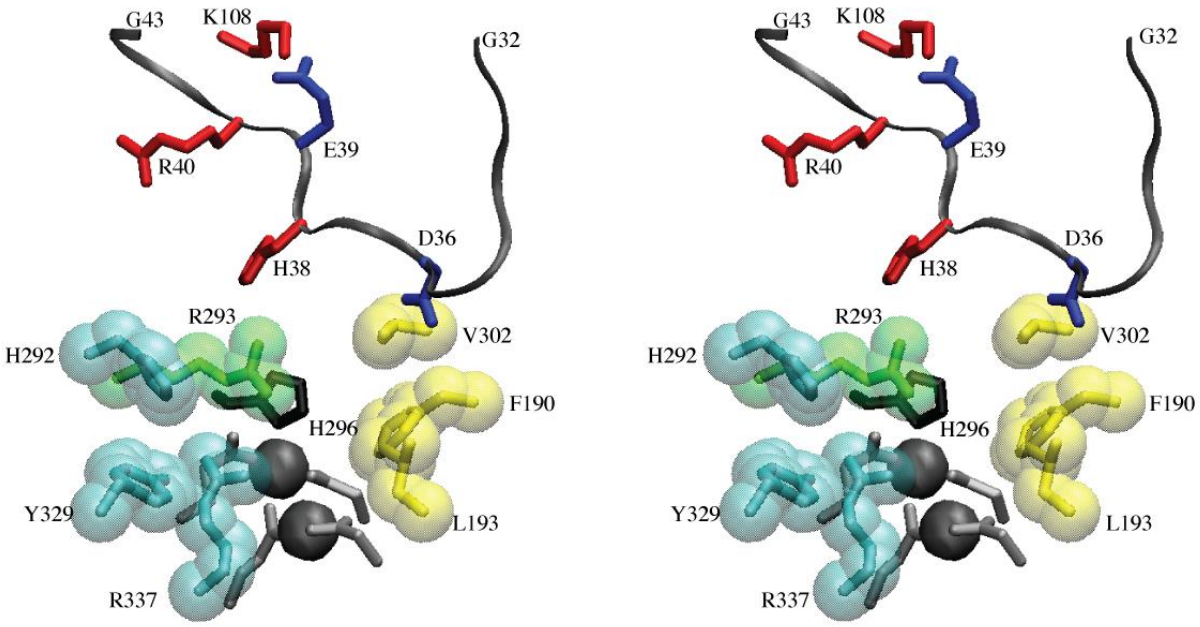

Figure 6.1-2 Stereodiagram of *Lla*prol active site.
Loop$^{32\text{-}43}$ is shown in gray ribbon; negatively charged residues (Asp^{36} and Glu^{39}) and positively charged residues (His^{38}, Arg^{40} and Lys^{108}) are shown in red and blue, respectively. In the active site cleft, zinc atoms are shown in gray spheres and the catalytic residue His^{296} is black. S_1' site residues (His^{292}, Tyr^{329}, and Arg^{337}) and S_1 site residues (Phe^{190}, Leu^{193}, and Val^{302}) are shown in cyan and yellow, respectively. Arg^{293}, a key residue for the allostery and substrate inhibition of *Lla*prol, is shown in green.

state, which narrows down or even blocks substrates from the active site, resulting in no activity. Both R40S and H38S/R40S lost activity for Leu-Pro, indicating Arg^{40} is an important residue to keep the activity of *Lla*prol. Judged from the molecular model of *Lla*prol, Arg^{40} may be in the hinge region of the lid. I hypothesize that Arg^{40} may play a role in triggering $Loop^{32-43}$ into a closed conformation, through charge-charge interaction with Glu^{39} (Figure 6.1-1) to transform $Loop^{32-43}$ between open and closed conformations. To test this hypothesis, R40K and R40E were constructed and studied. Interestingly, no activity was observed in both mutants R40K and R40E, disproving the interaction between Arg^{40} and Glu^{39}. However, these results suggest that not only the charged property of Arg^{40} is important, but also its bulky property is necessary to maintain the activity of *Lla*prol. Due to the inactivation of Arg^{40} mutants, the detailed mechanism has to be further investigated through X-ray crystallography.

The inactivation by Δ36-40, E39S, R40S, R40K and R40E mutations observed in this study proves that the flexible $Loop^{32-43}$, especially Glu^{39} and Arg^{40} on it, is required to maintain the activity of *Lla*prol. In addition, the flexibility of $Loop^{32-43}$ seems critical for the functionality of *Lla*prols. In the following sections, the flexibility and important roles of this loop are further discussed in terms of allosteric behaviour and substrate inhibition.

6.2 The Relationship of Asp^{36} and Arg^{293} to the Allosteric Behaviour of *Lla*prol

Allostery is one of interesting properties of *Lla*prol and it is not reported in prolidases from other sources. This study is the first attempt to solve the molecular mechanism of the allosteric behaviour observed in *Lla*prol.

As discussed in section 6.1, *Lla*prol $Loop^{32-43}$ is flexible over the active site and can act as a flap structure undergoing conformational changes during the catalytic cycle. Allosteric regulation, being an essential part of the catalytic cycle, is likely attributed to the motions of the

flap Loop$^{32\text{-}43}$. A loop (from position-178 to 192; Loop$^{178\text{-}192}$) in α subunit of tryptophan synthase participates in the allosteric regulation (Ferrari et al., 2003). This loop is highly flexible and can switch from an open to a closed state in response to ligand bindings. Gly^{181} located on Loop$^{178\text{-}192}$ forms a hydrogen bond with Ser^{178} of β subunit and this interaction is proved to be fundamental to transit allosteric signal between subunits (Spyrakis et al., 2006). Since *Lla*prol Loop$^{32\text{-}43}$ is suggested to protect the catalytic environment similar to Loop$^{178\text{-}192}$ in tryptophan synthase, we expect interactions among Loop$^{32\text{-}43}$ and residues in the active site cleft contribute to the allosteric signal transition.

In this study, mutants D36S and D36E/R293K provide interesting results in terms of the allosteric behaviour of *Lla*prol. When the negative charge of position 36 on the Loop$^{32\text{-}43}$ was neutralized in D36S, mutant D36S showed 96% activity of WT and lost the allosteric behaviour with a Hill constant of 0.90 (Table 5.2-1), which suggested a negative charge at the position 36 was necessary for maintaining the allosteric subsite of *Lla*prol. Combined two observations that 1) positive charged Arg^{293} is a key residue for allostery (Zhang et al. 2009) and 2) Arg^{293} is close to Asp^{36}, it is logical to conclude a charge-charge interaction between Asp^{36} and Arg^{293} exists to form a substrate subsite for the allostery. Double mutant D36E/R293K, mimicking the charge-charge interaction and keeping the distance of their α carbons, exhibited the allosteric behaviour, although it dramatically decreased the catalytic activity (Table 5.2-1). Moreover, the thermal denaturing temperatures of D36S and D36E/R293K determined with CD did not show significant changes compared to WT, which indicates that the structure of these mutants likely fail in undergoing major structural changes. Thus changes in observed behaviours are due to the mutations themselves. These results provides the strong evidence to conclude the

significant roles of charge-charge interaction between Asp^{36} (the tip of the loop) and Arg^{293} (beside the active site cleft) in the allosteric regulation.

To generate allosteric behaviours, no matter how they are regulated, allosteric proteins must have at least a substrate binding subsite for the allostery. The substrate binding subsite for the allostery (effector site) is normally located apart from the productive substrate binding site (active site). Different subsites played diverse roles during the catalytic cycle of enzymes. An effector site contributes to the allosteric regulation, whereas an active site provides a location for the catalytic reaction. Moreover, the binding of an effector to the allosteric subsite can trigger the exposure of the active site for substrate binding, which activates the allosteric enzyme.

In *Lla*prol, it is believed that the allosteric subsite is formed near the productive subsite because Asp^{36} and Arg^{293} (Figure 6.1-2) are located near the active site and influence the allosteric behaviour. Negative carboxyl group ($-COO^-$) of Asp^{36} and positive amine group ($-NH_3^+$) of Arg^{293} likely play important roles in forming the allosteric subsite. Results from the pH dependency and substrate specificity studies of D36S provided the evidence to support the above hypothesis. D36S had a significantly high activity at pH 5.5 (Figure 5.2.4-1) in comparison to other mutated and WT *Lla*prols, suggesting the loss of a negative charge at position 36 has an impact on the microenvironment for catalyst-His^{296} (Hu and Tanaka, 2009). For catalysis, His^{296} has to stay deprotonated to accept proton from the intermediate of the enzyme reaction. The more deprotonated population of His^{296} exists, the higher activity of this enzyme should be shown. D36S showed a much higher activity (129.8 %) at pH 5.5 than WT (5.6 %) and other mutant *Lla*prols (38.3% for D36E/R293K; 61.1 % for H38S), which was due to the disappearance of the negative charge of position 36. The removal of the negative charge

in D36S could indirectly increase the positive microenvironment of His^{296}, because the absence of the negative charge of Asp^{36} left the positive charge of Arg^{293} near His^{296}. The extra positive charged groups around His^{296} in D36S allows a higher population of deprotonated His^{296} at lower pH. Besides, D36S had a higher activity toward Lys-Pro than WT and D36E/R293K (Table 5.2-2). The small side chain of serine at position 36 was more capable to allow the docking of dipeptides with a long side chain (i.e., Lys-Pro) than a bulky side chain (glutamic acid or aspartic acid) at position 36. This indicated that Asp^{36} also limit the size of the productive substrate-binding pocket of WT when Asp^{36} formed an allsoteric subsite. It is of interest that the non-allosteric D36S withstood a higher temperature than other *Lla*prols in this study (Figure 5.2-5). This suggests that Asp^{36} influences the local structural stability of WT *Lla*prol. In another words, the absence of the interaction between Asp^{36} and Arg^{293} results in local structural changes of the active site in the event of substrate binding. Based on these analyses, we further conclud that the charge-charge interaction between Asp^{36} and Arg^{293} is most likely responsible for forming an allosteric binding subsite in *Lla*prol.

Induced-fit model introduced in section 2.3.1 can fit well in explaining the allosteric behaviour of *Lla*prol. When Leu-Pro as a substrate was introduced, the proline residue (P_1' residue) in a substrate docked in the substrate binding site (S_1' site), defined by His^{292}, Tyr^{329}, and Arg^{337}. Due to the flexible nature, Asp^{36} was able to interact with Arg^{293} forming an allosteric subsite when the loop takes the closed conformation. The negative charge of Asp^{36} would accommodate amine group of substrates (Xaa-Pro). The binding of the amine group of Xaa-Pro to the allosteric site further induces a conformational change of $Loop^{32\text{-}43}$ and the active site to expose the productive active site, which is discussed in next section.

6.3 Dual Roles of His^{38}, a Substrate Binding Residue for Activity and Inhibition

As mentioned in section 6.2, when the allosteric subsite is formed by Asp^{36} and Arg^{293} and is saturated with the effectors, the active site can be activated and bind to substrates for the catalysis. His^{38}, located at the tip of $Loop^{32-43}$, is likely involved in the formation of the productive binding site for the catalysis in *Lla*prol, judged from following observations. H38S had a significant decrease in its activity (10 % of WT), indicating the substitution of histidine to serine caused significant influence in the catalytic activity of *Lla*prol. In addition, the substrate specificities of H38S compared to WT had significant increases for Arg-Pro and Lys-Pro, which reveals the contribution of His^{38} in the recognition of substrate. His^{38} in WT likely had a larger influence than Asp^{36} on limiting the size of substrate, since D36S only changes behaviours in recognizing Lys-Pro. The residue (Leu^{37}) in *Pf*prol corresponding to this position (Figure 2.4-2-B) is suggested as a substrate-binding site for P_1 (Maher et al., 2004), which further supported that His^{38} of *Lla*prol was actually involved in forming the subsite for substrate binding. Combined with our previous study that Leu^{193}, Phe^{190} and Val^{302} are confirmed as the S_1 site residues in WT *Lla*prol (Hu and Tanaka, 2009), we believe His^{38} is another member of S_1 site and moves along with conformational changes of $Loop^{32-43}$. Therefore, in WT, the saturation of allosteric subsites (defined with Asp^{36} and Arg^{293}) with substrates Leu-Pro, incurs a conformational change of $Loop^{32-43}$, which is expressed as a right position of His^{38} to form the intact S_1 site with Leu^{193}, Phe^{190} and Val^{302} at the active site cleft. In this way, the P_1 residue (e.g., Leu) and P_1' residue (i.e., Pro) of the substrate can saturate the S_1 site (His^{38}, Leu^{193}, Phe^{190}, Val^{302}) and S_1' (His^{292}, Tyr^{329} and Arg^{337}) site, respectively. Then, a metal bound hydroxyl group acts as the nucleophile to attack the peptide bound and deprotonated catalyst-His^{296} immediately stabilize the intermediate product, as introduced in section 2.2.1.

As aforementioned, WT *Lla*prol showed the substrate inhibition. This study demonstrated that H38S exhibited little substrate inhibition. The K_i values for this mutant reached more than 1000 mM (Table 5.2-1), implying His^{38} significantly influenced the substrate inhibition of *Lla*prol. His^{38} is likely able to form a substrate binding subsite for inhibition, besides acting as a S_1 site residue. Zhang et al. (2009) considers Arg^{293} as a vital residue for the allostery and substrate inhibition because mutant R293S lost these two behaviours. As discussed in the previous section, Arg^{293} can form an allosteric subsite with Asp^{36}. The H38S mutant of this study indicated that His^{38} can interact with Arg^{293} for the substrate inhibition, which supported our hypothesis that the allosteric behaviour and substrate inhibition in *Lla*prol were correlated with each other. Phe^{190} is suggested as one of the key S_1 site residues for the substrate binding. The alteration of Phe^{190} is found to be lethal to the enzyme activity (Hu and Tanaka, 2009). This observation and the result acquired in this study (substrate inhibition of H38S) led us to suggest that S_1 site residues-His^{38} and Phe^{190} associate with Arg^{293} to mimic the S_1' site environment for binding proline through stacking forces between ring structures of His^{38} and Phe^{190}. When the substrates reached a higher concentration than the substrate molecules required for saturating the productive binding sites (S_1 and S_1'), extra population of free substrates are able to dock their proline into the new inhibition subsite formed by His^{38}, Phe^{190} and Arg^{293} (Figure 6.1-1), resulting in non-productive binding. These bindings prevent the $Loop^{32\text{-}43}$ from switching back to the open state, which results in inhibition of activity. In this explanation of substrate inhibition, *Lla*prol takes advantages of Arg^{293} and S_1 site residues (Phe^{190} and His^{38}), mimicking the binding environment of S_1' site (His^{292}, Tyr^{329} and Arg^{337}, shown in Figure 6.1-1) to form an inhibition subsite for binding the P_1' residues (proline) of substrates, which resulted in the substrate inhibition.

6.4 General Conclusion

To elucidate the contributions of residues on Loop$^{32\text{-}43}$ to the functions of *Lla*prol, ten mutated prolidases were constructed and characterized on their substrate specificity, pH dependency, allosteric behaviour, thermal dependency and metal ion dependency. The data were interpreted as follows.

Combining the arguments in section 6.1, 6.2, and 6.3, it is concluded that Loop$^{32\text{-}43}$ over the active site cleft is a key element in *Lla*prol to regulate and participate in the enzymatic reaction including allosteric activation, productive catalysis, and substrate inhibition. Its flexible nature offered by Gly^{32} and Gly^{43} provides advantages to permit the central portion of Loop$^{32\text{-}43}$ to communicate with the active site under certain circumstances. The central portion of Loop$^{32\text{-}43}$ includes charged residues (Asp^{36}, His^{38}, Glu^{39} and Arg^{40}), which are found to play specific roles at different stages of the catalysis.

Disordered crystallization of WT and ordered manner of loopless mutant (Δ36-40) imply that Loop$^{32\text{-}43}$ influences the inter-subunit conformational states, and supports the hypothesis that the loop is a 'lid' structure over the active site cleft. Glu^{39} and Arg^{40} are important residues for enzyme activity and they may play roles in regulating the open and closed conformation of Loop$^{32\text{-}43}$. Asp^{36} interacting with Arg^{293} through charge-charge attractions, contributes to the allosteric subsite formation and the interaction is likely the critical component of the allosteric site of *Lla*prol. His^{38} is a residue involved in forming substrate subsite for inhibition and it can recognize the substrates.

In a summary, Loop$^{32\text{-}43}$ is flexible and it has open and closed conformations. This nature, relying on the existence of Glu^{39}, Arg^{40} and possibly Lys^{108} (Figure 6.1-2), is important to maintain the activity of *Lla*prol. When the loop takes the closed conformation, the tip of the loop

(Asp[36] and His[38]) can extend over the active site pocket and be involved in the catalysis of *Lla*prol. Asp[36] interacting with Arg[293] forms an allosteric subsite, allowing the bound of the N-terminus amine group of the substrates (Xaa-Pro). The saturation of the allosteric site with substrates further allows the communications of His[38] with other substrate binding residues to form an intact active site (S_1 site for Xaa residue). When the substrate concentrations increase, His[38], Phe[190] and Arg[293] mimic the microenvironment of S_1' site and bind to the ring structure of proline residue in the substrates. The non-productive binding site is formed to block the appropriate binding for catalysis, which results in the substrate inhibition. Since Glu[39] and Arg[40] mutants are inactivated, the dynamic change and their specific roles during catalysis are still ambiguous. A model based on a real structure is really necessary. Further X-ray crystallization studies on *Lla*prol for additional evidences are being conducted.

7 FUTURE RESEARCH

This thesis research provides a platform to understand the mechanism of allosteric behaviour and substrate inhibition, whose mechanisms are still elusive. The molecular mechanisms of these interesting behaviours in *Lla*prol can be further studied at the atomic level with X-ray crystallography. Although several crystal structures of prolidase from different sources (such as *Pyrococcus* bacteria and *Homo sapiens*) are solved, the crystal structures in the presence of their substrate or analogues are scarce. These native structures of prolidase are not able to provide solid evidence in the substrate binding sites and catalytic mechanism. To prove the substrate binding subsites for allostery, catalysis, and substrate inhibition of *Lla*prol, crystal structures of both native *Lla*prol and its complex with substrate analogues, products and intermediate analogues, have to be solved at high resolutions (at least 2.0 Å). The interpretation from these structures would be able to provide more dynamic pictures of *Lla*prol and how these changes are related to its function.

In this thesis study, the crystallization conditions of *Lla*prol were successfully obtained, although the preliminary X-ray diffraction failed in generating sufficient data for the structure determination. Based on our knowledge, the bottleneck for this problem is obtaining well-ordered crystals. Crystal growth conditions have to be further optimized in order to obtain better diffractions for interpreting the protein structure of *Lla*prol. Besides, for solving the complex structure of *Lla*prol and its analogues, analogues have to be designed and synthesized.

When the crystal structure is successfully solved, its information shall be valuable to elucidate the mechanism of substrate specificity, allostery and substrate inhibition in *Lla*prol. This knowledge can further guide our practical manipulation of *Lla*prol to reduce the substrate inhibition and allostery, moreover to increase the substrate conversion as well as to broad the

substrate specificity, aiming to the applications in debittering process of cheese-making and treating prolidase deficiency patients as well as the never gas detoxification.

8 REFERENCES

Aguilar, C.F., Cronin, N.B., Badasso, M., Dreyer, T., Newman, M.P., Cooper, J.B., Hoover, D.J., Wood, S.P., Johnson, M.S., and Blundell, T.L. (1997). The three-dimensional structure at 2.4 angstrom resolution of glycosylated proteinase A from the lysosome-like vacuole of *Saccharomyces cerevisiae*. Journal of Molecular Biology *267*, 899-915.

Asao, M., Iwamura, H., Akamatsu, M., and Fujita, T. (1987). Quantitative structure-activity-relationships of the bitter thresholds of amino-acids, peptides, and their derivatives. Journal of Medicinal Chemistry *30*, 1873-1879.

Bazan, J.F., Weaver, L.H., Roderick, S.L., Huber, R., and Matthews, B.W. (1994). Sequence and structure comparison suggest that methionine aminopeptidase, prolidase, aminopeptidase-p, and creatinase share a common fold. Proceedings of the National Academy of Sciences *91*, 2473-2477.

Biertumpfel, C., Basquin, J., Suck, D., and Sauter, C. (2002). Crystallization of biological macromolecules using agarose gel. Acta Crystallographica section D *58*, 1657-1659.

Birnboim, H.C., and Doly, J. (1979). A rapid alkaline extraction procedure for screening recombinant plasmid DNA. Nucleic Acids Research *7*, 1513-1523.

Boggon, T.J., Chayen, N.E., Snell, E.H., Dong, J., Lautenschlager, P., Potthast, L., Siddons, D.P., Stojanoff, V., Gordon, E., Thompson, A.W., Zagalsky, P.F., Bi, R.C., Helliwell, J.R., (1998). Protein crystal movements and fluid flows during microgravity growth. Philosophical Transactions of the Royal Society A *356*, 1045-1061.

Braman, J., Papworth, C., and Greener, A. (1996). Site-directed mutagenesis using double-stranded plasmid DNA templates. Methods in Molecular Biology *57*, 31-44.

Broadbent, J.R., Strickland, M., Weimer, B.C., Johnson, M.E., and Steele, J.L. (1998). Peptide accumulation and bitterness in Cheddar cheese made using single-strain *Lactococcus lactis* starters with distinct proteinase specificities. Journal of Dairy Science *81*, 327-337.

Bukrinsky, J.T., and Poulsen, J.C.N. (2001). pH, conductivity and long-term stability in the Crystal Screen solutions. Journal of Applied Crystallograph *34*, 533-534.

Bumberger, E., and Belitz, H.D. (1993). Bitter taste of enzymic hydrolysates of casein. I. Isolation, structural and sensorial analysis of peptides from tryptic hydrolysates of beta-casein. Z Lebensm Unters Forsch *197*, 14-19.

Buxbaum, E. (2005). Fundamentals of protein structure and function (New York, NY, Springer).

Chayen, N.E., and Saridakis, E. (2008). Protein crystallization: from purified protein to diffraction-quality crystal. Nature Methods *5*, 147-153.

Chevrier, B., Schalk, C., D'Orchymont, H., Rondeau, J.M., Moras, D., and Tarnus, C. (1994). Crystal structure of *Aeromonas proteolytica* aminopeptidase: a prototypical member of the co-catalytic zinc enzyme family. Structure *2*, 283-291.

Christen, B., Perez, D.R., Hornemann, S., and Wuthrich, K. (2008). NMR structure of the Bank Vole Prion Protein at 20 degrees C contains a structured loop of residues 165-171. Journal of Molecular Biology *383*, 306-312.

Coll, M., Knof, S.H., Ohga, Y., Messerschmidt, A., Huber, R., Moellering, H., Russmann, L., and Schumacher, G. (1990). Enzymatic mechanism of creatine amidinohydrolase as deduced from crystal-structures. Journal of Molecular Biology *214*, 597-610.

Colonna, C., Conti, B., Perugini, P., Pavanetto, F., Modena, T., Dorati, R., Iadarola, P., and Genta, I. (2008). Ex vivo evaluation of prolidase loaded chitosan nanoparticles for the enzyme replacement therapy. European Journal of Pharmaceutics and Biopharmaceutics *70*, 58-65.

Davis, N.C., and Smith, E.L. (1957). Purification and some properties of prolidase of swine kidney. Journal of Biological Chemistry *224*, 261-275.

Ditargiani, R.C., Chandrasekaran, L., Belinskaya, T., and Saxena, A. (2010). In search of a catalytic bioscavenger for the prophylaxis of nerve agent toxicity. Chemico-Biological Interactions *187*, 349-354.

Doi, E., Shibata, D., and Matoba, T. (1981). Modified colorimetric ninhydrin methods for peptidase assay. Analytical Biochemistry *118*, 173-184.

Endo, F., Matsuda, I., Ogata, A., and Tanaka, S. (1982). Human-erythrocyte prolidase and prolidase deficiency. Pediatric Research *16*, 227-231.

Fernandez-Espla, M.D., Martin-Hernandez, M.C., and Fox, P.F. (1997). Purification and characterization of a prolidase from *Lactobacillus casei* subsp. casei IFPL 731. Applied and Environmental Microbiology *63*, 314-316.

Ferrari, D., Niks, D., Yang, L.H., Miles, E.W., and Dunn, M.F. (2003). Allosteric communication in the tryptophan synthase bienzyme complex: roles of the beta-subunit aspartate 305-arginine 141 salt bridge. Biochemistry-Us *42*, 7807-7818.

Fersht, A. (1985). Enzyme structure and mechanism, 2nd edition (New York, W.H. Freeman).

Fujii, M., Nagaoka, Y., Imamura, S., and Shimizu, T. (1996). Purification and characterization of a prolidase from *Aureobacterium esteraromaticum*. Bioscience Biotechnology and Biochemistry *60*, 1118-1122.

Fukushima, D. (1979). Fermented Vegetable (Soybean) Protein and related foods of Japan and China. Journal of the American Oil Chemists' Society *56*, 357-362.

Ghosh, M., Grunden, A.M., Dunn, D.M., Weiss, R., and Adams, M.W. (1998). Characterization of native and recombinant forms of an unusual cobalt-dependent proline dipeptidase (prolidase) from the hyperthermophilic archaeon *Pyrococcus furiosus*. Journal of Bacteriology *180*, 4781-4789.

Gilboa, R., Spungin-Bialik, A., Wohlfahrt, G., Schomburg, D., Blumberg, S., and Shoham, G. (2001). Interactions of *Streptomyces griseus* aminopeptidase with amino acid reaction products and their implications toward a catalytic mechanism. Proteins *44*, 490-504.

Han, B.Z., Rombouts, F.M., and Nout, M.J.R. (2004). Amino acid profiles of sufu, a Chinese fermented soybean food. Journal of Food Composition and Analysis *17*, 689-698.

Hechtman, P., Richter, A., Corman, N., and Leong, Y.M. (1988). Insitu activation of human-erythrocyte prolidase - potential for enzyme replacement therapy in prolidase deficiency. Pediatric Research *24*, 709-712.

Holm, R.H., Kennepohl, P., and Solomon, E.I. (1996). Structural and functional aspects of metal sites in biology. Chemical Review *96*, 2239-2314.

Hu, K.K., and Tanaka, T. (2009). *S*-1 site residues of *Lactococcus lactis* prolidase affect substrate specificity and allosteric behaviour. Biochim Biophys Acta, Proteins Proteomics *1794*, 1715-1724.

Hu, T., Wu, D., Chen, J., Ding, J., Jiang, H., and Shen, X. (2008). The catalytic intermediate stabilized by a "down" active site loop for diaminopimelate decarboxylase from *Helicobacter pylori*. Enzymatic characterization with crystal structure analysis. Journal of Biological Chemistry *283*, 21284-21293.

Ishibashi, N., Kubo, T., Chino, M., Fukui, H., Shinoda, I., Kikuchi, F., Okai, H., and Fukui, S. (1988). Studies on Flavored Peptides .4. Taste of Proline-Containing Peptides. Agricultural and Biological Chemistry Tokyo *52*, 95-98.

Kaminogawa, S., Azuma, N., Hwang, I.K., Suzuki, Y., and Yamauchi, K. (1984). Isolation and characterization of a prolidase from *Streptococcus-Cremoris* H61. Agricultural and Biological Chemistry Tokyo *48*, 3035-3040.

Kato, H., Tanaka, T., Yamaguchi, H., Hara, T., Nishioka, T., Katsube, Y., and Oda, J. (1994). Flexible loop that is novel catalytic machinery in a ligase - atomic-structure and function of the loopless glutathione synthetase. Biochemistry-Us *33*, 4995-4999.

Kelders, H.A., Kalk, K.H., Gros, P., and Hol, W.G. (1987). Automated protein crystallization and a new crystal form of a subtilisin:eglin complex. Protein Engineering Design and Selection *1*, 301-303.

Kempf, J.G., Jung, J.Y., Ragain, C., Sampson, N.S., and Loria, J.P. (2007). Dynamic requirements for a functional protein hinge. Journal of Molecular Biology *368*, 131-149.

Kempner, E.S. (1993). Movable lobes and flexible loops in proteins - structural deformations that control biochemical-activity. FEBS Letters *326*, 4-10.

Kendrew, J.C., Bodo, G., Dintzis, H.M., Parrish, R.G., Wyckoff, H., and Phillips, D.C. (1958). A three-dimensional model of the myoglobin molecule obtained by x-ray analysis. Nature *181*, 662-666.

Kim, M.R., Kawamura, Y., and Lee, C.H. (2003). Isolation and identification of bitter peptides of tryptic hydrolysate of soybean 11S glycinin by reverse-phase high-performance liquid chromatography. Journal of Food Science *68*, 2416-2422.

Kim, S.L., Kim, H.M., Chun, S.C., Kim, J.T., Kim, M.Y., Chi, H.Y., Kim, E.H., Kim, H.B., Kim, M.J., Seo, B.R., *et al.* (2008). Characterization of 7S and 11S globulins in soybean varieties differing in seed size and their effects on the properties of soybean curd. Food Science and Biotechnology *17*, 135-143.

Kiw, M.R., Yukio, K., Kim, K.M., and Lee, C.H. (2008). Tastes and structures of bitter peptide, asparagine-alanine-leucine-proline-glutamate, and its synthetic analogues. J Agr Food Chem *56*, 5852-5858.

Koshland, D.E., Jr., Nemethy, G., and Filmer, D. (1966). Comparison of experimental binding data and theoretical models in proteins containing subunits. Biochemistry-Us *5*, 365-385.

Lee, K.P.D., and Warthesen, J.J. (1996). Preparative methods of isolating bitter peptides from cheddar cheese. Journal of Agricultural and Food Chemistry *44*, 1058-1063.

Leszczynski, J.F., and Rose, G.D. (1986). Loops in globular proteins: a novel category of secondary structure. Science *234*, 849-855.

Li, M., Phylip, L.H., Lees, W.E., Winther, J.R., Dunn, B.M., Wlodaawer, A., Kay, J., and Gustchina, A. (2000). The aspartic proteinase from *Saccharomyces cerevisia*e folds its own inhibitor into a helix. Nature Structural & Molecular Biology *7*, 113-117.

Liu, S.P., Widom, J., Kemp, C.W., Crews, C.M., and Clardy, J. (1998). Structure of human methionine aminopeptidase-2 complexed with fumagillin. Science *282*, 1324-1327.

Lorber, B., Sauter, C., Robert, M.C., Capelle, B., and Giege, R. (1999). Crystallization within agarose gel in microgravity improves the quality of thaumatin crystals. Acta Crystallographica Section D *55*, 1491-1494.

Lowther, W.T., and Matthews, B.W. (2000). Structure and function of the methionine aminopeptidases. Biochimica Et Biophysica Acta-Protein Structure and Molecular Enzymology *1477*, 157-167.

Lowther, W.T., and Matthews, B.W. (2002). Metalloaminopeptidases: Common functional themes in disparate structural surroundings. Chemical Reviews *102*, 4581-4607.

Lupi, A., Della Torre, S., Campari, E., Tenni, R., Cetta, G., Rossi, A., and Forlino, A. (2006). Human recombinant prolidase from eukaryotic and prokaryotic sources. Expression, purification, characterization and long-term stability studies. FEBS Journal *273*, 5466-5478.

Maehashi, K., and Huang, L. (2009). Bitter peptides and bitter taste receptors. Cellular and Molecular Life Sciences *66*, 1661-1671.

Maher, M.J., Ghosh, M., Grunden, A.M., Menon, A.L., Adams, M.W., Freeman, H.C., and Guss, J.M. (2004). Structure of the prolidase from *Pyrococcus furiosu*s. Biochemistry-Us *43*, 2771-2783.

Manao, G., Camici, G., Cappugi, G., Nassi, P., and Ramponi, G. (1972). Swine kidney prolidase - assay, isolation procedure, and molecular properties. Physiological Chemistry and Physics *4*, 75-87.

Mcdonald, J.K., Zeitman, B.B., Reilly, T.J., and Ellis, S. (1969). New observations on substrate specificity of cathepsin c (dipeptidyl aminopeptidase i) - including degradation of beta-corticotropin and other peptide hormones. Journal of Biological Chemistry *244*, 2693-2709.

Monod, J., Changeux, J.P., and Jacob, F. (1963). Allosteric proteins and cellular control systems. Journal of Molecular Biology *6*, 306-329.

Monod, J., Wyman, J., and Changeux, J.P. (1965). On the nature of allosteric transitions: a plausible model. Journal of Molecular Biology *12*, 88-118.

Morel, F., Frot-Coutaz, J., Aubel, D., Portalier, R., and Atlan, D. (1999). Characterization of a prolidase from *Lactobacillus delbrueckii* subsp. bulgaricus CNRZ 397 with an unusual regulation of biosynthesis. Microbiology *145 (Pt 2)*, 437-446.

Myara, I., Cosson, C., Moatti, N., and Lemonnier, A. (1994). Human kidney prolidase - purification, preincubation properties and immunological reactivity. International Journal of Biochemistry *26*, 207-214.

Ney, K. H., (1971). Voraussage der Bitterkeit von Peptiden aus deren Aminosaure-zusammensetzung. Z. Lebensm. Unters. Forsch. 147, 64-71.

Ogata, A., Tanaka, S., Tomoda, T., Murayama, E., Endo, F., and Kikuchi, I. (1981). Autosomal recessive prolidase deficiency - 3 patients with recalcitrant leg ulcers. Archives of Dermatology *117*, 689-694.

Okoniewska, M., Tanaka, T., and Yada, R.Y. (1999). The role of the flap residue, threonine 77, in the activation and catalytic activity of pepsin A. Protein Engineering Design and Selection *12*, 55-61.

Okoniewska, M., Tanaka, T., and Yada, R.Y. (2000). The pepsin residue glycine-76 contributes to active-site loop flexibility and participates in catalysis. Biochemical Journal *349*, 169-177.

Otagiri, K., Nosho, Y., Shinoda, I., Fukui, H., and Okai, H. (1985). Studies on a model of bitter peptides including arginine, proline and phenylalanine residues .1. bitter taste of dipeptides and tripeptides, and bitterness increase of the model peptides by extension of the peptide-chain. Agricultural and Biological Chemistry *49*, 1019-1026.

Palka, J.A., and Phang, J.M. (1997). Prolidase activity in fibroblasts is regulated by interaction of extracellular matrix with cell surface integrin receptors. Journal of Cellular Biochemistry *67*, 166-175.

Pandit, J., Forman, M.D., Fennell, K.F., Dillman, K.S., and Menniti, F.S. (2009). Mechanism for the allosteric regulation of phosphodiesterase 2A deduced from the X-ray structure of a near full-length construct. Proceedings of the National Academy of Sciencei U S A *106*, 18225-18230.

Park, J.N., Ishida, K., Watanabe, T., Endoh, K., Watanabe, K., Murakami, M., and Abe, H. (2002). Taste effects of oligopeptides in a Vietnamese fish sauce. Fisheries Science *68*, 921-928.

Park, M.S., Hill, C.M., Li, Y., Hardy, R.K., Khanna, H., Khang, Y.H., and Raushel, F.M. (2004). Catalytic properties of the *Pep*Q prolidase from *Escherichia c*oli. Archives of Biochemistry and Biophysics *429*, 224-230.

Perozzo, M.A., Ward, K.B., Thompson, R.B., and Ward, W.W. (1988). X-ray diffraction and time-resolved fluorescence analyses of Aequorea green fluorescent protein crystals. Journal of Biological Chemistry *263*, 7713-7716.

Popovych, N., Sun, S., Ebright, R.H., and Kalodimos, C.G. (2006). Dynamically driven protein allostery. Nature Structural & Molecular Biology *13*, 831-838.

Powell, G.F., Rasco, M.A., and Maniscal.Rm (1974). Prolidase deficiency in man with iminopeptiduria. Metabolism - Clinical and Experimental *23*, 505-513.

Raksakulthai, R., and Haard, N.F. (2003). Exopeptidases and their application to reduce bitterness in food: a review. Critical Reviews in Food Science and Nutrition *43*, 401-445.

Rantanen, T., and Palva, A. (1997). *Lactobacilli* carry cryptic genes encoding peptidase-related proteins: characterization of a prolidase gene *(pep*Q) and a related cryptic gene (*orf*Z) from *Lactobacillus delbrueckii* subsp. bulgaricus. Microbiology *143*, 3899-3905.

Roberts, A.K., and Vickers, Z.M. (1994). Cheddar cheese aging - changes in sensory attributes and consumer acceptance. Journal of Food Science *59*, 328-334.

Roderick, S.L., and Matthews, B.W. (1993). Structure of the cobalt-dependent methionine aminopeptidase from *Escherichia coli*: a new type of proteolytic enzyme. Biochemistry-Us *32*, 3907-3912.

Rowsell, S., Pauptit, R.A., Tucker, A.D., Melton, R.G., Blow, D.M., and Brick, P. (1997). Crystal structure of carboxypeptidase G(2), a bacterial enzyme with applications in cancer therapy. Structure *5*, 337-347.

Sakoda, M., and Hiromi, K. (1976). Determination of the best-fit values of kinetic parameters of the Michaelis-Menten equation by the method of least squares with the Taylor expansion. Journal of Biochemistry *80*, 547-555.

Sauter, C., Balg, C., Moreno, A., Dhouib, K., Theobald-Dietrich, A., Chenevert, R., Giege, R., and Lorber, B. (2009). Agarose gel facilitates enzyme crystal soaking with a ligand analog. Journal of Applied Crystallography *42*, 279-283.

Shannon, R.D. (1976). Revised effective ionic-radii and systematic studies of interatomic distances in halides and chalcogenides. Acta Crystallographica Section A *32*, 751-767.

Sielecki, A.R., Fedorov, A.A., Boodhoo, A., Andreeva, N.S., and James, M.N.G. (1990). Molecular and crystal-structures of monoclinic porcine pepsin refined at 1.8-a resolution. Journal of Molecular Biology *214*, 143-170.

Silva, J.J.R.F.d., and Williams, R.J.P. (2001). The biological chemistry of the elements: the inorganic chemistry of life, 2nd edn (Oxford ; New York, Oxford University Press).

Sjostrom, H., Noren, O., and Josefsso.L (1973). Purification and specificity of pig intestinal prolidase. Biochimica Et Biophysica Acta *327*, 457-470.

Smialowski, P., Schmidt, T., Cox, J., Kirschner, A., and Frishman, D. (2006). Will my protein crystallize? A sequence-based predictor. Proteins-Structure Function and Bioinformatics *62*, 343-355.

Spyrakis, F., Raboni, S., Cozzini, P., Bettati, S., and Mozzarelli, A. (2006). Allosteric communication between alpha and beta subunits of tryptophan synthase: modelling the open-closed transition of the alpha subunit. Biochimica et Biophysica Acta *1764*, 1102-1109.

Strater, N., and Lipscomb, W.N. (1995). Two-metal ion mechanism of bovine lens leucine aminopeptidase: active site solvent structure and binding mode of L-leucinal, a gem-diolate transition state analogue, by X-ray crystallography. Biochemistry-Us *34*, 14792-14800.

Stucky, K., Klein, J.R., Schuller, A., Matern, H., Henrich, B., and Plapp, R. (1995). Cloning and DNA-Sequence Analysis of *Pep*q, a Prolidase Gene from *Lactobacillus-Delbrueckii* Subsp Lactis Dsm7290 and Partial Characterization of Its Product. Molecular & General Genetics *247*, 494-500.

Suga, K., Kabashima, T., Ito, K., Tsuru, D., Okamura, H., Kataoka, J., and Yoshimoto, T. (1995). Prolidase from *Xanthomonas maltophilia*: purification and characterization of the enzyme. Bioscience, Biotechnology, and Biochemistry *59*, 2087-2090.

Suh, J.H. (1992). Model studies of metalloenzymes involving metal-ions as lewis acid catalysts. Accounts of Chemical Research *25*, 273-279.

Tahirov, T.H., Oki, H., Tsukihara, T., Ogasahara, K., Yutani, K., Ogata, K., Izu, Y., Tsunasawa, S., and Kato, I. (1998). Crystal structure of methionine aminopeptidase from hyperthermophile, *Pyrococcus furiosus*. Journal of Molecular Biology *284*, 101-124.

Tamura, M., Miyoshi, T., Mori, N., Kinomura, K., Kawaguchi, M., Ishibashi, N., and Okai, H. (1990). Mechanism for the bitter tasting potency of peptides using O-aminoacyl sugars as model compounds. Agricultural Biology and Chemistry *54*, 1401-1409.

Tanaka, T., Kato, H., Nishioka, T., and Oda, J. (1992). Mutational and proteolytic studies on a flexible loop in glutathione synthetase from *Escherichia-coli* b - the loop and arginine-233 are critical for the catalytic reaction. Biochemistry-Us *31*, 2259-2265.

Tanaka, T., Teo, K.S.L., Lamb, K.M., Harris, L.J., and Yada, R.Y. (1998). Effect of replacement of the conserved Tyr75 on the catalytic properties of porcine pepsin A. Protein Peptide Letter *5*, 19-26.

Tanaka, T., Yamaguchi, H., Kato, H., Nishioka, T., Katsube, Y., and Oda, J. (1993). Flexibility impaired by mutations revealed the multifunctional roles of the loop in glutathione synthetase. Biochemistry-Us *32*, 12398-12404.

Thomas, T.D., and Pritchard, G.G. (1987). Proteolytic-enzymes of dairy starter cultures. FEMS Microbiology Reviews *46*, 245-268.

Thompson, J.D., Higgins, D.G., and Gibson, T.J. (1994). Clustal-W - Improving the sensitivity of progressive multiple sequence alignment through sequence weighting, position-specific gap penalties and weight matrix choice. Nucleic Acids Research *22*, 4673-4680.

Toelstede, S., and Hofmann, T. (2008). Sensomics mapping and identification of the key bitter metabolites in Gouda cheese. Journal of Agricultural and Food Chemistry *56*, 2795-2804.

Tzeng, S.R., and Kalodimos, C.G. (2009). Dynamic activation of an allosteric regulatory protein. Nature *462*, 368-U139.

Visser, S., Hup, G., Exterkate, F.A., and Stadhouders, J. (1983). Bitter flavor in cheese .2. model studies on the formation and degradation of bitter peptides by proteolytic-enzymes from calf rennet, starter cells and starter cell-fractions. Netherlands Milk and Dairy Journal *37*, 169-180.

Volkman, B.F., Lipson, D., Wemmer, D.E., and Kern, D. (2001). Two-state allosteric behavior in a single-domain signaling protein. Science *291*, 2429-2433.

Vyas, N.K., Nickitenko, A., Rastogi, V.K., Shah, S.S., and Quiocho, F.A. (2010). Structural insights into the dual activities of the nerve agent degrading organophosphate anhydrolase/prolidase. Biochemistry-Us *49*, 547-559.

Walter, H.E., Sadler, A.M., and Mattingl.Wa (1969). Semisoft skimmilk cheese . pilot plant procedure. Journal of Dairy Scienc *52*, 1133-1136.

Wiens, M., Koziol, C., Batel, R., and Muller, W.E.G. (1999). Prolidase in the marine sponge suberites domuncula: enzyme activity, molecular cloning, and phylogenetic relationship. Marine Biotechnology *1*, 191-199.

Wilce, M.C., Bond, C.S., Dixon, N.E., Freeman, H.C., Guss, J.M., Lilley, P.E., and Wilce, J.A. (1998). Structure and mechanism of a proline-specific aminopeptidase from *Escherichia coli*. Proceedings of the National Academy of Science U S A *95*, 3472-3477.

Yan, B.X., and Sun, Y.Q. (1997). Glycine residues provide flexibility for enzyme active sites. Journal of Biological Chemistry *272*, 3190-3194.

Yang, S.I., and Tanaka, T. (2008). Characterization of recombinant prolidase from *Lactococcus lactis*- changes in substrate specificity by metal cations, and allosteric behavior of the peptidase. FEBS Journal *275*, 271-280.

Yang, S.I., and Tanaka, T. (2008). Characterization of recombinant prolidase from *Lactococcus lactis*- changes in substrate specificity by metal cations, and allosteric behavior of the peptidase. FEBS Journal *275*, 271-280.

Yanicek, C. (2003). Accelerated protein crystallization with FID. Scientist *17*, 44-44.

Yoshimoto, T., Matsubara, F., Kawano, E., and Tsuru, D. (1983). Prolidase from bovine intestine - purification and characterization. Journal of Biochemistry-Tokyo *94*, 1889-1896.

Zhang, G.D., Chen, J.A., and Tanaka, T. (2009). Deregulation of allosteric response of *Lactococcus lactis* prolidase and its effects on enzyme activity. Biochim Biophys Acta, Proteins Proteomics *1794*, 968-975.

Zhao, G.P., and Somerville, R.L. (1993). A single amino-acid switch within the hinge region of the tryptophan synthase beta-subunit of *Escherichia-coli* that leads to diminished association with alpha-subunit and arrested conversion of esii to product. Journal of Biological Chemistry *268*, 14921-14931.

APPENDIX A

Series of Self-Made Crystallization Screening Solutions

Tube #	Recipe
A1	18% PEG8000, 0.1M NaCacodylate (pH 6.5), 0.1M ZnAcetate
A2	18% PEG8000, 0.1M NaCacodylate (pH 6.5), 0.1M CaAcetate
A3	18% PEG8000, 0.1M NaCacodylate (pH 6.5), 0.1M MnCl2
A4	18% PEG8000, 0.1M NaCacodylate (pH 6.5), 0.1M CoNO3
A5	18% PEG8000, 0.1M NaCacodylate (pH 6.5), 0.1M MgAcetate
A6	20% PEG8000, 0.1M NaCacodylate (pH 6.5), 0.1M ZnAcetate
A7	20% PEG8000, 0.1M NaCacodylate (pH 6.5), 0.1M CaAcetate
A8	20% PEG8000, 0.1M NaCacodylate (pH 6.5), 0.1M MnCl2
A9	20% PEG8000, 0.1M NaCacodylate (pH 6.5), 0.1M CoNO3
A10	20% PEG8000, 0.1M NaCacodylate (pH 6.5), 0.1M MgAcetate
A11	22% PEG8000, 0.1M NaCacodylate (pH 6.5), 0.1M ZnAcetate
A12	22% PEG8000, 0.1M NaCacodylate (pH 6.5), 0.1M CaAcetate
A13	22% PEG8000, 0.1M NaCacodylate (pH 6.5), 0.1M MnCl2
A14	22% PEG8000, 0.1M NaCacodylate (pH 6.5), 0.1M CoNO3
A15	22% PEG8000, 0.1M NaCacodylate (pH 6.5), 0.1M MgAcetate
B1	36% PEG3350, 0.1M NaCacodylate (pH 6.5), 0.1M ZnAcetate
B2	36% PEG3350, 0.1M NaCacodylate (pH 6.5), 0.1M CaAcetate
B3	36% PEG3350, 0.1M NaCacodylate (pH 6.5), 0.1M MnCl2
B4	36% PEG3350, 0.1M NaCacodylate (pH 6.5), 0.1M CoNO3
B5	36% PEG3350, 0.1M NaCacodylate (pH 6.5), 0.1M MgAcetate
B6	42% PEG3350, 0.1M NaCacodylate (pH 6.5), 0.1M ZnAcetate
B7	42% PEG3350, 0.1M NaCacodylate (pH 6.5), 0.1M CaAcetate
B8	42% PEG3350, 0.1M NaCacodylate (pH 6.5), 0.1M MnCl2
B9	42% PEG3350, 0.1M NaCacodylate (pH 6.5), 0.1M CoNO3
B10	42% PEG3350, 0.1M NaCacodylate (pH 6.5), 0.1M MgAcetate
B11	48% PEG3350, 0.1M NaCacodylate (pH 6.5), 0.1M ZnAcetate
B12	48% PEG3350, 0.1M NaCacodylate (pH 6.5), 0.1M CaAcetate
B13	48% PEG3350, 0.1M NaCacodylate (pH 6.5), 0.1M MnCl2
B14	48% PEG3350, 0.1M NaCacodylate (pH 6.5), 0.1M CoNO3
B15	48% PEG3350, 0.1M NaCacodylate (pH 6.5), 0.1M MgAcetate
C1	18% PEG8000, 0.1M NaCacodylate (pH 6.0), 0.1M CaAcetate
C2	18% PEG8000, 0.1M NaCacodylate (pH 6.0), 0.1M MgAcetate
C3	20% PEG8000, 0.1M NaCacodylate (pH 6.0), 0.1M CaAcetate
C4	20% PEG8000, 0.1M NaCacodylate (pH 6.0), 0.1M MgAcetate
C5	22% PEG8000, 0.1M NaCacodylate (pH 6.0), 0.1M CaAcetate
C6	22% PEG8000, 0.1M NaCacodylate (pH 6.0), 0.1M MgAcetate
C7	18% PEG8000, 0.1M NaCacodylate (pH 7.0), 0.1M CaAcetate
C8	18% PEG8000, 0.1M NaCacodylate (pH 7.0), 0.1M MgAcetate
C9	20% PEG8000, 0.1M NaCacodylate (pH 7.0), 0.1M CaAcetate

C10	20% PEG8000, 0.1M NaCacodylate (pH 7.0), 0.1M MgAcetate
C11	22% PEG8000, 0.1M NaCacodylate (pH 7.0), 0.1M CaAcetate
C12	22% PEG8000, 0.1M NaCacodylate (pH 7.0), 0.1M MgAcetate
C13	18% PEG8000, 0.1M NaCacodylate (pH 6.0), 0.1M CaAcetate, 5% iProOH
C14	18% PEG8000, 0.1M NaCacodylate (pH 6.0), 0.1M MgAcetate, 5% iProOH
C15	20% PEG8000, 0.1M NaCacodylate (pH 6.0), 0.1M CaAcetate, 5% iProOH
C16	20% PEG8000, 0.1M NaCacodylate (pH 6.0), 0.1M MgAcetate, 5% iProOH
C17	22% PEG8000, 0.1M NaCacodylate (pH 6.0), 0.1M CaAcetate, 5% iProOH
C18	22% PEG8000, 0.1M NaCacodylate (pH 6.0), 0.1M MgAcetate, 5% iProOH
C19	18% PEG8000, 0.1M NaCacodylate (pH 7.0), 0.1M CaAcetate, 5% iProOH
C20	18% PEG8000, 0.1M NaCacodylate (pH 7.0), 0.1M MgAcetate, 5% iProOH
C21	20% PEG8000, 0.1M NaCacodylate (pH 7.0), 0.1M CaAcetate, 5% iProOH
C22	20% PEG8000, 0.1M NaCacodylate (pH 7.0), 0.1M MgAcetate, 5% iProOH
C23	22% PEG8000, 0.1M NaCacodylate (pH 7.0), 0.1M CaAcetate, 5% iProOH
C24	22% PEG8000, 0.1M NaCacodylate (pH 7.0), 0.1M MgAcetate, 5% iProOH
D1	18% PEG8000, 0.1M Na Citrate (pH 6.0), 0.1M CaAcetate
D2	18% PEG8000, 0.1M Na Citrate (pH 6.0), 0.1M MgAcetate
D3	20% PEG8000, 0.1M Na Citrate (pH 6.0), 0.1M CaAcetate
D4	20% PEG8000, 0.1M Na Citrate (pH 6.0), 0.1M MgAcetate
D5	22% PEG8000, 0.1M Na Citrate (pH 6.0), 0.1M CaAcetate
D6	22% PEG8000, 0.1M Na Citrate (pH 6.0), 0.1M MgAcetate
D7	18% PEG8000, 0.1M Na Citrate (pH 6.5), 0.1M CaAcetate
D8	18% PEG8000, 0.1M Na Citrate (pH 6.5), 0.1M MgAcetate
D9	20% PEG8000, 0.1M Na Citrate (pH 6.5), 0.1M CaAcetate
D10	20% PEG8000, 0.1M Na Citrate (pH 6.5), 0.1M MgAcetate
D11	22% PEG8000, 0.1M Na Citrate (pH 6.5), 0.1M CaAcetate
D12	22% PEG8000, 0.1M Na Citrate (pH 6.5), 0.1M MgAcetate
D13	18% PEG8000, 0.1M MOPS (pH 6.5), 0.1M CaAcetate
D14	18% PEG8000, 0.1M MOPS (pH 6.5), 0.1M MgAcetate
D15	20% PEG8000, 0.1M MOPS (pH 6.5), 0.1M CaAcetate
D16	20% PEG8000, 0.1M MOPS (pH 6.5), 0.1M MgAcetate
D17	22% PEG8000, 0.1M MOPS (pH 6.5), 0.1M CaAcetate
D18	22% PEG8000, 0.1M MOPS (pH 6.5), 0.1M MgAcetate
D19	18% PEG8000, 0.1M MES (pH 6.5), 0.1M CaAcetate
D20	18% PEG8000, 0.1M MES (pH 6.5), 0.1M MgAcetate
D21	20% PEG8000, 0.1M MES (pH 6.5), 0.1M CaAcetate
D22	20% PEG8000, 0.1M MES (pH 6.5), 0.1M MgAcetate
D23	22% PEG8000, 0.1M MES (pH 6.5), 0.1M CaAcetate
D24	22% PEG8000, 0.1M MES (pH 6.5), 0.1M MgAcetate
E1	14% PEG8000, 0.1M NaCacodylate (pH 6.5), 0.1M CaAcetate
E2	14% PEG8000, 0.1M NaCacodylate (pH 6.5), 0.1M CaAcetate, 10mM Leu
E3	14% PEG8000, 0.1M NaCacodylate (pH 6.5), 0.1M CaAcetate, 10mM Pro
E4	14% PEG8000, 0.1M NaCacodylate (pH 6.5), 0.1M CaAcetate, 1 mM DTT
E5	14% PEG8000, 0.1M NaCacodylate (pH 6.5), 0.1M CaAcetate, 1 mM DTT, 10 mM Pro
E6	14% PEG8000, 0.1M NaCacodylate (pH 6.5), 0.1M CaAcetate, 1 mM DTT, 10 mM Pro,

	10mM Leu
E7	14% PEG8000, 0.1M NaCacodylate (pH 6.5), 0.1M MgAcetate
E8	14% PEG8000, 0.1M NaCacodylate (pH 6.5), 0.1M MgAcetate, 10 mM Leu
E9	14% PEG8000, 0.1M NaCacodylate (pH 6.5), 0.1M MgAcetate, 10 mM Pro
E10	14% PEG8000, 0.1M NaCacodylate (pH 6.5), 0.1M MgAcetate, 1 mM DTT
E11	14% PEG8000, 0.1M NaCacodylate (pH 6.5), 0.1M MgAcetate, 1 mM DTT, 10 mM Pro
E12	14% PEG8000, 0.1M NaCacodylate (pH 6.5), 0.1M MgAcetate, 1 mM DTT, 10 mM Pro, 10 mM Leu
E13	16% PEG8000, 0.1M NaCacodylate (pH 6.5), 0.1M CaAcetate
E14	16% PEG8000, 0.1M NaCacodylate (pH 6.5), 0.1M CaAcetate, 10 mM Leu
E15	16% PEG8000, 0.1M NaCacodylate (pH 6.5), 0.1M CaAcetate, 10 mM Pro
E16	16% PEG8000, 0.1M NaCacodylate (pH 6.5), 0.1M CaAcetate, 1 mM DTT
E17	16% PEG8000, 0.1M NaCacodylate (pH 6.5), 0.1M CaAcetate, 1 mM DTT, 10 mM Pro
E18	16% PEG8000, 0.1M NaCacodylate (pH 6.5), 0.1M CaAcetate, 1 mM DTT, 10 mM Pro, 10 mM Leu
E19	16% PEG8000, 0.1M NaCacodylate (pH 6.5), 0.1M MgAcetate
E20	16% PEG8000, 0.1M NaCacodylate (pH 6.5), 0.1M MgAcetate, 10 mM Leu
E21	16% PEG8000, 0.1M NaCacodylate (pH 6.5), 0.1M MgAcetate, 10 mM Pro
E22	16% PEG8000, 0.1M NaCacodylate (pH 6.5), 0.1M MgAcetate, 1 mM DTT
E23	16% PEG8000, 0.1M NaCacodylate (pH 6.5), 0.1M MgAcetate, 1 mM DTT, 10 mM Pro
E24	16% PEG8000, 0.1M NaCacodylate (pH 6.5), 0.1M MgAcetate, 1 mM DTT, 10 mM Pro, 10 mM Leu
F1	10% PEG8000, 0.1M NaCacodylate (pH 6.5), 0.1M CaAcetate
F2	10% PEG8000, 0.1M NaCacodylate (pH 6.5), 0.1M CaAcetate, 10 mM Leu
F3	10% PEG8000, 0.1M NaCacodylate (pH 6.5), 0.1M CaAcetate, 1 mM DTT
F4	10% PEG8000, 0.1M NaCacodylate (pH 6.5), 0.1M CaAcetate, 1 mM DTT, 10mM Leu
F5	10% PEG8000, 0.1M NaCacodylate (pH 6.5), 0.1M MgAcetate
F6	10% PEG8000, 0.1M NaCacodylate (pH 6.5), 0.1M MgAcetate, 10 mM Leu
F7	10% PEG8000, 0.1M NaCacodylate (pH 6.5), 0.1M MgAcetate, 1 mM DTT
F8	10% PEG8000, 0.1M NaCacodylate (pH 6.5), 0.1M mgAcetate, 1 mM DTT, 10 mM Leu
F9	10% PEG8000, 0.1M NaCacodylate (pH 6.5), 0.1M MnCl2
F10	10% PEG8000, 0.1M NaCacodylate (pH 6.5), 0.1M MnCl2, 10 mM Leu
F11	10% PEG8000, 0.1M NaCacodylate (pH 6.5), 0.1M MnCl2, 1 mM DTT
F12	10% PEG8000, 0.1M NaCacodylate (pH 6.5), 0.1M MnCl2, 1 mM DTT, 10mM Leu
F13	12% PEG8000, 0.1M NaCacodylate (pH 6.5), 0.1M CaAcetate
F14	12% PEG8000, 0.1M NaCacodylate (pH 6.5), 0.1M CaAcetate, 10 mM Leu
F15	12% PEG8000, 0.1M NaCacodylate (pH 6.5), 0.1M CaAcetate, 1 mM DTT
F16	12% PEG8000, 0.1M NaCacodylate (pH 6.5), 0.1M CaAcetate, 1 mM DTT, 10 mM Leu
F17	12% PEG8000, 0.1M NaCacodylate (pH 6.5), 0.1M MgAcetate
F18	12% PEG8000, 0.1M NaCacodylate (pH 6.5), 0.1M MgAcetate, 10 mM Leu
F19	12% PEG8000, 0.1M NaCacodylate (pH 6.5), 0.1M MgAcetate, 1 mM DTT
F20	12% PEG8000, 0.1M NaCacodylate (pH 6.5), 0.1M mgAcetate, 1 mM DTT, 10 mM Leu
F21	12% PEG8000, 0.1M NaCacodylate (pH 6.5), 0.1M MnCl2
F22	12% PEG8000, 0.1M NaCacodylate (pH 6.5), 0.1M MnCl2, 10 mM Leu
F23	12% PEG8000, 0.1M NaCacodylate (pH 6.5), 0.1M MnCl2, 1 mM DTT

F24	12% PEG8000, 0.1M NaCacodylate (pH 6.5), 0.1M MnCl2, 1 mM DTT, 10 mM Leu
G1	12% PEG8000, 0.1M NaCacodylate (pH 5.5), 0.1M CaAcetate
G2	12% PEG8000, 0.1M NaCacodylate (pH 5.5), 0.1M MgAcetate
G3	12% PEG8000, 0.1M NaCacodylate (pH 5.5), 0.1M MnCl2
G4	12% PEG8000, 0.1M NaCacodylate (pH 6.0), 0.1M CaAcetate
G5	12% PEG8000, 0.1M NaCacodylate (pH 6.0), 0.1M MgAcetate
G6	12% PEG8000, 0.1M NaCacodylate (pH 6.0), 0.1M MnCl2
G7	12% PEG8000, 0.1M NaCacodylate (pH 6.5), 0.1M CaAcetate
G8	12% PEG8000, 0.1M NaCacodylate (pH 6.5), 0.1M MgAcetate
G9	12% PEG8000, 0.1M NaCacodylate (pH 6.5), 0.1M MnCl2
G10	12% PEG8000, 0.1M NaCacodylate (pH 7.0), 0.1M CaAcetate
G11	12% PEG8000, 0.1M NaCacodylate (pH 7.0), 0.1M MgAcetate
G12	12% PEG8000, 0.1M NaCacodylate (pH 7.0), 0.1M MnCl2
H1	6% PEG8000, 0.1M NaCacodylate (pH 6.5), 0.1M MgAcetate
H2	8% PEG8000, 0.1M NaCacodylate (pH 6.5), 0.1M MgAcetate
H3	10% PEG8000, 0.1M NaCacodylate (pH 6.5), 0.1M MgAcetate
H4	12% PEG8000, 0.1M NaCacodylate (pH 6.5), 0.1M MgAcetate
H5	20% PEG8000, 0.1M NaCacodylate (pH 6.5), 0.1M MgAcetate
H6	22% PEG8000, 0.1M NaCacodylate (pH 6.5), 0.1M MgAcetate
H7	25% PEG8000, 0.1M NaCacodylate (pH 6.5), 0.1M MgAcetate
H8	30% PEG8000, 0.1M NaCacodylate (pH 6.5), 0.1M MgAcetate
I1	12% PEG8000, 0.1M NaCacodylate (pH 6.5), 0.1M MgAcetate
I2	12% PEG8000, 0.1M NaCacodylate (pH 6.5), 0.1M MgAcetate, 5% glycerol
I3	12% PEG8000, 0.1M NaCacodylate (pH 6.5), 0.1M MgAcetate, 10% glycerol
I4	12% PEG8000, 0.1M NaCacodylate (pH 6.5), 0.1M MgAcetate, 15% glycerol
I5	12% PEG8000, 0.1M NaCacodylate (pH 6.5), 0.1M MgAcetate, 20% glycerol
I6	12% PEG8000, 0.1M NaCacodylate (pH 6.5), 0.1M MgAcetate, 25% glycerol
I7	12% PEG8000, 0.1M NaCacodylate (pH 6.5), 0.1M MgAcetate, 30% glycerol
I8	12% PEG8000, 0.1M NaCacodylate (pH 6.5), 0.1M MgAcetate, 35% glycerol
I9	12% PEG8000, 0.1M NaCacodylate (pH 6.5), 0.1M MgAcetate, 50% glycerol
J1	10% PEG8000, 0.1M NaCacodylate (pH 6.5), 0.1M MgAcetate, 1% glycerol
J2	10% PEG8000, 0.1M NaCacodylate (pH 6.5), 0.1M MgAcetate, 2% glycerol
J3	10% PEG8000, 0.1M NaCacodylate (pH 6.5), 0.1M MgAcetate, 3% glycerol
J4	10% PEG8000, 0.1M NaCacodylate (pH 6.5), 0.1M MgAcetate, 4% glycerol
J5	10% PEG8000, 0.1M NaCacodylate (pH 6.5), 0.1M MgAcetate, 5% glycerol
J6	10% PEG8000, 0.1M NaCacodylate (pH 6.5), 0.1M MgAcetate, 6% glycerol
J7	10% PEG8000, 0.1M NaCacodylate (pH 6.5), 0.1M MgAcetate, 7% glycerol
J8	10% PEG8000, 0.1M NaCacodylate (pH 6.5), 0.1M MgAcetate, 8% glycerol
J9	10% PEG8000, 0.1M NaCacodylate (pH 6.5), 0.1M MgAcetate, 9% glycerol
J10	10% PEG8000, 0.1M NaCacodylate (pH 6.5), 0.1M MgAcetate, 10% glycerol
J11	12% PEG8000, 0.1M NaCacodylate (pH 6.5), 0.1M MgAcetate, 1% glycerol
J12	12% PEG8000, 0.1M NaCacodylate (pH 6.5), 0.1M MgAcetate, 2% glycerol
J13	12% PEG8000, 0.1M NaCacodylate (pH 6.5), 0.1M MgAcetate, 3% glycerol
J14	12% PEG8000, 0.1M NaCacodylate (pH 6.5), 0.1M MgAcetate, 4% glycerol
J15	12% PEG8000, 0.1M NaCacodylate (pH 6.5), 0.1M MgAcetate, 5% glycerol

J16	12% PEG8000, 0.1M NaCacodylate (pH 6.5), 0.1M MgAcetate, 6% glycerol
J17	12% PEG8000, 0.1M NaCacodylate (pH 6.5), 0.1M MgAcetate, 7% glycerol
J18	12% PEG8000, 0.1M NaCacodylate (pH 6.5), 0.1M MgAcetate, 8% glycerol
J19	12% PEG8000, 0.1M NaCacodylate (pH 6.5), 0.1M MgAcetate, 9% glycerol
J20	12% PEG8000, 0.1M NaCacodylate (pH 6.5), 0.1M MgAcetate, 10% glycerol

Note: Percentage for PEG8000 and glycerol are expressed as weight per volume and volume per volume, respectively.